Effects of preovulatory aging on the developmental competence of mouse oocytes

Inaugural-Dissertation

zur

Erlangung des Doktorgrades

Dr. rer. nat.

der Fakultät für Biologie

an der

Universität Duisburg-Essen

vorgelegt von

Hannah Demond

aus Bergisch Gladbach

Februar 2016

Die der vorliegenden Arbeit zugrunde liegenden Experimente wurden am Institut für Humangenetik der Universität Duisburg-Essen durchgeführt.

1. Gutachter: Prof. Dr. Bernhard Horsthemke

2. Gutachter: Prof. Dr. Gunther Wennemuth

3. Gutachter: Prof. Dr. Thomas Haaf

Vorsitzender des Prüfungsausschusses: Prof. Dr. Dominik Boos

Tag der mündlichen Prüfung: 09.05.2016

List of Papers

This thesis is based on the following papers:

Dankert D.*, **Demond H.***, Trapphoff T., Heiligentag M., Eichenlaub-Ritter U., Horsthemke B., Grümmer R. (2014). Pre- and postovulatory aging of murine oocytes affect the transcript level and poly(A) tail length of maternal effect genes. *PLoS One* 9(10): e108907.

*shared first authorship

Demond, H., T. Trapphoff, D. Dankert, M. Heiligentag, B. Horsthemke, R. Grümmer, U. Eichenlaub-Ritter. Preovulatory aging in vivo and in vitro affects maturation rates, abundance of selected proteins, histone methylation and spindle integrity in murine oocytes. Submitted to *PLoS One.*

Table of contents

1 Introduction

1.1 Oocyte development

Mammalian oocytes originate from primordial germ cells (PGCs) that are formed during female embryonic development and migrate from the gut to the genital ridge (Molyneaux et al. 2001). In mice, the PGCs enter the genital ridge around embryonic day 11.5 where their numbers vastly increase through mitotic divisions (Figure 1; Tam and Snow 1981). These divisions continue once the cells reach the gonad, resulting in millions of gamete precursors that commence meiosis. At birth mammalian oocytes are arrested at prophase I at the diplotene stage. This stage of the first meiotic cycle is also known as germinal vesicle (GV) stage, based on the large nucleus that is visible in these oocytes (Lüllmann-Rauch 2003).

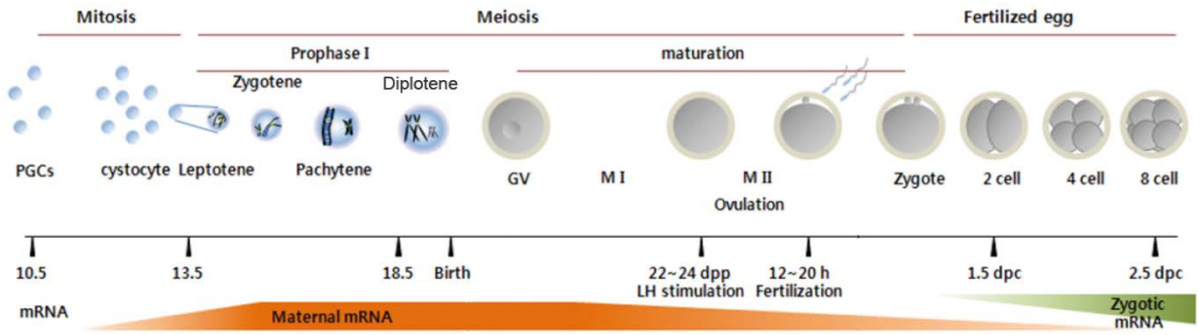

Figure 1: Messenger RNA levels during oocyte growth, maturation and early embryonic development. During embryonic development PGCs migrate to the genital ridge, where they increase in number through mitotic divisions. At day 13.5 of embryonic development meisosis is initiated, which coincides with oocyte growth and enrichment of maternal mRNAs. At the pachytene stage of meiosis, transcription is arrested and maternal transcripts are stored. These stored mRNAs are recruited for protein translation during oocyte maturation, which is followed by their degradation. Since embryonic genome activation does not occur before the 2-cell stage, maternal transcripts present in the zygote regulate early preimplantation development. Figure adapted from Kang and Han (2011).

Oocytes resume their development in a process called oocyte maturation consisting of three major steps: 1) resumption of meiosis, which is characterized by germinal vesicle breakdown, chromosome condensation and spindle formation; 2) passage from meiosis I to meiosis II; and 3) subsequent arrest in metaphase II of the second meiotic cycle. Meiosis I resumes as a response to the surge of luteinizing hormone (LH) prior to ovulation, which leads to the separation of the homologues chromosomes and the expulsion of the first polar body.

Completion of meiosis II is triggered by fertilization and leads to division of the sister chromatids and extrusion of the second polar body (Lüllmann-Rauch 2003).

Fertilization is followed by the first cleavage stages of embryonic development (Figure 1). During this time, the embryo migrates from the oviduct to the uterus, which it reaches at the blastocyst stage ready for implantation. The first embryonic cell divisions still depend largely on maternal factors that are stored and recruited by the oocyte during growth and maturation (Figure 1; Li et al. 2013). Therefore, the developmental competence of the oocyte is of crucial importance for embryonic development and reproductive outcome and, amongst others, defined by these maternal factors that regulate the preimplantation phase.

1.2 Preovulatory aging

Since oocyte growth, maturation, fertilization and preimplantation development are tightly coordinated processes that depend on many highly regulated factors, disturbances of these processes may severely impact the developmental competence of the oocyte. Deregulation of the timely development of the oocytes is an example of such a disturbance. For instance, delay in ovulation or fertilization cause oocyte overripeness, also known as pre- and postovulatory aging. These deregulations have been postulated long ago as causative for a significant amount of birth defects in humans (Butcher 1976). The present study focused mainly on the effects of preovulatory aging on oocyte developmental competence since much less is known about this form of oocyte overripeness.

Delayed ovulation can happen naturally in animals and humans due to an irregular menstrual cycle. In women this can occur during the whole reproductive life span, but is more frequent in certain phases, such as the first postmenarchal years, the last premenopausal years and the first months following pregnancy (Smits et al. 1995). Prolonged menstrual cycles correlate with an increased incidence in congenital malformations in women (Spira et al. 1985). Preovulatory aging can also arise in the course of assisted reproduction techniques (ART), which is getting increasingly important since more and more children are born this way (Kupka et al. 2014). Over 5 million babies worldwide have been born after ART treatment since the birth of the first in vitro fertilization (IVF) baby, Louise Brown, in 1978. Prolonged hormonal treatment prior to superovulation is avoided during ART, since it coincides with a lower number of oocytes. Due to ethical reasons the sparse knowledge about the effects of preovulatory aging in humans has been gathered through indirect evidence (Smits et al. 1995). Therefore, animal models are essential for understanding the consequences of preovulatory

oocyte overripeness on the developmental capacity of the oocyte and the embryo that derives from it.

Preovulatory aging in vivo has been studied in several different animal species and was shown to decrease the developmental competence of the oocyte and impair embryonic and fetal development in e.g. fish, frogs, urodeles and guinea pigs. In rats an induced delay of ovulation for 24-48 hours (h) decreased the fertilization rate of the aged oocytes and led to chromosome aberrations, abnormal development of the preimplantation embryo, implantation failure, fetal malformations and high mortality rates (Smits et al. 1995). Hardly anything is known about the molecular processes in the oocyte during preovulatory aging that cause the decreased oocyte quality. In rats induced preovulatory aging is known to alter the cell organization and RNA transcription of the oocyte as well as the hormonal levels of the animals. Natural preovulatory aging, defined by spontaneously delayed cycles, has been described to cause cytoplasmic degeneration in the oocyte and to lead to increased implantation failure and embryonic malformations in rats (Smits et al. 1995). Recently an in vivo mouse model has been established to investigate the consequences of preovulatory aging in more detail (Bittner et al. 2011).

1.2.1 In vivo mouse model for preovulatory aging

The in vivo mouse model that was used in this study was established by Bittner and colleagues (2011). It is based on the gonadotropin releasing hormone (GnRH) antagonist cetrorelix that also finds broad application in human ART (Al-Inany 2007; Al-Inany et al. 2011). GnRH is secreted by the hypothalamus and stimulates the pituitary to produce follicle stimulating hormone (FSH) and LH (Lüllmann-Rauch 2003). FSH in turn, induces the secretion of aromatase by the granulosa cells which mediates the modulation of androgens into estrogens in the ovary. It stimulates follicle growth and ripening. LH is responsible for inducing ovulation (Lüllmann-Rauch 2003). By blocking GnRH, cetrorelix suppresses the whole intrinsic sex-hormonal axis and allows regulating follicle ripening and ovulation by external application of hormones. This way ovulation can be postponed inducing preovulatory aging of oocytes (see Figure 4 for detailed hormone application scheme).

It was shown with this mouse model that preovulatory aging leads to an increase in embryo resorption after implantation and a decreased embryonic weight (Bittner et al. 2011). This indicates that preovulatory aging in this mouse model impairs oocyte quality and interferes with embryo development. The preovulatory-aged oocytes that derive from these cetrorelix-

treated mice have not been analyzed on a molecular level so far; neither have the processes of fertilization and preimplantation development. That is why the present study focused on the investigation of molecular mechanisms in preovulatory in vivo-aged oocytes and embryos that derived from these oocytes.

1.2.2 Preovulatory aging in a follicle culture model

Another possible setting to investigate the molecular consequences of preovulatory aging is in vitro in a follicle culture model. The importance of growth and maturation in follicle culture is increasing, for instance in the context of cryopreservation or as experimental model (Cortvrindt and Smitz 2002; Sun et al. 2004; Chian et al. 2013). Cryopreservation of oocytes, also known as vitrification, is the most commonly used method for fertility preservation in women. In the case of cancer patients it is not always possible to collect mature oocytes after hormonal treatment for vitrification. In these cases, unstimulated ovarian tissue or immature oocytes from this tissue can be preserved and maturated in vitro (Chian et al. 2013). In vitro culture allows a strict control of the environment in which the follicles develop and can therefore serve as a suitable experimental model to investigate the impact of adverse exposures, altered follicle environment or prolonged follicle culture time (Cortvrindt and Smitz 2002; Sun et al. 2004). The fertilization rate as well as the developmental competence of preovulatory-aged oocytes to the blastocyst stage is known to be reduced when prolonging the culture period (Segers et al. 2010). Not much is known though about the molecular mechanisms, such as RNA dynamics, in preovulatory-aged in vitro-grown oocytes.

1.3 Postovulatory aging

Another form of oocyte overripeness can result from postovulatory aging caused by a delay in fertilization. Early research on pre- and postovulatory aging of mammalian oocytes found similarities between the two mechanisms of timely interference of oocyte development leading to the hypothesis that similar pathogeneses might apply (Smits et al. 1995). In contrast to preovulatory aging, delayed fertilization has been studied much more intensely and it is known to have detrimental effects on molecular processes in the oocyte, impairing fertilization and embryonic development (Lord and Aitken 2013). For example, one important cause for the reduced oocyte quality after postovulatory aging is oxidative stress caused by accumulation of electrophilic aldehydes. This sets off many cascades that influence oocyte developmental competence, like mitochondrial dysfunction, DNA damage, DNA methylation defects and perturbed Ca^{2+} homeostasis, eventually leading to apoptosis (Chi et al. 1988;

Liang et al. 2008; Miao et al. 2009; Zhang et al. 2011; Lord et al. 2015). It has been shown for *Xenopus tropicalis* that also disturbances in posttranscriptional regulation of transcripts such as degradation of maternal mRNA or loss of poly(A) tail length might decrease the developmental potential of the oocyte and lead to a decline in fertilization rates and aberrant embryonic development (Kosubek et al. 2010). To investigate if effects on posttranscriptional regulation can also be found in mammals, the current study analyzed poly(A) tail dynamics in the postovulatory-aged mouse oocyte on a transcriptome-wide level.

1.4 Epigenetic histone modifications in the growing oocyte

Around midgrowth in prophase I, transcription declines progressively until it is nearly halted, such that full-grown oocytes are essentially transcriptionally quiescent (Moore and Lintern-Moore 1978). Transcriptional silencing of the oocyte genome is mediated by epigenetic histone modifications and DNA methylation. Genomic DNA in eukaryotes is folded around histones and other proteins to form chromatin. Histones are small proteins that consist of a globular domain and a flexible and charged NH_2-terminus, the histone tail that obtrudes from the nucleosome. Epigenetic modifications such as methylation, acetylation and phosphorylation of amino acids in this histone tail determine the functional characteristics of the chromatin (Jenuwein and Allis 2001). The structural organization of chromatin can be divided into two major categories: euchromatin and heterochromatin. Euchromatin is less condensed and it is therefore generally thought to be easier accessible and transcribed. Heterochromatin is highly condensed, inaccessible and is well known to function in gene silencing and repression of recombination, although there is evidence for a multifaceted role of heterochromatin in both transcriptional repression as well as activation of target loci (Li 2002; Grewal and Jia 2007). Euchromatin is typically characterized by a histone-modification profile that includes histone acetylation and methylation of histone H3 at lysine 4 (H3K4me), whereas heterochromatin is marked by hypoacetylation and trimethylation of histone H3 at lysine 9 and 27 (H3K9me3 and H3K27me3; Grewal and Jia 2007).

Histone modifications can influence transcription of DNA directly. For example, H3K9me3 prohibits binding of transcription factors to the DNA, by making DNA binding domains inaccessible to them (Soufi et al. 2012). On a longer term, histone modifications can also organize DNA methylation levels, by recruiting or inhibiting binding of DNA methyltransferases (Cedar and Bergman 2009). For instance, H3K4 interacts with the DNA methyltransferase Dnmt3a and its regulatory factor Dnmt3l, inducing DNA methylation (Jia et al. 2007). Methylation of H3K4 at CpG islands inhibits the binding of Dnmt3l, therefore

repressing DNA methylation at these sites (Ooi et al. 2007). During oogenesis histone modifications and DNA methylation change, establishing the epigenetic landscape of the oocyte. For example, H3K4 di- and trimethylation increases, which is followed by inhibition of DNA methylation in these regions (Stewart et al. 2015). In contrast, H3K36 trimethylation is a marker for sites in the genome that will be methylated on DNA in the course of oocyte growth (Stewart et al. 2015).

H3K9me3 has long been thought to be involved in silencing repetitive sequences, such as tandem-repeat satellites near centromeres and telomeres, retrotransposons and endogenous retroviruses (Becker et al. 2016). When active, these regions pose a risk for the genome integrity, which is why it is important to keep them physically inaccessible by packing them in condensed heterochromatin. These regions are classified as constitutive heterochromatin and they are silenced universally in all tissues (Saksouk et al. 2015). In contrast, facultative heterochromatin is dynamically regulated during development and tissue specific. It affects cell-type specific genes and enhancers (Trojer and Reinberg 2007). More recent genome-wide mapping studies suggested a role of H3K9me3 in cell type specific regulation of facultative heterochromatin during development and differentiation (Vogel et al. 2006; O'Geen et al. 2007; Hawkins et al. 2010; Zhu et al. 2013). For example, during human embryonic development H3K9me3 mediates the differentiation from pluripotent stem cells to differentiated cells by blocking access to pluripotent transcription factors such as Oct4 and Sox2 (Soufi et al. 2012). H3K9 trimethylation is nearly absent at the time of oogenesis that takes place during early postnatal development from day 5 until day 15. Then it increases prominently in the GV stage of oocyte maturation and is thought to function in the silencing of the oocyte genome at this stage (Kageyama et al. 2007).

At the pericentric regions of heterochromatin H3K9 is methylated through the selective histone methyltransferase Suv39h1 and Suv39h2, creating a binding site for the chromatin modulator HP1 (Bannister et al. 2001; Lachner et al. 2001). HP1 is a member of the highly conserved chromodomain protein family and involved in gene silencing and genome organization (Jones et al. 2000). The Suv39h histone methyltransferases are required in mice for normal pre- and postnatal development (Peters et al. 2001). Loss of Suv39h leads to growth retardation and infertility. H3K9 methylation is dependent on Suv39h and protects genomic stability at the pericentric regions of constitutive heterochromatin. Suv39h is also required for H3K9 methylation during male meiosis, since impairments lead to aberrant centromere clustering and nonhomologous interactions (Peters et al. 2001). It is likely that Suv39h mediated H3K9 methylation is also important for female meiosis. Other H3K9

methyltransferases are Eset, EuHmt1 and G9a (Li 2002). Whereas Suv39h is required for H3K9me in pericentric heterochromatin, G9a methylates histone H3K9 in euchromatin regions. G9a and Suv39h have distinct, non-overlapping regions of the chromosomes to which they localize, which indicates different functions in chromatin organization for the two proteins, but also for H3K9 methylation depending on whether it is associated with euchromatin or heterochromatin (Tachibana et al. 2002). Like Suv39h, G9a is indispensible for postimplantation embryonic development (Tachibana et al. 2002). If G9a also functions in oocytes and preimplantation embryos is unknown.

1.5 Posttranscriptional regulation of protein synthesis in the oocyte

Oocyte volume increases 200- to 300-fold during oocyte growth. In this time, the oocyte accumulates a vast amount of RNA in the cytoplasm (Figure 1) resulting in a fully grown oocyte containing approximately 80 pg of mRNA and 350-500 pg of total RNA (Bachvarova et al. 1985). After accumulation of RNA, transcription is arrested until the time point of embryonic genome activation. Following transcriptional silencing meiosis is accompanied with a slow but steady decrease of maternal mRNA levels, which accelerates after fertilization during the oocyte-to-embryo transition (Figure 1). In between, the stored transcripts are needed to regulate the processes of oocyte maturation, fertilization or oocyte-to-embryo transition. They are essential for oocyte survival and recruited for translation in a time-dependent manner (Kang and Han 2011).

Due to the absence of transcription, synthesis of proteins during oocyte growth and maturation has to be regulated almost exclusively on a posttranscriptional level. RNA storage and protein synthesis are closely regulated. One important and well-studied mechanism of RNA storage and translation in the oocyte is modification of the poly(A) tail length (Weill et al. 2012). It is known that postovulatory aging reduces the transcript levels and poly(A) tail length in *Xenopus* oocytes, which might be a cause for the reduced developmental competence that is observed in oocytes with delayed fertilization (Kosubek et al. 2010). But also subcellular localization and factors like Musashi1, Dazl and Y-box proteins (e.g. Ybx2) regulate storage and translation of transcripts (Molyneaux et al. 2001; Flemr et al. 2010; Yurttas et al. 2010; Chen et al. 2011). If preovulatory aging also affects transcript storage has not been studied so far.

1.5.1 Ybx2-mediated mRNA storage and recruitment

Ybx2 (Y-box protein 2; formerly known as Msy2) is a germ cell specific RNA binding protein that belongs to the family of the Y-box proteins (Gu et al. 1998). Y-box proteins form a large family that is conserved from bacteria to humans (Yu et al. 2002). Ybx2 for example, is the mouse ortholog of the *X. laevis* FRGY2 and human CONTRTIN proteins (Matsumoto and Wolffe 1998; Tekur et al. 1999). It is one of the most abundant proteins in growing oocytes, constituting approximately 2% of total protein in the cell (Yu et al. 2002). It has a major role in regulating mRNA stability and repressing protein translation during oocyte growth (Yu et al. 2002). Considering the importance, it is not surprising that loss of Ybx2 was found to lead to infertility in mice (Yang et al. 2005). The growth rate of oocytes lacking Ybx2 is reduced, leading to improper maturation. Furthermore, oocytes fail to become transcriptional quiescent, show transcript and poly(A) tail instability, spindle malformations, deficiencies in chromosome arrangement and a dramatic perturbation of the transcriptome in absence of Ybx2 expression (Medvedev et al. 2011).

1.5.2 Poly(A) tail dynamics

In eukaryotic cells, DNA is transcribed into pre-mRNA which has to be modified in the nucleus after transcription. First introns are spliced out, then an m^7Gppp group is attached to the 5’ end (the cap structure) of the mRNA and finally a poly(A) tail of approximately 250-300 adenosine residues is added to the 3’ end (Piccioni et al. 2005). After transportation of the mRNA into the cytoplasm, the 5’ cap and the 3’ poly(A) tail facilitate the initiation of translation, the rate-limiting step of protein translation (Figure 2A; Sachs 2000; Preiss and Hentze 2003). The 5’ cap binds the eukaryotic translation initiation factor eIF4E, which in turn binds the scaffolding protein eIF4G (Sonenberg et al. 1978; 1979; Lamphear et al. 1995; Mader et al. 1995). The poly(A) binding protein (PABP) binds to the 3’end and associates to eIF4G (Tarun and Sachs 1995; 1996). Together, these interactions form a platform for the recruitment of several other eIFs including the RNA helicase eIF4A, which in the end leads to the formation of the eIF4F complex and a closed-loop formation of the mRNA (Figure 2A; Wells et al. 1998; Preiss and Hentze 2003). This pseudo-circularization of the mRNA stabilizes the eIF4F complex. At last, the eIF4F complex recruits the ribosome subunits and the initiation of translation is completed (Preiss and Hentze 2003).

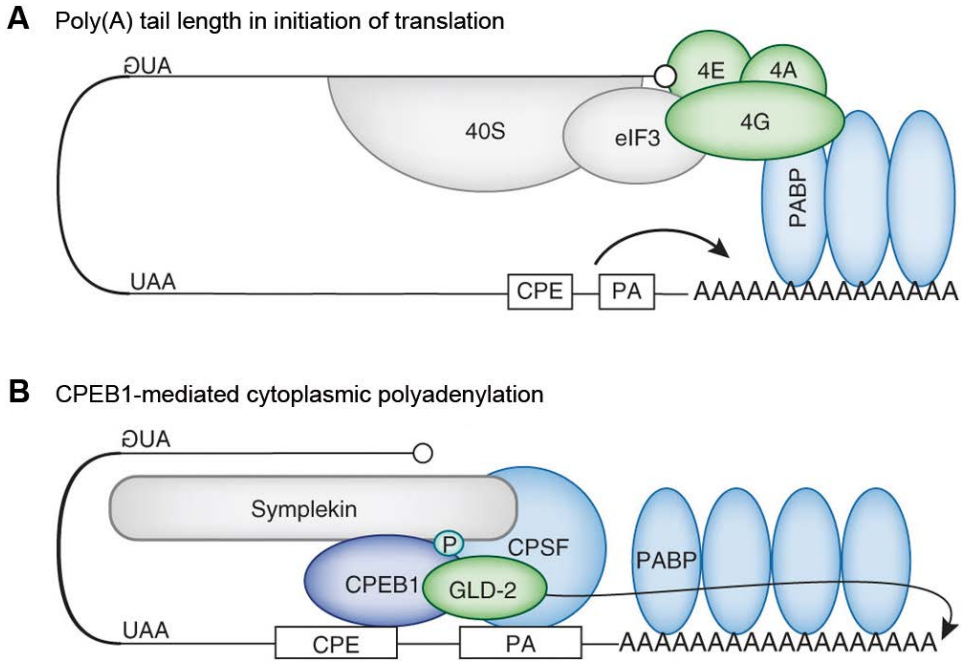

Figure 2: The role of the poly(A) tail during initiation of translation (A) and the process of cytoplasmic polyadenylation through CPEB1 phosphorylation (B). A) The poly(A) tail is bound by PABPs, which interact with eIF4G, the scaffolding protein of the eIF4F complex that induces the initiation of translation. This leads to a closed-loop formation of the mRNA, enhancing translation efficiency. Motifs in the 3'UTR, such as CPE and PA, promote cytoplasmic polyadenylation and therefore translation. **B)** CPEB1 binds to CPEs and interacts with the scaffolding protein Symplekin that is also associated with CPSF-bound PAs. When CPEB1 is phosphorylated it recruits the poly(A) polymerase GLD-2, which elongates the poly(A) tail. However, without its phosphorylation mark, CPEB1 attracts the poly(A) deadenylase PARN that blocks GLD-2 and shortens the poly(A) tail, giving this protein a dual function in the regulation of poly(A) tail length. Figure adapted from Weill et al. 2012.

Translation efficiency is known to depend on the poly(A) tail length although a recent study found that this correlation can only be found in certain tissues or cells such as oocytes and early embryos (Beilharz and Preiss 2007; Subtelny et al. 2014). The oocyte seems to be a very special in regard to poly(A) tail dynamics. In most tissues mRNA turnover in the cytoplasm starts with the degradation of the poly(A) tail inducing a pathway that leads to translation followed by degradation of the transcript (Parker and Song 2004). In contrast, oocytes have the possibility to protect certain transcripts after deadenylation. This allows them to store mRNAs in a dormant state until they are needed. They are recruited for translation by elongating their poly(A) tail again through a process known as cytoplasmic polyadenylation. The best studied mechanism of cytoplasmic de- and polyadenylation in the oocyte is mediated by the cytoplasmic polyadenylation element binding protein 1 (CPEB1; Figure 2B; Richter 2007; Weill et al. 2012). This process depends on two elements in the 3' untranslated region (UTR) of the mRNA: 1) a polyadenylation site (PA), which is also required for nuclear

polyadenylation and found in all mRNAs and 2) a cytoplasmic polyadenylation element (CPE; McGrew et al. 1989; Paris and Richter 1990; Gebauer et al. 1994). CPEs can only be found in certain transcripts (15-20% of the vertebrate genome) and are recognized by CPEB1 (Paris et al. 1991; Hake and Richter 1994; Pique et al. 2008).

CPEB1 has a dual function in mediating poly(A) tail length of maternal transcripts during oogenesis depending on its phosphorylation status (Kim and Richter 2006). Non-phosphorylated CPEB1 bound to a CPE recruits a ribonucleoprotein complex containing the poly(A) deadenylase PARN, which deadenylates the transcripts and leads to the repression of maternal mRNAs. Phosphorylation of CPEB1 causes expulsion of PARN from this complex (Kim and Richter 2006). Through the scaffolding protein Symplekin phosphorylated CPEB1 can interact with the cleavage and polyadenylation specific factor (CPFS) that binds to the PA (Dickson et al. 1999; Barnard et al. 2004). Together CPEB1 and CPSF recruit the cytoplasmic poly(A) polymerase GLD-2 to elongate the poly(A) tail and promote translation of the transcript (Figure 2B; Barnard et al. 2004).

It is known that transcript levels are reduced after postovulatory aging. It was shown in *Xenopus* that this coincides with deadenylation of certain maternal transcripts which contain a CPE and PA in their 3'UTR (Kosubek et al. 2010). If this also applies to mammalian oocytes and whether the poly(A) tail length is also affected by preovulatory aging has not been studied so far.

1.6 Oocyte-to-embryo transition

The process of oocyte-to-embryo transition describes the conversion of a fully grown, highly specialized and almost transcriptionally quiescent oocyte into a developmentally active and mitotically dividing embryo (Robertson and Lin 2013). This process starts with oocyte maturation and includes fertilization, embryonic genome activation and the transition from maternal-to-zygotic control.

1.6.1 Maternal effect genes

The oocyte-to-embryo transition is mainly regulated by maternal effect (ME) genes. These are genes are expressed by the oocyte but function in the early embryo. Some ME genes are exclusive to the oocyte and function during the oocyte-to-embryo transition, while others are needed later during embryo development and are expressed by both the oocyte and the embryo. This makes it difficult to distinguish between maternal and embryonic defects. ME

genes have three major roles: 1) processing of the paternal genome, 2) removal of maternal factors and 3) the activation of the embryonic genome (Li et al. 2010). Defects in ME genes usually lead to developmental impairments and embryonic arrest during early preimplantation stages (Acevedo and Smith 2005). The present study investigated a selection of the over 30 described ME genes (Li et al. 2010), focusing mainly on genes involved in early embryonic genetic processes, e.g. RNA dynamics (*Zar1*), embryonic genome activation (*Smarca4*) and epigenetic reprogramming (*Tet3*, *Trim28*, *Zfp57*, *Dnmt1*). Furthermore, the transcription factor *Pou5f1* as well as members of the *Nlrp* gene family were analyzed.

Zar1 (Zygotic arrest 1) is an example of an ME gene that is involved in the very early processes after fertilization, probably in syngamy of the pronuclei. It is essential for development past the 1-cell stage (Wu et al. 2003). Studies in *Xenopus* indicate that *Zar1* encodes an RNA-binding protein involved in posttranscriptional regulation in the oocyte. It binds to the translational control region in the 3'UTR of maternal mRNAs, leading to their translational repression (Yamamoto et al. 2013).

One very crucial ME gene seems to be *Pou5f1* (encoding the Oct4 protein), which is better known as a marker for pluripotent stem cells during early embryonic development (Pesce et al. 1998; Foygel et al. 2008). During oocyte growth *Pou5f1* is first down regulated during early oogenesis, to be up regulated de novo in the final stages of meiotic prophase I (Pesce et al. 1998). *Pou5f1* plays a critical role by controlling the expression of many transcription regulators involved in embryonic genome activation, maternal RNA degradation and reprogramming processes (Foygel et al. 2008). This *Pou5f1*-regulated transcriptional network in the oocyte consists of 182 genes (Zuccotti et al. 2011). Within this network there is a core group of 80 ME genes, which escape post-fertilization degradation and which are involved in oocyte-to-embryo transition (Zuccotti et al. 2011). It has been proposed that *Pou5f1* can directly or indirectly affect many essential processes such as chromatin remodeling, epigenetic regulation, apoptosis, cell cycle regulation and signaling during early developmental reprogramming (Foygel et al. 2008; Zuccotti et al. 2011).

Several members of the *Nlrp* gene family have been found to be ME genes. *Nlrp* (also known as *Nalp*) stands for nucleotide-binding oligomerization domain, leucine rich repeat and pyrin domain containing gene and the *Nlrp* genes are members of the *Nlr* (Nod-like receptor) gene family. *Nlrp*s were previously found to be involved in the innate immune system of mammals but recently they have been discovered to play a role in reproduction (Zhang et al. 2008; Tian et al. 2009). In mice *Nlrp2*, *4*, *5*, *9* and *14*, all situated on chromosome 11, are known to be

involved in reproduction. Their exact functions as well as the mechanisms in which they act are mainly unknown. *Nlrp2* and *Nlrp14* are both oocyte specific ME genes required for proper embryonic preimplantation development (Horikawa et al. 2005; Peng et al. 2012). *Nlrp5* (also known as *Mater*) is an oocyte specific gene and was one of the first described ME genes (Tong et al. 2000). Nlrp5 protein is part of the subcortical maternal complex (SCMC), where it interacts with other proteins such as Filia, Floped and Tle6 (Li et al. 2008a). The SCMC is known to be essential for preimplantation development and required for symmetric division of the zygote (Li et al. 2008a; Yu et al. 2014). Nlrp5 is known to function in mitochondria localization and activity and distribution of the endoplasmatic reticulum and calcium homeostasis. *Nlrp4* and *9* are also oocyte specific genes and are expansive in rodents, having 7 and 3 copies respectively (Tian et al. 2009). Their function in early embryonic development remains unknown. Therefore, and because *Nlrp4* and *9* are difficult to assess due to the many isoforms that exist, the focus in this study lay on the remaining *Nlrp* genes known to be involved in mouse reproduction (*Nlrp2, 5 and 14*).

To release the genome from its repressive state and initiating transcription maternal factors are required. *Smarca4* (SWI/SNF related, matrix associated, actin dependent regulator of chromatin, subfamily a, member 4, also known as *Brg1*) is an ME gene involved in chromatin remodeling and required for development past the 2-cell stage (Bultman et al. 2006). Smarca4 protein is the catalytic subunit of SWI/SNF-related complexes and has a DNA-dependent ATPase activity. The energy derived from ATP hydrolysis alters the conformation and position of nucleosomes, causing DNA-histone contacts to break and histone octamers to slide several hundred base pairs upstream or downstream (Bazett-Jones et al. 1999; Kingston and Narlikar 1999; Whitehouse et al. 1999). This chromatin remodeling then in turn makes promoters accessible for transcription initiation by inducing H3K9 demethylation. Smarca4 is known to regulate the expression of 30% of the genes expressed at the 2-cell stage, of which most are involved in transcription, RNA processing and cell cycle regulation (Bultman et al. 2006).

Other ME genes investigated in this study are *Tet3*, *Trim28*, *Zfp57* and *Dnmt1*. They will be described later, in the context of epigenetic reprogramming and DNA methylation maintenance of genomic imprints.

1.6.2 Embryonic genome activation

Embryonic genome activation is the first major step to occur after fertilization, in which control of the developmental program switches from regulation by maternally inherited mRNAs and proteins to regulation by embryonic genes. The parental genomes that were repressed during germ cell growth and maturation have to be reactivated, which involves epigenetic reprogramming. In the course of embryonic genome activation maternal factors have to be degraded and replaced by embryonic factors. Also extensive reprogramming has to take place since the transition from a highly specialized oocyte and sperm to totipotent blastomers requires a large-scale change of the gene expression pattern (Schultz 2002).

In mice transcription is activated in several waves. The first major step occurs around the 2-cell stage (Schultz 1993; Hamatani et al. 2004; Wang et al. 2004). In comparison, in other vertebrate species the embryonic genome activation is later, e.g. at the 4- to 8-cell stage in other mammals like ovine, bovine, porcine and human embryos or after 12 rounds of DNA replication at the mid-blastula stage in *Xenopus* (Newport and Kirschner 1982; Telford et al. 1990). The first minor wave of transcription occurs in the S-phase of the 1-cell embryo and mRNAs during this first wave of transcription are mainly transcribed from the male pronucleus (Nothias et al. 1996; Aoki et al. 1997). This is possibly due to a higher concentration of transcription factors in the male pronucleus (Worrad et al. 1994). Because the first minor wave of transcription correlates with the start of DNA replication, it was hypothesized that DNA replication might be a trigger for the transcriptional onset in the zygote. This is supported by the observation that inhibiting DNA replication leads to a decrease in transcription in the early embryo although it does not inhibit transcription completely (Aoki et al. 1997). It is thought that maternal proteins translated from maternal transcripts during the 1-cell stage trigger the first minor wave of embryonic genome activation (Hamatani et al. 2004).

A second, bigger wave of transcription starts during the S- and G2-phase in the 2-cell embryo and continues until the 4-cell stage (Aoki et al. 1997; Hamatani et al. 2004; Wang et al. 2004). Several other waves of genome activation follow around the 8-cell, morula and blastocyst stage (Hamatani et al. 2004). Each wave activates a specific group of genes of which the majority is downregulated again soon after. The maternal proteins and the proteins from the first wave are in subsequent steps required for initiation of the next waves of transcription (Hamatani et al. 2004). Chromatin remodeling such as histone acetylation that is needed for DNA replication might allow access for maternally inherited transcription machineries to

promotors which were silenced during oocyte maturation (Wiekowski et al. 1993; Patterton and Wolffe 1996). Indeed, hyperacetylation was shown to increase transcription in the 2-cell embryo (Aoki et al. 1997). Due to the focus on how maternal transcripts in preovulatory-aged oocytes affect the developmental competence, the present study concentrated on the first major wave of embryonic genome activation at the 2-cell stage.

1.7 DNA methylation

DNA methylation of cytosines (5-methyl-cytosine, 5mC) within CpG dinucleotides is the most widely studied epigenetic modification in mammals and has for example a central role in imprinting (Li et al. 1993; Peters 2014). DNA methylation of CpGs is generally related with transcriptional silencing and chromosome stability. Even though CpGs are underrepresented in the genome, there are certain regions in which the sequence differs significantly from the rest in being CpG-rich. These DNA sequences are known as CpG islands and are mainly nonmethylated (Deaton and Bird 2011).

One of the most important regulators of DNA methylation is the family of DNA methyltransferases (Dnmt; Bestor 2000; Goll and Bestor 2005). This family consists of three members with methyltransferase activity, Dnmt1, Dnmt3a and Dnmt3b, who are conserved in the plant and animal kingdom (Bestor 2000). A fourth member, Dnmt2, shows sequence similarities but does not show DNA methylation catalyzing activity (Okano et al. 1998). Instead it was found to specifically methylate cytosine 38 of the aspartic acid tRNA (Goll et al. 2006). All DNA methyltransferases use S-adenosyl-methionine as a methyl-donor (Goll and Bestor 2005). The first eukaryotic DNA methyltransferase to be found in mammals was Dnmt1 (Bestor et al. 1988). It is known as the maintenance methyltransferase and restores DNA methylation during the S-phase of each cell replication cycle (Leonhardt et al. 1992; Lyko et al. 1999; Goll and Bestor 2005). It binds preferentially to hemimethylated DNA and catalyzes methylation of the unmethylated newly synthesized DNA strand (Yoder et al. 1997). Dnmt1 is crucial to maintain DNA methylation patterns of certain regions, such as imprinting control centers and repetitive sequences during pre- and postimplantation embryonic development (Li et al. 1992; Howell et al. 2001; Gaudet et al. 2004; Kurihara et al. 2008). In contrast, Dnmt3a and Dnmt3b are de novo methyltransferases that are required for the establishment of DNA methylation and, like Dnmt1, are also mandatory for successful embryonic development (Okano et al. 1999). Function of Dnmt3 depends on Dnmt3l, which itself has no enzymatic activity but interacts with Dnmt3a and Dnmt3b during imprint establishment (Bourc'his et al. 2001; Hata et al. 2002).

DNA methylation is an important and widely employed mechanism of epigenetic control. It has a central role in e.g. X-chromosome inactivation, retrotransposon repression, chromosome structure and gene silencing (Dean et al. 2005; Brockdorff 2011; Probst and Almouzni 2011). One of the best studied mechanisms of DNA methylation function is genomic imprinting, which is of special interest due to its heritability to the next generation (Reik and Walter 2001).

1.7.1 Genomic imprinting

For successful embryonic development a maternal and paternal copy of the genome is required. Manipulation of murine zygotes to generate embryos with either two maternal or two paternal pronuclei showed that uniparental diploid embryos are non-viable due to severe developmental failures (Barton et al. 1984; McGrath and Solter 1984; Surani et al. 1984). The requirement for both the maternal and the paternal genome is a result of asymmetric DNA methylation, causing parent-of-origin specific gene expression pattern at certain gene loci known as genomic imprinting (Li et al. 1993). Approximately 150 of these imprinted genes have been identified in mice and roughly half of them also in humans (www.mousebook.org/mousebook-catalogs/imprinting-resource and http://igc.otago.ac.nz/home.html). Most imprinted genes (>80%) are organized in clusters, which enclose a cis-acting imprinting control region (ICR) that contains a differentially methylated CpG island (Barlow 2011; Peters 2014). Methylation of an ICR is maintained throughout development and preserved in adult tissues.

There are several strategies how DNA methylation is involved in gene regulation of imprinted genes. Most ICRs are methylated on the maternal allele, e.g. the *Snrpn* and *Igf2r* clusters (Stoger et al. 1993; Shemer et al. 1997). Maternally methylated ICRs often enclose promoters of long non-coding RNAs (lncRNA), which silence protein-coding gene(s) in the cluster in cis by running antisense to it/them (Barlow 2011; Peters 2014). In the case of the *Snrpn* cluster the maternally methylated ICR inhibits the expression of *Snrpn* on the maternal allele (Shemer et al. 1997). On the paternal allele *Snrpn* is expressed, as well as the lncRNA *Ube3a-as* that in the brain extends into the *Ube3a* gene and inhibits *Ube3a* expression from the paternal allele (Rougeulle et al. 1998; Chamberlain and Brannan 2001; Horsthemke and Wagstaff 2008). *Ube3a* is expressed only from the maternal allele in the brain but biallelic in other tissues (Rougeulle et al. 1997; Vu and Hoffman 1997). In the case of the *Igf2r* locus, maternal methylation of an intronic DMR in the *Igf2r* gene inhibits the expression of the lncRNA *Airn* in mice (Wutz et al. 1997; Sleutels et al. 2002). This leads to maternal

expression of *Igf2r* in murine post-implantation embryos (Lerchner and Barlow 1997). *Airn* is expressed from the unmethylated paternal allele where its transcription overlaps and therefore interferes with *Igf2r* expression causing *Igf2r* silencing (Sleutels et al. 2002; Latos et al. 2012). In contrast to mice, the human *Igf2r* locus appears to be mainly biallelically expressed (Kalscheuer et al. 1993; Ogawa et al. 1993; Xu et al. 1993).

Paternal methylated ICRs are typically located in intergenic regions, e.g. the *Igf2*/*H19* cluster (Bartolomei et al. 1993; Peters 2014). The *Igf2*/*H19* cluster is an example of the insulator model for regulation of imprinted gene expression (Bell and Felsenfeld 2000; Hark et al. 2000; Nordin et al. 2014). The ICR is located between the two genes. It is methylated on the paternal allele resulting in maternal expression of *H19*. The ICR contains a binding site for the zinc-finger protein CCCTC-binding factor (CTCF). CTCF binds to the non-methylated maternal ICR, thereby blocking access of downstream enhancers to *Igf2* promotors and inhibiting transcription of *Igf2* from the maternal allele (Bell and Felsenfeld 2000; Hark et al. 2000). Genetic or epigenetic defects such as deletions or impaired methylation levels can cause disruption of imprinted gene expressions. This is related with diseases and imprinting disorders in humans, for instance Angelman and Prader-Willi syndromes (*SNRPN* cluster) or Beckwith-Wiedemann and Silver-Russel syndromes (*IGF2/H19* cluster; Horsthemke and Wagstaff 2008; Eggermann 2009).

1.7.2 Epigenetic reprogramming of the embryo

Throughout mammalian development two major waves of epigenetic reprogramming occur (Dean et al. 2003). The first takes place in primordial germ cells, where DNA methylation of imprints is erased upon entry to the genital ridge and then reset during germ cell development (Hajkova et al. 2002; Lee et al. 2002). The reacquisition of imprints is mediated by Dnmt3a in dependence of Dnmt3l in growing germ cells (Figure 3; Bourc'his et al. 2001; Hata et al. 2002; Kaneda et al. 2004). In males imprints are set in the genital ridge during late fetal development (Davis et al. 2000; Ueda et al. 2000). In females imprints are established postnatally in a time-specific manner for each gene in the growing oocyte (Obata and Kono 2002; Lucifero et al. 2004). Especially in the oocyte the imprint setting seems to be highly dependent on Dnmt3l (Kobayashi et al. 2012).

The second wave of epigenetic reprogramming is during preimplantation development and involves large scale demethylation during embryonic genome activation from which imprinted genes need to be protected (Figure 3; Messerschmidt 2012). The oocyte and sperm

genome are very distinct, which requires different approaches to process the DNA after fertilization in order to activate the zygotic genome. The oocyte only completes meiosis after fertilization, whereas the sperm has a haploid genome packed around protamines. So, upon fertilization the sperm genome has to undergo nuclear envelope breakdown, replacement of protamines by histones and chromatin decondensation to form the male pronucleus (Wright 1999). Protamine replacement is directly followed by chromatin decondensation and completed within the first hour after fertilization (Santos et al. 2002).

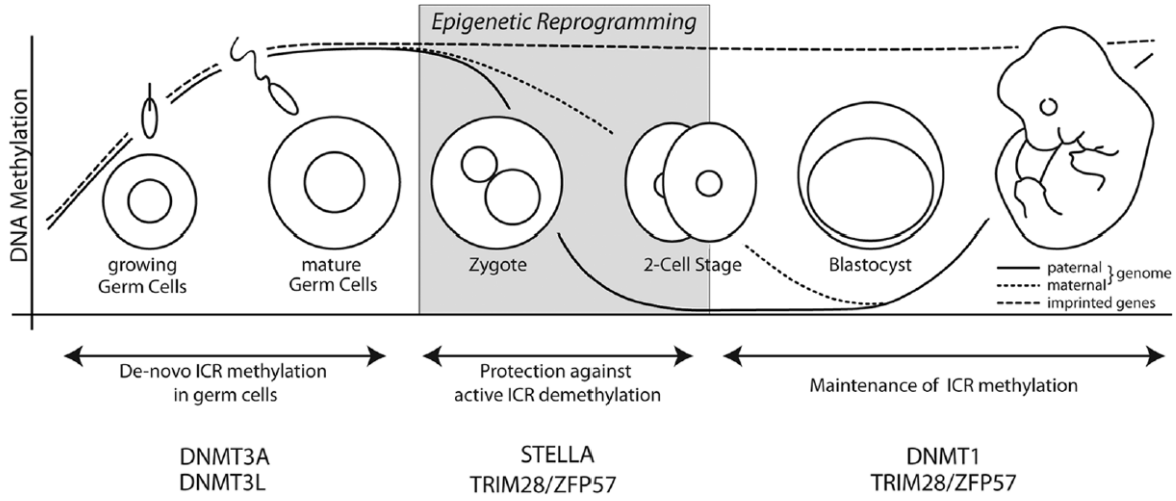

Figure 3: DNA methylation levels throughout mammalian development and protection of DNA methylation of imprinted genes. DNA methylation levels rise in growing germ cells until they reach a peak in mature germ cells. In this phase Dnmt3a and Dnmt3l set genomic imprints by de novo methylation of ICRs. After fertilization major epigenetic reprogramming takes place, in which first the paternal genome is actively demethylated and then the maternal genome is passively demethylated. In the blastocyst, both parental genomes of the cells in the inner cell mass undergo de novo methylation. ICRs have to be protected and maintained during these demethylation and remethylation events. This is mediated by Stella (Dppa3), Trim28, Zfp57 and Dnmt1. Figure from Messerschmidt 2012.

While the paternal genome is highly methylated prior to fertilization (89%), the maternal genome is undermethylated (40%; Monk et al. 1987; Kobayashi et al. 2012). Further processing of the parental genomes in the zygote then involves global demethylation. Maybe due to the different levels of methylation, demethylation seems to be differentially regulated for the maternal and paternal genome (Mayer et al. 2000; Oswald et al. 2000; Santos et al. 2002). The exact mechanisms are not completely clear but it is thought that first the paternal genome undergoes progressive demethylation. This is completed within 4-8 hours after fertilization before the first DNA replication (Mayer et al. 2000; Oswald et al. 2000; Santos et al. 2002). It is therefore commonly known as active demethylation. *Tet3* (Ten-eleven translocation protein 3) is an ME gene that has been associated with this active demethylation

in zygotes (Gu et al. 2011). The Tet3 protein is enriched in the male pronucleus where it oxidates 5mC to 5-hydroxymethylcytosine (5hmC), which is thought to be the first step in active demethylation (Gu et al. 2011; Wossidlo et al. 2011; Santos et al. 2013).

The maternal genome was thought to be protected from active demethylation and mainly passively demethylated through exclusion of Dnmt1 from the nucleus during cell replication (Carlson et al. 1992; Rougier et al. 1998; Santos et al. 2002). Processing of the maternal genome takes until the morula stage. This is longer than active demethylation causing a delay in demethylation of the maternal genome in comparison to the paternal genome (Santos et al. 2002; Dean et al. 2003). However, a recent study showed that also the maternal genome is subject to Tet3 oxidation suggesting multiple demethylation pathways in the embryo that might function redundantly (Peat et al. 2014). After completion of global demethylation, massive de novo methylation occurs in the inner cell mass but not in the trophectoderm of the blastocyst (Santos et al. 2002).

1.7.3 Imprint maintenance in preimplantation embryos

As described above, imprinted genes must be protected from demethylation during epigenetic reprogramming (Figure 3). There are several proteins that are encoded by ME genes, which are known to be involved in this imprint maintenance during preimplantation development (Messerschmidt 2012). *Dppa3* (Developmental pluripotency-associated 3 protein, also known as *Pgc7* or *Stella*) was the first identified ME gene encoding a protein with an imprint protection function (Payer et al. 2003; Nakamura et al. 2007). It prevents demethylation at certain imprinted regions, e.g. *Snrpn* and *Peg3* (Nakamura et al. 2007). Trim28 (tripartite motif-containing 28; previously named Kap1 or Tif1β) is a central scaffolding component of an epigenetic modifying corepressor complex. It binds for instance the H3K9me3-catalizing histone methyltransferase Setdb1, which in turn recruits the heterochromatin protein Hp1 that is involved in epigenetic silencing (Schultz 2002). This heterochromatin-inducing complex binds DNA specifically through interaction of Trim28 with Krüppel-associated box-containing zinc-finger proteins (KRAB-ZFPs) such as Zfp57 (Li et al. 2008b). *Trim28* and *Zfp57* are both ME genes that are essential for imprint maintenance during preimplantation development (Li et al. 2008b; Messerschmidt et al. 2012). They encode proteins that bind selectively to all H3K9 and DNA methylation bearing ICRs in embryonic stem cells and conserve the imprints through recruitment of Setb1 and Hp1 to methylated DNA (Quenneville et al. 2011). Zfp57 recognizes ICRs and several other locis that carry Zfp57-dependent methylation in ESCs through a hexanucleotide motif that is found in all murine ICRs

(Quenneville et al. 2011). This hexanucleotide motif (TGCCGC) contains a CpG and Zfp57 binds more efficiently to the sequence when it is methylated, explaining the parent-of-origin specific sequence recognition by Zfp57. Trim28/Zfp57 was also found to be associated with DNA methyltransferases Dnmt1, Dnmt3a and Dnmt3b (Quenneville et al. 2011). *Dnmt1* is another ME gene, which is not only important for processing of the maternal genome after methylation but also required for imprint maintenance (Howell et al. 2001; Borowczyk et al. 2009). In oocytes both a truncated, oocyte specific variant (*Dnmt1o*) and, although to a far lesser extent, the somatic variant (*Dnmt1s*) are expressed (Mertineit et al. 1998; Kurihara et al. 2008). Dnmt1o and Dnmt1s proteins are present at all times during oocyte growth, maturation and preimplantation development and protect methylation and ICRs (Cirio et al. 2008; Hirasawa et al. 2008; Kurihara et al. 2008). Since at the same time exclusion of Dnmt1 is supposed to cause passive demethylation of the maternal genome, a scenario is assumed that in the early embryo Dnmt1 binds specifically to imprinted gene loci enabling the majority of the genome to be demethylated. Indeed a region conserved in mammals in the N-terminus of the Dnmt1 protein has been found that seems to be associated with binding to specific regions like ICRs and some repetitive sequences (Borowczyk et al. 2009).

Correct imprint establishment in the oocyte and imprint maintenance during epigenetic reprogramming are of vital importance for oocyte quality and developmental potential. It is not known if preovulatory aging might affect imprint setting and protection in oocytes.

1.8 Aim

Hardly anything is known on the molecular mechanisms that occur in the preovulatory-aged oocyte. Therefore, the aim of the present study was to investigate the effects of preovulatory aging on several aspects of RNA dynamics and the developmental competence of preimplantation embryos. For this, a previously described in vivo mouse model was employed in which ovulation is delayed using the GnRH antagonist cetrorelix (Bittner et al. 2011).

First, RNA dynamics in preovulatory aged oocytes were assessed on different levels using several methods: 1) as indicator of transcriptional silencing and stability of the oocyte genome (Kageyama et al. 2007) the repressive histone modification mark H3K9me3 was assessed by immunofluorescent analysis. 2) The germ cell-specific RNA-binding protein Ybx2 is one of the most abundant proteins in the growing oocyte and required for RNA storage and recruitment of transcripts for protein translation (Yu et al. 2002; Medvedev et al. 2011). Because it is essential for oocyte developmental potential, it was analyzed on transcript and

protein level by qRT-PCR and immunofluorescent analysis. 3) ME-genes are of crucial importance for oocyte quality since they are needed for regulation of early embryonic development (Li et al. 2010). Transcript levels of selected ME-genes were determined by qRT-PCR. Considering that poly(A) tail length is an important regulator of translation efficiency in the oocyte (Kang and Han 2011) changes in poly(A) tail length after preovulatory aging of the investigated ME genes were analyzed by priming cDNA conversion with random or oligo(dT) primers. RNA dynamics of ME genes in oocytes aged in vivo were compared to preovulatory-aged oocytes grown and maturated in vitro in a follicle culture system.

In postovulatory-aged *Xenopus* oocytes, it is known that poly(A) tail length is affected (Kosubek et al. 2010). To determine if this is also true for mammals, it was aimed to establish a poly(A) RNA sequencing method to investigate poly(A) tail length after postovulatory aging on a transcriptome-wide level in mouse oocytes.

Possible effects on RNA dynamics in preovulatory-aged oocytes are likely to affect the developmental potential of oocytes. It has been previously shown that preovulatory aging in the cetrorelix mouse model impairs postimplantation development (Bittner et al. 2011). The current study investigated the developmental potential of preovulatory-aged oocytes in preimplantation embryos at several stages: 1) Fertilization success after preovulatory aging was determined by assessing the 2-cell rate after natural mating. 2) For embryonic development, the onset of transcription in the course of embryonic genome activation is essential (Schultz 2002). The first major wave of embryonic genome activation at the 2-cell stage was analyzed by determining BrUTP incorporation into nascent RNA. 3) Early embryonic development is dominated by the oocyte-to-embryo transition which involves extensive epigenetic reprogramming. During this phase, DNA methylation levels of imprinted genes need to be maintained (Messerschmidt 2012). The present study investigated DNA methylation levels of 3 imprinted genes (*H19, Snrpn, Igf2r*) and one unmethylated control gene (*Pou5f1*) at the 8-cell stage of preimplantation development by deep amplicon bisulfite sequencing of single embryos after preovulatory aging.

This study was the first, to address molecular processes in the preovulatory-aged oocyte in such detail and to find mechanisms that might give possible explanations for the low fertilization rates and impaired embryonic development previously described in the present mouse model or other animal models (Smits et al. 1995; Bittner et al. 2011).

2 Materials and Methods

2.1 Ethics statement

This study was conducted according to the recommendations stated in the Guide for the Care and Use of Laboratory Animals of the German government. The investigations were authorized by the Committee on the Ethics of Animal Experiments of the responsible authorities (*Landesamt für Natur, Umwelt und Verbraucherschutz*, LANUV AZ 84-02.04.2011. A374).

2.2 Materials

2.2.1 Chemicals and Substances

4′,6-Diamidin-2-phenylindol (DAPI; Sigma Aldrich)

5-Bromouridine-5'-triphosphate (BrUTP; Sigma Aldrich)

DABCO (Sigma Aldrich)

Fluoresceinisothyiocyanate (FITC; Sigma Aldrich)

Forene (Isoflurane; Abbvie)

Oligo$(dT)_{25}$ Dynabeads (Life Technologies)

Poly-L-Lysin Hydrobromide (Sigma Aldrich)

Triton X-100 (AppliChem)

6xMassRuler DNA Loading Dye (Thermo Scientific)

Vectashield Mounting Medium with DAPI (Vector Laboratories)

All other chemicals not mentioned here were obtained from Applichem, Life Technologies, Merck, Peqlab Biotechnologie and Sigma Aldrich in pro analysis quality.

2.2.2 Buffers and solutions

Purchased buffers and solutions:

1x Dulbecco's Phosphate-Buffered Saline (DPBS; Life Technologies)

10x Tris-acetate-EDTA (TAE; Applichem)

Prepared buffers:

All buffers were mixed using double distilled water, unless stated otherwise.

Blocking buffer for immunofluorescent analysis of H3K9me3 and BrUTP:

Bovine serum albumin (BSA)	1.0	% (w/v)
Milk powder	0.2	% (w/v)
Norm goat serum	2.0	% (v/v)
Glycine	0.1	M
Triton X-100	10.0	% (v/v)

Chemicals were filled up with DPBS and sterilized by filtration.

Blocking buffer for immunofluorescent analysis of Ybx2:

Tween 20	0.01	% (v/v)
BSA	0.10	% (v/v)

Chemicals were filled up with DPBS and sterilized by filtration.

FITC solution:

FITC	10	mg
C_3H_7NO	1	ml

Guanidine thiocyanate (GTC) buffer:

$C_2H_6N_4S$	4	M
$Na_3C_6H_5O_7$	25	mM
C_2H_6OS	2	% (v/v)

pH7.1

Sodium carbonate buffer:

Na_2CO_3	160	mM
$NaHCO_3$	333	mM

pH9.5

Paraformaldehyde (PFA) 4%:

PFA	8	g
DPBS	200	ml

PFA was dissolved in approximately 170 ml hot DPBS (80 °C). The pH was set with NaOH to 7.3 and the solution filled up with DPBS to 200 ml. Aliquots of 50 µL were stored at -20 °C.

Physiological buffer:

CH_3CO_2K	100.0	mM
KCl	30.0	mM
$MgCl_2$	1.0	mM
Na_2HPO_4 ($7H_2O$)	10.0	mM
ATP	1.0	mM
DTT	1.0	mM
PMSF	0.2	mM
RNasin	40.0	U/ml

Physiological buffer with BrUTP:

Adenosine triphosphate (ATP)	2.0	mM
Guanosine-5'-triphosphate (GTP)	0.4	mM
Cytosinetriphosphate (CTP)	0.4	mM
BrUTP	0.4	mM
$MgCl_2$	2.0	mM

All chemicals were dissolved in physiological buffer.

20x Saline sodium citrate (SSC) buffer:

NaCl	3.0	M
$Na_3C_6H_5O_7$	0.3	M

pH 7.3

2.2.3 Hormones

PMSG (Intergonan; MSD)

hCG (Ovogest; MSD)

Cetrorelix (Cetrotide; Merck-Serono)

2.2.4 Media

For isolation of oocytes and 2-cell embryos the HEPES buffered M2-Medium (Sigma Aldrich) was used. Embryos were cultivated to the 8-cell stage in KSOM medium (GlobalStem).

2.2.5 Antibodies

Monoclonal mouse anti-BrU (1:50; Roche)

Polyclonal rabbit anti-H3K9me3 (1:40; Epigentek)

Polyclonal goat anti-Ybx2 (1:300; Santa Cruz)

Polyclonal rabbit anti-goat IgG-Cy3 (1:200; Sigma Aldrich)

Monoclonal goat anti-rabbit IgG-TRITC (1:40; Epigentek)

2.2.6 Oligonucleotides, UPL-Probes, Taqman assays and DNA marker

Random hexamer primers and oligo$(dT)_{16}$ primers for reverse transcription were obtained from Life Technologies. Oligonucleotides and UPL-Probes for qRT-PCR analysis were designed using the Universal ProbeLibrary Assay Design Center (Roche; https://lifescience.roche.com/webapp/wcs/stores/servlet/CategoryDisplay?tab=Assay+Design+Center&identifier=Universal+Probe+Library&langId=-1). Oligonucleotides were obtained from Biomers and UPL-Probes from Roche. Pre-designed Taqman assays for qRT-PCR analysis were obtained from Life Technologies. All assays are listed in Supplementary Table S1.

For the ePAT analysis an anchor primer containing a poly(A) stretch at the 3'end and gene specific forward primers were ordered from Eurofins. Oligonucleotide sequences are listed in Supplementary Table S2.

Oligonucleotide sequences for Sanger or Bisulfite Sequencing were previously described in (El Hajj et al. 2011) and ordered from Metabion (Supplementary Table S3).

The pUC19 DNA/MspI (HpaII) Marker (Thermo Scientific) was used for size determination of the PCR product length by agarose gel electrophoresis. This marker has a range from 34 bp to 501 bp.

2.2.7 Enzymes

DNase I (Qiagen)

ExoSAP-IT (Affymetrix)

HotStarTaq DNA Polymerase (Qiagen)

Hyaluronidase (Sigma Aldrich)

Klenow Fragment (New England Biolabs)

Pronase E (Sigma Aldrich)

RiboLock RNase Inhibitor (Thermo Scientific)

2.2.8 Kits

Agencourt AMPure XP System (Beckman Coulter)

Agilent DNA 1000 Kit (Agilent Technologies)

Agilent High Sensitivity DNA Kit (Agilent Technologies)

Agilent RNA 6000 Pico Kit (Agilent Technologies)

Arcturus Pico Pure RNA Isolation Kit (Life Technologies)

BigDyeTerminator v1.1 Cycle Sequencing Kit (Life Technologies)

EZ DNA Methylation-Direct Kit (Zymo Research)

GeneAmp RNA PCR Core Kit (Life Technologies)

Multiplex PCR Kit (Qiagen)

Ovation Single Cell RNA-Seq System (NuGEN)

QiaShredder (Qiagen)

ReadyMix Taq PCR Reaction Mix (Sigma Aldrich)

RNeasy MinElute Clean up Kit (Qiagen)

Superscript III Reverse Transkriptase (Life Technologies)

2.2.9 Mouse strains

C57Bl/6J inbred female mice (*Mus musculus*) were used for all experiments, except for the in vitro follicle culture. The benefit of using an inbred strain is the homogeneous genetic background. This should provide low genetic variability within one experimental group and therefore lower the amount of replicates (animals) needed. The disadvantage is the inbred depression, which reduces fertility of animals from the C57Bl/6J strain. For in vitro follicle culture C57Bl/6J mice were therefore mated with animals from the CBA inbred strain and follicles were isolated from the hybrid C57Bl/6J x CBA females obtained out of this breeding.

For the generation of 2-cell embryos to study BrUTP incorporation, C57Bl/6J female mice were mated with C57Bl/6J x CBA hybrid males to increase the reproductive success. DNA-methylation analysis was carried out with 8-cell embryos derived from C57Bl/6J female mice mated with CAST/EiJ male mice. CAST/EiJ (*M. m. castaneous*) is also an inbred strain but it is not as closely related to C57Bl/6J as the CBA strain. Therefore, heterozygous single nucleotide polymorphisms (SNPs) can be found in the offspring allowing the differentiation between maternal and paternal allele during DNA-methylation analysis.

All strains were bred in the Central Animal Facility of the University Hospital Essen. Founding animals of the C57Bl/6J and CBA strains were obtained from Harlan Laboratories. CAST/EiJ breeding founder pairs were kindly provided by Prof. Ulrich Zechner, University of Mainz, Germany. All mice were housed under standard conditions (food and water ad libitum, 12:12 h dark-light cycles). Cages were supplied with bedding and nesting material. Breeding pairs additionally obtained a house of red acrylic glass.

2.3 Methods

2.3.1 Generation and collection of preovulatory-aged oocytes

2.3.1.1 In vivo maturation and preovulatory aging of oocytes

For in vivo growth and maturation of MII oocytes, female 4-6 weeks old C57Bl/6J mice were stimulated hormonally to induce superovulation (Figure 4A). On day 0 all mice were injected intra peritoneal (i.p.) with 10 IU pregnant mare serum gonadotropin (PMSG) to stimulate follicle growth and maturation. PMSG is a gonadotropic hormone, produced by pregnant mares during gestation and shows similar activity as FSH in mice. Intrinsic hormones were suppressed by daily subcutaneous (s.c.) application of 50 mg cetrorelix during the phase of oocyte growth and maturation starting from day 0. For the collection of control oocytes 10 IU

human chorionic gonadotropin (hCG) was applied i.p. 48 h later at day 2 of stimulation to induce ovulation. These 48 h represent the intrinsic cycle of the mouse. Human CG is produced during human pregnancy in the placenta and mimics the effect of LH by inducing ovulation.

Due to inhibition of the intrinsic hormone levels with cetrorelix it was possible to delay ovulation and age oocytes for 3 or 4 days (d) in vivo. Ovulation of preovulatory-aged oocytes (PreOA) was induced at day 5 or 6. To ensure that PMSG levels stayed high during the course of aging, PMSG was applied every 2 d. Fifteen hours after hCG injection on day 3 (control), 6 or 7 (PreOA), mice were anesthetized with 1-2 ml isoflurane in a bell jar for 30-60 seconds (s) and then sacrificed by cervical dislocation. Mice were dissected to isolate the female reproductive tract, including the uterus, fallopian tubes and ovaries. These organs were then further dissected using a binocular, to collect the oviduct, which was transferred into a 25 µl drop of M2-medium. The oviductal ampulla was then torn using forceps, releasing the cumulus-oocytes-complex (COC). To dissociate the cumulus cells from the oocytes, the COC was transferred into another 25 µl drop of M2-medium, which was enriched with 2 µl (10 mg/ml) hyaluronidase. The oocytes were afterwards washed 3-4 times in M2-medium to remove all cumulus cells and stored at -80 °C until further use.

2.3.1.2 In vitro growth and preovulatory aging of oocytes

The follicle culture system used for in vitro preovulatory aging (Figure 4B) was established in the Department of Gene Technology and Microbiology at the University of Bielefeld. Oocytes were grown, maturated and preovulatory-aged for 3 or 4 d in vitro by Dr. Tom Trapphoff and Martyna Heiligentag under the supervision of Prof. Ursula Eichenlaub-Ritter and send to our laboratory for further analysis. The follicle culture system has been described in Traphoff et al. (2010), Demant et al. (2012) and Wigglesworth et al. (2012). Briefly, preantral follicles were isolated from female F1 hybrid C57Bl/6J x CBA/Ca mice and grown and maturated in vitro. Follicle growth was stimulated with recombinant FSH (rFSH) and recombinant LH (rLH) for 12 d. Then ovulation was induced with recombinant epidermal growth factor (rEGF) and recombinant hCG (rhCG). Control MII oocytes were collected 18 h later on day 13. To age oocytes preovulatory, the in vitro culture was prolonged for 3 or 4 d before application of rEGF and rhCG.

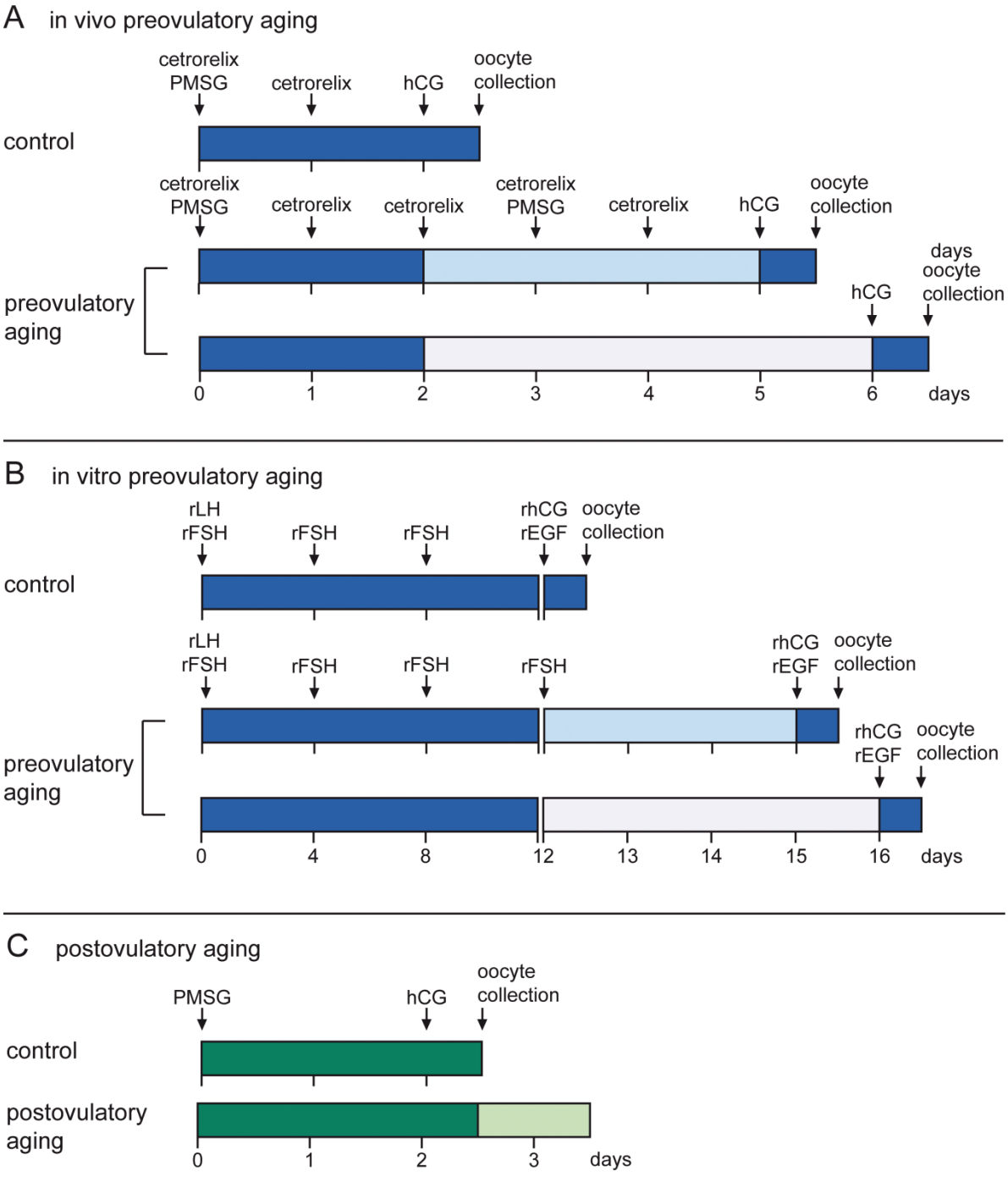

Figure 4: Treatment scheme of the mouse models for preovulatory oocyte aging in vivo (A) and in vitro (B) and postovulatory aging (C). A) Oocyte growth in vivo was induced by application of PMSG at day 0 and ovulation was induced at day 2 by hCG injection. Oocytes were retrieved from the oviductal ampullae the next morning. Delaying ovulation with the GnRH antagonist cetrorelix caused in vivo preovulatory aging for either 3 or 4 days. **B)** In vitro growth and preovulatory-aging was performed using a follicle culture system. Oocyte growth was stimulated by application of rLH and rFSH and ovulation was induced after 12 days with rhCG and rEGF. Oocytes were collected 18 h later. Delaying ovulation for 3 or 4 days caused preovulatory aging of oocytes in vitro. **C)** Growth and ovulation of postovulatory-aged oocytes was performed as described in **A**. After oocyte collection, oocytes were incubated in M2-medium for an extra day, causing postovulatory aging. This figure was modified from Dankert et al. (2014).

2.3.2 Generation and collection of postovulatory-aged in vivo-maturated oocytes

For the generation of postovulatory-aged oocytes (PostOA), C57Bl/6J female mice were stimulated hormonally to induce superovulation, similar as described above (2.3.1.1). Mice received PMSG to stimulate follicle growth and oocyte maturation. Ovulation was induced by hCG application 48 h later. MII oocytes were collected 15 h after hCG injection from the oviductal ampullae as described above. After removal of the cumulus cells, oocytes were either frozen at -80 °C (controls) or aged for 24 h in 100 µl M2-medium covered by mineral oil at 37 °C and 5% CO_2 (PostOA). After 24 h, aged oocytes were also stored at -80 °C until further use.

2.3.3 Generation and collection of embryos derived from preovulatory-aged oocytes

To generate embryos from control and preovulatory-aged oocytes, female C57Bl/6J mice (> 8 weeks) were stimulated hormonally (2.3.1.1). After induction of ovulation by application of hCG females were mated over night with either C57Bl/6J x CBA hybrid males or CAST/EiJ males. The next morning males and females were separated and females were checked for the presence of a vaginal plug. Twenty-four hours later plugged females were sacrificed by cervical dislocation and the oviducts were isolated. Two-cell embryos were collected in M2-medium by flushing the oviduct with DPBS using a syringe. After subsequent washing of the embryos in M2-medium, the 2-cell embryos were either used immediately for immunohistochemical analyses or further cultured to the 8-cell stage in 100 µl KSOM under mineral oil at 37 °C and 5% CO2 for 24 h. Eight-cell embryos were frozen individually in 10 µl DPBS at -80 °C.

2.3.4 RNA isolation from oocytes

Total RNA was isolated from oocytes using the Arcturus PicoPure RNA Isolation Kit according to manufacturer instructions with small adaptations. For homogenization of samples, cell mixtures were transferred into a QIAshredder column and centrifuged at full speed (20108xg) for 5 min. Any residual DNA, which might interfere with later analysis was removed by DNase I treatment according to the guidelines of the kit. RNA was eluted in 14 µL elution buffer, which was applied directly to the membrane. Elution buffer was incubated for 1 min followed by two centrifugation steps; 1 min at 8000xg and 1 min at 16,000xg. RNA was stored at -80 °C until further use.

2.3.5 RNA expression analysis

To analyze RNA expression and relative polyadenylation of transcripts of genes in preovulatory-aged and control oocytes, RNA from pooled oocytes was reverse transcribed (RT) into cDNA and analyzed by quantitative real-time polymerase chain reaction (qPCR). For all experimental groups 3 samples of 20 pooled oocytes each were analyzed. For reverse transcription of total RNA or poly(A) mRNA in oocytes, cDNA was either primed with random hexamers or with oligo$(dT)_{16}$primers.

2.3.5.1 Reverse transcription of RNA

For the reverse transcription of oocyte RNA into cDNA, the GeneAmp RNA PCR Core Kit was used. Reactions were prepared as shown in Table 1. To control for successful DNA digestion during RNA preparation in subsequent PCR reactions a -RT control reaction lacking the reverse transcriptase was included. Samples were incubated in a thermocycler for 10 min at 21 °C followed by cDNA synthesis for 30 min at 42 °C and reverse transcriptase inhibition for 5 min at 99 °C.

Table 1: Reverse transcription reaction.

Sample	**+RT**	**-RT**
Total RNA	9.00 µl	2.25 µl
$MgCl_2$ (25 mM)	8.20 µl	2.05 µl
10x PCR Buffer II	5.00 µl	1.25 µl
dGTP	5.00 µl	1.25 µl
dATP	5.00 µl	1.25 µl
dTTP	5.00 µl	1.25 µl
dCTP	5.00 µl	1.25 µl
Primer (10 µM)	2.50 µl	0.63 µl
RNase inhibitor (20 U/µl)	2.50 µl	0.63 µl
MuLV Reverse Transcriptase (50 U/µl)	2.50 µl	-
RNase free water	add to 50 µl	add to 12.5 µl

2.3.5.2 Quantitative real-time PCR

Real-time qPCR is a PCR method used to quantify specific DNA elements amplified during PCR by analyzing fluorescent intensity during each amplification cycle. Here, the technology was utilized for relative quantification of RNA expression by amplification of cDNA after reverse transcription. Samples were amplified and quantified on the LightCycler 480 II

(Roche) using the assays designed by the Universal Probe Library (UPL) design center. The UPL probes consist of a short sequence (8-9 bp) labeled at the 5' end with the fluorophore FAM (fluorescein amidite) and at the 3' end with a dark quencher dye. The UPL probe binds to the amplified sequence in between the primer pair. During amplification, the probe is digested by the 5'-3'-exonuclease activity of the DNA polymerase resulting in the separation of the quencher and the FAM dye. As a result of amplification, the quencher will no longer suppress FAM fluorescence, which will be measured by the LightCycler in each amplification cycle. The intensity of fluorescence is proportional to target amplification.

An internal reference gene, also known as housekeeping gene, is commonly used for quantitative analysis of relative RNA-levels. It is unclear whether murine housekeeping genes are affected by preovulatory aging. A previous study investigated several housekeeping genes, including *GAPDH*, *ACTB*, Histone *H2A* and *18S* rRNA in bovine oocytes, during development (Robert et al. 2002). They showed that housekeeping genes are affected by the general maternal RNA-decay seen during oocyte maturation and early embryonic development. It is likely that a similar effect might be happening in the mouse oocyte. Therefore, *Luciferase* mRNA was spiked into the oocyte pools before RNA isolation (1 pg/oocyte), to serve as an external reference for analysis of candidate maternal effect (ME) genes. Investigation of *Ybx2* transcript levels was normalized using a *Luciferase* standard curve.

UPL assays were used for the investigation of *Ybx2*, 7 ME genes (*Brg1*, *Tet3*, *Trim28*, *Zfp57*, *Nlrp14*, *Pou5f1*, *Zar1*) and *Luciferase*. *Dnmt1*, *Nlrp2* and *Nlrp5* were analyzed using pre-designed Taqman assays, which are based on the same principle as the UPL asssays and include a primer pair and a hydrolysis probe. All primers and UPL-probes are summarized in Supplementary Table S1.

Table 2 shows the preparation of a 20 µL qRT-PCR reaction mix using either UPL or Taqman assays. All samples were analyzed in technical triplicates, a sample containing water instead of cDNA and a sample containing the –RT control were used as negative controls.

Table 2: qRT-PCR reaction.

Assay	UPL	Taqman
cDNA	1.0 µl	1.0 µl
2x Light Cycler Master Mix	10.0 µl	10.00 µl
Fwd Primer (10 µM)	0.8 µl	-
Rev Primer (10 µM)	0.8 µl	-
UPL Probe	1.6 µl	-
Taqman Assay	-	1.0 µl
Water	5.8 µl	9.0 µl

The following PCR conditions were applied:

95 °C	10 min	
95 °C	10 s	50 cycles
60 °C	30 s	
72 °C	1 s	

The fold change of each ME gene in preovulatory-aged oocytes compared to control oocytes was calculated for both random-primed and oligo(dT)-primed cDNA using the Ct-value and the $2^{-\Delta\Delta Ct}$ method. The Ct-value is the cycle number where the fluorescent signal intensity starts to rise exponentially. To eliminate possible outliers, the median Ct of each triplicate was taken for analysis. First, the Ct-value of both aged and control oocytes for each ME-gene (target) had to be normalized against *Luciferase* expression (reference) for each of the 3 biological replicates (oocyte pools) per condition:

$$\Delta Ct = medianCt(Target) - medianCt(Reference)$$

To calculate the difference in expression between aged and control oocytes, the mean ΔCt of the 3 control replicates was calculated and then subtracted for each single ΔCt-value:

$$\Delta\Delta Ct = \Delta Ct - mean\Delta Ct(Control)$$

Then, the fold change was calculated:

$$Fold\ change = 2^{-\Delta\Delta Ct}$$

Last, the fold change was normalized against controls:

$$Normalized\ Fold\ change = \frac{Fold\ change}{mean\ Fold\ change(Control)}$$

The mean of the normalized fold change of preovulatory-aged oocytes was compared to control oocytes after random hexamer priming to determine possible effects of aging on total transcript levels. A change in poly(A) content was defined as a significant difference in fold changes between random hexamer-primed and oligo(dT)-primed cDNA.

2.3.6 Agarose gel electrophoresis

Agarose gel electrophoresis was used to determine the size of DNA fragments. During gel electrophoresis, DNA samples are added to an agarose gel to which an electric field is applied. The negatively charged nucleic acids will migrate through the gel towards the anode and are separated by size (smaller fragments move faster than larger fragments). A DNA marker with DNA fragments of known size was used as reference for size determination. 1-2% agarose gels were prepared in 1x TAE buffer and enriched with 4 µg/ml ethidium bromide (EtBr). EtBr intercalates into DNA and can be visualized under ultra violet (UV) light of 302 nm. DNA fragments were transferred to the gel with 1x Loading Dye. The pUC19 DNA/MspI (HpaII) Marker was used as reference for size determination. Electrophoresis was carried out at 100-120 V.

2.3.7 Immunofluorescent analysis of oocytes and embryos

Immunofluorescent (IF) analysis was used to analyze the histone modification H3K9 trimethylation (H3K9me3) and Ybx2 protein expression of in vivo preovulatory-aged and control oocytes. Also, BrUTP incorporation in two-cell embryos derived from either in vivo preovulatory-aged or control oocytes was detected using IF. This technique uses the antigene-antibody binding affinity to visualize epitopes in a cell or tissue. A primary antibody specific for an antigen, in this case the histone methylation H3K9me3 or the protein Ybx2, first binds to the epitope. To visualize this bond a secondary antibody that is specific for the primary antibody and carries a fluorophore is added. The secondary antibody has to be raised against the IgG of the host animal species in which the primary antibody was raised. The fluorescent label of the secondary antibody can be detected using a light microscope. The protocols for detection of H3K9me3 and Ybx2 expression in embryos were established by the group of Prof. Ursula Eichenlaub-Ritter.

2.3.7.1 Coating of microscope slides with poly-L-lysin

For analysis, all oocytes were applied to poly-L-lysin coated microscope slides after the IF reaction. Poly-L-lysin is positively charged and surfaces covered with it support binding of the mainly negatively charged cell membranes. This allows binding of oocytes to the microscope slide. To coat the slides with poly-L-lysin, first a ring of vulcanized rubber was applied to the slides. After the ring had dried a poly-L-lysin solution in water (0.1 mg/mL) was applied to the surface of the slide within the ring. After drying of the poly-L-lysin solution the slides were rinsed with demineralized water and dried again. The oocytes were placed inside the ring after the IF reaction, which protected them from being crushed underneath the cover slip. After mounting, the rim of the cover slip was fixed using nail polish.

2.3.7.2 Ybx2 expression in oocytes

Oocytes were isolated as described previously (2.3.1.1) and placed into a Terasaki plate. Each well contained 13 µl of a buffer, solution or antibody. Oocytes were transferred from one well to the next. All following steps occurred at room temperature. The first well contained 4% PFA in DPBS in which the oocytes were fixed for 1 h. Afterwards, the plasma membrane was permeabilized in 0.5% Triton X-100 and oocyte were then transferred into a first well of blocking buffer to wash the oocytes briefly. In a second well of blocking buffer, blocking occurred during a 30 min incubation period. Oocytes were transferred into a well containing the primary antibody goat anti-Ybx2 in blocking buffer (1:300) and incubated for 1 h. Then oocytes were washed 4 times in subsequent wells in blocking buffer for 10 min each and transferred into the secondary antibody rabbit anti-goat IgG-Cy3 in blocking buffer (1:200) for 1 h. Oocytes were washed again 4 times in blocking buffer for 10 min each and transferred into the ring on the poly-L-lysin coated slides. Oocytes were mounted with Vectashield containing DAPI, which is a fluorescent stain that intercalates into the DNA and therefore visualizes cell nuclei.

2.3.7.3 H3K9me3 expression in oocytes

The protocol of H3K9me3 IF was very similar to Ybx2 analysis. The beginning of the protocol was different because the zona pellucida needed to be removed to allow better penetration of the antibody into the cell. After removal of the cumulus cells with hyaluronidase the zona was digested in pronase at 37 °C under constant visual monitoring. After the zona had dissolved, the oocytes were washed in two drops of M2-medium and then fixed in PFA, permeabilized in Triton X-100, and blocked in blocking buffer for 30 min. Oocytes were then transferred into the primary antibody rabbit anti-H3K9me3 in DPBS (1:40)

and incubated for 1 h. After a brief washing and blocking for 30 min in two subsequent wells of blocking buffer, oocytes were incubated for 1 h in the secondary antibody goat anti-rabbit IgG-TRITC in DPBS (1:40). Oocytes were washed twice shortly in blocking buffer and then transferred into DAPI for 15 min. Last, the oocytes were transferred into blocking buffer again, transferred into the ring on the poly-L-lysin coated microscope slides and mounted with DABCO.

2.3.7.4 BrUTP incorporation in two-cell embryos

To assess the embryonic genome activation at the two-cell stage of embryos derived from either preovulatory-aged or control oocytes, incorporation of bromouridine-triphosphate (BrUTP) into the cell nuclei was detected using IF. The protocol was adapted from Aoki et al. 1997 by Dr. Debora Dankert at the Institute of Anatomy, University Hospital Essen. Embryos were incubated in BrUTP, which is a nucleotide analogue that is incorporated into the RNA during transcription (Jackson et al. 1993). There it is converted into Bromouridine (BrU), which can be detected with an antibody by IF. Instead of an indirect visualization using a secondary antibody, the primary antibody was directly labeled with a fluorescent dye (FITC).

In detail, after flushing the two-cell embryos out of the fallopian tube, they were transferred into a Terasaki plate and washed in DPBS. The membrane was permeabilized for 1-2 min in 0.05% Triton X-100 in physiological buffer (PB) until a slight swelling of the cells was observed. Embryos were washed 3 times in PB and then incubated in BrUTP solution for 10 min at 33 °C. All BrU that did not incorporate into the RNA was washed out in 3 subsequent wash steps in PB. Then, embryos were incubated in 0.2% Triton X-100 in PB for 3 min to permeabilize the nuclear membrane. Embryos were washed 3 times in PB and then fixed in 4% PFA in PB for 30 min at room temperature or overnight at 4 °C.

For IF analysis of BrUTP incorporation the primary antibody was labeled with FITC. For this, 10 µl FITC-solution (10 mg/mL) was added to 300 µl mouse anti-BrU (300 ng/µl) and diluted with 1690 µl sodium carbonate buffer to a total volume of 2 ml. This mixture was incubated for at least 1 h at room temperature or overnight at 4 °C, to allow binding of FITC to the antibody. To concentrate the antibody, the mixture was transferred to a Vivaspin 6 ultrafiltration spin column (Sartorius) and filled up with 4 ml DPBS. To wash out all unbound FITC and concentrate the primary antibody, the spin column was centrifuged for 5-7 min at 3600xg until 300-400 µl of the antibody mixture in the spin column were left. The supernatant was discarded.

After preparation of the primary antibody, embryos were washed 5 times in blocking buffer over a time period of 15 min. Then, the primary antibody in PB (1:50) was added and incubated for 1 h. The embryos were washed twice in blocking buffer and mounted with Vectashield containing DAPI as described above.

2.3.7.5 Analysis of fluorescence intensity

H3K9me3 and BrU IF reactions of oocytes and embryos were analyzed by quantification of fluorescence intensity of the samples. Detection of fluorescence was done with a LEICA DM4000B microscope. Ybx2 IF was analyzed by Dr. Tom Trapphoff by confocal laser scanning microscopy (CLSM). Intensity of fluorescence was quantified with the software Image J. Fluorescence intensity of the region of interest (I_{ROI}; e.g. the cell nucleus for H3K9me3 and BrUTP) was normalized against the background intensity ($I_{Background}$; e.g. cytoplasm). The ratio between normalized intensity (ΔI) of aged embryo and control embryos was calculated as follows:

$$\Delta I = I_{ROI} - I_{Background}$$

$$Relative\ Intensity = \frac{\Delta I(Embryo)}{mean\Delta I(Control\ Embryos)}$$

2.3.8 Poly(A) tail dependent fractionation of mRNA

To analyze the effect of postovulatory aging on the poly(A) tail on a transcriptome-wide level, mRNA was separated into fractions of different poly(A) tail lengths (Figure 5). The method is based on magnetic oligo$(dT)_{25}$ Dynabeads, that bind to poly(A) mRNA and was adapted from Meijer et al. (2007). The +Poly(A) mRNA bound to the beads can be separated from the unbound mRNA, containing the -Poly(A) mRNA fraction (fraction 1) and all other RNAs that do not contain poly(A) stretches (e.g. rRNA). The +poly(A) mRNA binds to the beads at a high salt concentration. The longer the poly(A) tail, the stronger the binding to the beads will be. A stepwise lowering of the salt concentration of the buffer will result in fractionated elution of transcripts differing in poly(A) tail length from short (fraction 2, medium salt buffer) to long (fraction 3, water). So after poly(A) mRNA fractionation there will be one -Poly(A) RNA fraction and several +Poly(A) mRNA fractions with increasing poly(A) tail length.

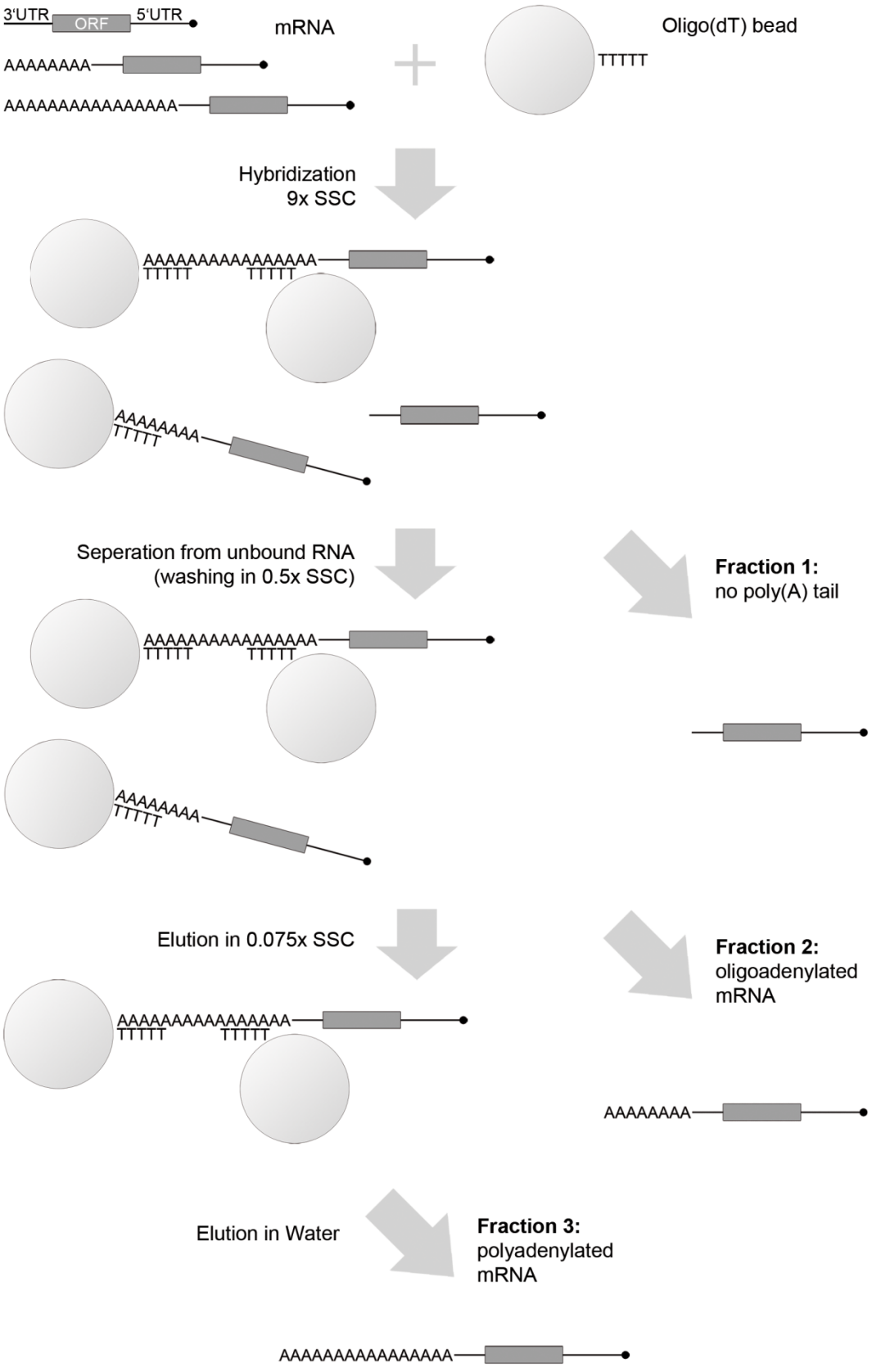

Figure 5: Fractionation of mRNA depending on the poly(A) tail length. Total RNA containing mRNAs with different poly(A) tail length were hybridized to oligo(dT) beads at high salt concentration (9x SSC buffer). Unbound RNA, containing –Poly(A) mRNA was separated (fraction 1). With decreasing salt concentrations, mRNAs with increasing poly(A) tail length were eluted. First, oligoadenylated mRNA (fraction 2) was eluted in 0.075x SSC buffer and second polyadenylated mRNA (fraction 3) was eluted in water. The method and this figure are based on Meijer et al. 2007 (ORF: open reading frame; UTR: untranslated region).

2.3.8.1 Poly(A)-mRNA fractionation

First, the oligo(dT) beads were adapted to room temperature for at least 30 min and then washed 3 times in 200 µl 0.5xSSC buffer. For fractionation a pool of 200 in vivo postovulatory-aged and 200 control oocytes was used. Oocytes were incubated in 10 µl Pronase for 10 min at 37 °C to digest the zona pellucida. RNA was extracted from oocytes by mixing them with 30 µl GTC buffer and incubation for 5 min at room temperature. After adding 100 µl dilution buffer (salt concentration: 9xSSC), the mixture was incubated for 5 min at 70 °C to denature RNA and remove any secondary structures, which might interfere with binding to the oligo(dT) beads. The RNA mixture was applied to the oligo(dT) beads, placed on a rotator and incubated for 30 min at room temperature to allow RNA binding to the beads. Rotation prevented sedimentation of the beads and therefore intermixture of RNA and oligo(dT) beads during binding. The tube was then placed onto the magnet for 1 minute to let the beads with the bound +Poly(A) mRNA bind to the magnet. The supernatant, containing fraction 1 (-Poly(A) mRNA), was removed and saved. Beads were washed 3 times in 200 µl 0.5xSSC buffer. The +Poly(A) mRNA was eluted in two steps, in decreasing salt concentrations. For this, beads were first resuspended in 100 µl 0.075xSSC buffer and incubated for 5 min at room temperature. The sample was then transferred to a magnet, incubated for 1 min and the supernatant containing fraction 2 (oligoadenylated mRNA) was removed and saved. The second elution step was conducted using 100 µl RNase free water for elution of fraction 3 (polyadenylated mRNA).

2.3.8.2 RNA cleanup and concentration

After fractionation, the 3 fractions were all suspended in different buffers with varying salt concentrations. To clean up and concentrate the RNA the RNeasy MinElute Cleanup Kit was used according to manufacturer's instructions. Before cleanup, *Luciferase* RNA was spiked into each fraction as an external reference for normalization of later analysis. This was not done before fractionation since *Luciferase* RNA has a poly(A) tail of 30 adenosines and would have been fractionated. An on-column DNA-digestion was carried out using DNase I as described in the kits user instructions. RNA was eluted in 14 µl RNase-free water.

The RNA quantity and quality was assessed by capillary electrophoresis on the Agilent 2100 Bioanalyzer (Agilent Technologies) using the RNA 6000 Pico Chip and following the manufacturer's user manual.

2.3.9 Transcriptome-wide RNA-sequencing analysis

The 3 mRNA fractions of both, postovulatory-aged and control oocytes were analyzed by transcriptome-wide RNA-sequencing on the Illumina HiSeq 2000. As a control, non-fractionated total RNA of 20 postovulatory-aged and 20 control oocytes was used to determine loss of RNA during the mRNA fractionation. If no RNA would have been lost the sum of all fractions would add up to the total RNA control. As a second control, 3 µL RNA from each of the 3 fractions was pooled together to check for biases during library preparation and sequencing process, which might occur since the fractions do not contain the same type of RNA: the unbound fraction contains other RNA types such as rRNA and tRNA next to mRNA, whereas the other fractions contain pure mRNA, which differ in length of the poly(A) tail. If these differences in RNA do not affect the RNA-sequencing, then the pool of fractions should be identical with the sum of the single fractions.

2.3.9.1 Library preparation

The sequencing libraries were prepared using the Ovation Single Cell RNA-Seq system, which is designed for very low amounts of total RNA, following the recommendations of NuGEN (User Guide “Ovation Single Cell RNA-Seq system”, Version M01363 v6). Briefly, the RNA fractions were first reverse-transcribed into single stranded antisense cDNA. The cDNA was then processed with a restriction enzyme into fragments of approximately 300 bp. A forward adaptor with a semi random primer attached was ligated to the 3’end of the fragments. The semi random primer mix was specific for mRNA to enrich for transcripts in the library. This was followed by second strand synthesis and end repair. Last, a reverse primer was ligated to the 5’end of the double stranded fragments and the library was amplified and enriched in two subsequent PCR steps. The reverse primer contained a 6 bp barcode that allowed identification of the sample during the sequencing analysis. Each sample got its own barcode enabling pooling of all samples together in one flow cell during sequencing. The fragment length, library quality and quantity were analyzed on a High Sensitivity DNA chip on the Agilent Bioanalyzer 2100.

2.3.9.2 RNA-sequencing on the Illumina HiSeq

Sequencing of the cDNA library was conducted on the Illumina HiSeq 2000 in the Biochip Laboratory of the University Hospital Essen by PD Dr. Ludger Klein-Hitpass and Claudia Haak. The HiSeq 2000 is an ultra-high-throughput next generation sequencing system, based on a four-colour cyclic reversible terminator system. During sequencing, each of the four nucleotides is labeled with its own fluorescent dye, which emits a signal when incorporated

into the DNA template. The fluorescent signals are captured in so-called flowgrams and converted into sequences.

The library was automatically clustered and amplified on the cBot (Illumina) using the HiSeq Cluster Kit v4 (Illumina). The cDNA molecules of the library all contain a forward and reverse primer, which both include an adaptor sequence (dual-indexed). The molecules are captured by covalent binding to oligonucleotides that are complementary to the adaptor sequence and attached to the flow cell. A clonal cluster of each of these cDNA molecules arises by solid-phase bridge amplification on the flow cell. One flow cell contains 8 lanes. All samples (fractions and controls) were pooled and loaded to 1 lane of the flow cell. The flow cell was then transferred to the HiSeq 2000, which was loaded with the HiSeq SBS Kit v4. A dual-indexed paired-end sequencing protocol was applied, in which 100 bp sequences were generated.

2.3.9.3 Analysis of RNA-Seq data

The data produced by the Illumina HiSeq were transferred to the Department of Genome Informatics of the University Hospital Essen, where they were analyzed by Prof. Sven Rahmann, Dr. Daniela Beißer and Dr. Inken Wohlers. First, reads were mapped against the mouse transcriptome with Tophat2. Short reads and duplicate reads were excluded. Then the data were filtered by searching for genes with HTSeq-Count. Fractions were normalized against the two control groups (total RNA and pooled fractions). *Luciferase* RNA that was spiked into each sample as external control was also included into the normalization. Genes represented in the control and postovulatory-aged fractions with over 500 counts were included into the analysis. A so called delta-score was determined to investigate changes in poly(A) tail length between the control and aged group. For this, first the proportion of reads per fraction (f1, f2 and f3) was calculated for each of the two groups separately. Then the score was determined with the following equation:

$$Delta = \frac{\big(f1(Control) - f1(PostOA)\big) - \big(f3(Control) - f3(PostOA)\big)}{2}$$

Genes with |Delta| ≥ 0.2 were defined as having a differentially changed poly(A) tail length. Fraction 2 was excluded from this analysis to increase the robustness of the score.

A gene ontology analysis was conducted with all genes that showed either differential deadenylation or polyadenylation using the Panther Classification System

(http://pantherdb.org/). A statistical overrepresentation test using default settings was performed searching for biological processes, molecular function and cellular compartments.

2.3.10 Analysis of poly(A) tail length by ePAT

The extension poly(A) test (ePAT) is a method to determine the poly(A) tail length of a transcript. It was first described by Jänicke et al. (2012) and established here in the institute by Dr. Debora Dankert. This technique is based on adding an anchor primer to the total RNA, which contains an oligo(dT) stretch. Klenow fragment of polymerase I ligates the primer to the 3' end of adenylated mRNA transcripts. Reverse transcription starting with the anchor primer is then used to transcribe the transcript including the poly(A) tail into cDNA. A subsequent PCR with the anchor primer and a gene specific primer then generates fragments of different size dependent on the poly(A) tail length.

Total RNA was extracted from 200 control and 200 postovulatory-aged oocytes as described above (2.3.4). RNA (7 µl from a 12 µl elution during RNA isolation) was mixed with 1 µl anchor primer (100 µM) and incubated for 5 min at 80 °C. The ePAT reaction was set up according to Table 3, incubated for 1 h at 37 °C and inactivated for 10 min at 80 °C. The reaction was then cooled to 55 °C and 1 µl Superscript II Reverse Transcriptase was added, incubated for 1 h and inactivated at 80 °C for 10 min.

Table 3: ePAT reaction.

Chemical	Volume
RNA-anchor-primer mix	8.0 µl
5x Superscript III Buffer	4.0 µl
DTT (100 mM)	1.0 µl
RiboLock RNase Inhibitor (1 U/µl)	1.0 µl
Klenow fragment (5 U/µl)	1.0 µl
Water	12.0 µl

Next a PCR reaction was set up using a gene specific primer in combination with the anchor primer. The optimal primer annealing temperature was determined using a temperature gradient PCR (55 °C – 65 °C). The PCR was set up using the ReadyMix Taq PCR Reaction Mix (Table 4).

Table 4: PCR-reaction for ePAT.

Sample	+DNA	-DNA
2x ReadyMix Taq PCR Reaction Mix	10.0 µl	10.0 µl
Anchor primer (5 µM)	2.0 µl	2.0 µl
Gene specific primer (5 µM)	2.0 µl	2.0 µl
Template from ePAT reaction	2.0-10.0 µl	-
Water	Ad to 20 µl	Ad to 20 µl

The following PCR conditions were applied:

93 °C	5 min	
93 °C	30 s	⎫
Primer annealing temperature	60 s	⎬ 35 cycles
72 °C	60 s	⎭
72 °C	7 min	

PCR products were verified by Sanger sequencing and then analyzed on a 1000 DNA Chip using the Agilent Bioanalyzer 2100 according to manufacturer's instructions.

2.3.11 Sanger sequencing

The didesoxy chain terminating sequencing technique described by Sanger et al. (1977) was used to validate the sequence of DNA amplicons. During the sequencing reaction, the incorporation of fluorescence-labeled didesoxynucleotides induces chain termination. This can happen at any point of the sequence and leads to fragments with different sizes. An automated sequencer separates these fragments based on their size by electrophoresis and detects the fluorescent signals.

2.3.11.1 ExoSAP-IT

For analysis of PCR-products using Sanger sequencing, all free nucleotides and primer dimers had to be removed from the sample, since this would disturb the sequencing reaction. The USBExoSAP-ITPCR Product Cleanup kit was used for this. 5 µl PCR-product were mixed with 2 µl ExoSAP-IT and incubated in a thermocycler for 15 min at 37 °C. The reaction was stopped by heating the sample to 80 °C for 15 min.

2.3.11.2 Sequencing reaction

The BigDyeTerminator v1.1 Cycle Sequencing Kit was used to set up a 10 µl sequencing reaction:

Template	**DNA**	**Bis-DNA**
PCR-Product	1.0 µl	1.0 µl
BigDye	2.0 µl	4.0 µl
BigDye Buffer	1.0 µl	-
Primer (5 µM; FWD or REV)	1.0 µl	1.0 µl
Water	5.0 µl	4.0 µl

The following program was applied for the sequencing reaction:

96 °C	1:00 min	
96 °C	0:10 min	35 cycles
Primer annealing temperature	0:05 min	
60 °C	2:50 min	

After the sequencing reaction, 10 µl water was added to each sample. Free didesoxynucleotides were removed by sephadex gelfiltration. Then samples were mixed with 10 µl formamide and sequenced on the ABI PRISM 3130XL Genetic Analyzer (Life Technologies). Data analysis was carried out employing the Sequencing Analysis (Life Technologies) and Geneious (Biomatters) software.

2.3.12 DNA-methylation analysis of 8-cell embryos

DNA-methylation of imprinted genes in single 8-cell embryos was assessed using deep bisulfite next-generation amplicon sequencing. For this sequencing technology, DNA is first treated with bisulfite, which converts unmethylated cytosine bases into uracil. If a cytosine base is methylated, it is protected against this conversion. In a subsequent PCR step the uracil bases are replaced by thymidine bases. After sequencing the bisulfite strand is compared to a reference strand. At CpG positions in the reference strand, a T is found in the bisulfite strand, except for methylated CpGs that were protected from bisulfite conversion and still contain a C. Next-generation sequencing allows a resolution of the methylation status of single amplicon copies.

2.3.12.1 DNA extraction and bisulfite conversion

The DNA of single 8-cell embryos was extracted and treated with bisulfite using the EZ DNA Methylation-Direct Kit according to the manufacturer's manual. Briefly, DNA was extracted from the cells with Proteinase K. DNA denaturation and bisulfite treatment were combined into a single step in which DNA was incubated in conversion reagent for 3.5 h at 64 °C. After bisulfite conversion the DNA was purified on a spin-column and eluted in 10 µl elution buffer.

2.3.12.2 Generation of amplicon libraries

Three imprinted genes (*H19*, *Snrpn* and *Igf2r*) and 1 control gene (*Pou5f1*) were analyzed by bisulfite sequencing. To generate the amplicon libraries a 3-step protocol was established, each step containing a PCR. The first 2 PCR steps were based on a nested PCR protocol to amplify DNA from such limited material as single 8-cell embryos. For the outer PCR a multiplex protocol was used with a primer pool for all 4 loci. For the inner PCR all 4 loci were amplified separately. The primer sequences for the inner PCR contained of a specific and a universal tag-sequence. In the third step, a so-called Re-PCR, primers binding to the tag-sequence of the amplicon were added. These primers contained sample-specific barcodes (multiplex identifiers, MIDs), a 4 bp key and adaptor sequences A or B. These primers are used for clonal amplification of the sequences in an emulsion PCR (emPCR). The MIDs allow multiplexing of samples during sequencing and the key sequences are needed for filtering during data analysis.

All primer sequences are summarized in Supplementary Table S3. Primers for the nested PCR have previously been described by El Hajj et al. (2011). For the outer PCR the Multiplex PCR kit was used and a 25 µl reaction was set up with a 10x primer mix (2 µM per primer):

Table 5: Outer PCR reaction.

Sample	+DNA	-DNA
2x Multiplex PCR Mastermix	12.5 µl	12.5 µl
10x Primer mix	2.5 µl	2.5 µl
Bisulfite converted DNA	10.0 µl	-
RNase free water	-	10.0 µl

The following PCR conditions were applied:

95 °C	15 min	
94 °C	30 s	⎫
52 °C	90 s	⎬ 30 cycles
72 °C	45 s	⎭
72 °C	10 min	

The HotStarTaq Mastermix was used to set up a 25 µl inner PCR reaction, as shown in Table 6.

Table 6: Inner PCR reaction.

Sample	**+DNA**	**-DNA**
2x HotStarTaq Mastermix	12.5 µl	12.5 µl
FWD Primer (5 µM)	2.5 µl	2.5 µl
REV Primer (5 µM)	2.5 µl	2.5 µl
Outer PCR product	3.0 µl	-
RNase free water	4.5 µl	7.5 µl

A touchdown PCR protocol was employed to increase primer specificity. A touchdown protocol starts at a high primer annealing temperature. During the first cycles this temperature is reduced in each step. In this protocol the annealing temperature was reduced by 0.5 °C in each cycle for 14 cycles from 64 °C to 57 °C:

95 °C	15 min	
94 °C	30 s	⎫
64 °C	30 s	⎬ 14 cycles: Δ -0.5 °C
72 °C	45 s	⎭
94 °C	30 s	⎫
57 °C	30 s	⎬ 25 cycles
72 °C	45 s	⎭
72 °C	10 min	

PCR-products were visualized by agarose gel electrophoresis. Products with a fragment of the expected size were further analyzed by Sanger sequencing to validate the sequence. A 50 µl Re-PCR reaction was set up with all validated inner PCR-products using the HotStarTaq Mastermix:

Table 7: Re-PCR reaction.

Sample	**+DNA**	**-DNA**
2x HotStarTaq Mastermix	25.0 µl	25.0 µl
FWD Primer (20 µM)	0.5 µl	0.5 µl
REV Primer (20 µM)	0.5 µl	0.5 µl
Inner PCR product	3.0 µl	-
RNase free water	21.0 µl	24.0 µl

Amplification took place applying the following PCR-conditions:

95 °C	15 min	
95 °C 72 °C	30 s 60 s	} 35 cycles
72 °C	10 min	

The PCR-product was again visualized by agarose gel electrophoresis for size-validation. 22.5 µl of validated products were diluted 1:1 with water and used for further sequencing analysis.

2.3.12.3 Next-generation bisulfite sequencing

For DNA-methylation analysis quantitative deep bisulfite sequencing on the 454/Roche genome sequencer (GS) Junior system was employed. Preparation of the samples and loading of the sequencer was conducted by Sabine Kaya at the Institute of Human Genetics of the University Hospital Essen according to the Roche emPCR Amplification Method Manual – Lib-A and the Roche Sequencing Method Manual.

Amplicon libraries were purified, according to recommendations by Roche, using the Agencourt AMPureXP System and quantified on the Nanodrop ND-1000 Spectrophotometer (Thermo Scientific). Samples were diluted depending on their concentration, pooled and amplified in a clonal emPCR (GS Junior Titanium emPCR Kit – Lib-A; Roche). This PCR takes place in an emulsion in which each droplet represents an individual reaction chamber

for clonal amplification of a single amplicon bound to a DNA capture bead. Each droplet contains Primer A and B that bind to the adaptor sequence of the primer that was added to the amplicon in the Re-PCR (Table 7). DNA capture beads containing amplified single-strand DNA sequences were washed, recovered and enriched. The enriched DNA capture beads were then transferred to a microtiter plate, where each well has place for one bead to avoid contaminations (GS Junior Titanium PicoTiterPlate Kit; Roche). The microtiter plate was loaded onto sequencing platform for analysis (GS Junior Titanium Sequencing Kit; Roche). The sequencing reaction on the 454/Roche GS Junior platform is similar to the Illumina HiSeq (2.3.9.2 RNA-sequencing on the Illumina HiSeq) except that the Roche is a single-colour fluorescent system. So each base has the same fluorescent label and has to be added separately in subsequent steps.

2.3.12.4 Sequencing data analysis

Data analysis was conducted using the Amplikyzer Software (Rahmann et al. 2013) with default settings based on the .ssf files generated by the 454/Roche GS Junior system. Due to the destruction of DNA during bisulfite treatment and the low input amount, it was not always possible to obtain reads for both, the maternal and the paternal allele. The parental alleles were distinguished by SNPs. The methylation level of the maternal and paternal allele was determined. In the case that both alleles were present for analysis the mean methylation level of the two alleles was calculated, which was expected to be 50% for imprinted genes and 0% for the *Pou5f1* control gene. A deviation of >10% was defined as aberrant methylation of the embryo at a specific locus. If only one allele was sequenced, a methylation failure was defined as a deviation of >10% from the expected methylation level of a certain allele (0 or 100%).

2.3.13 Statistical analysis

Statistical analysis was conducted with the SigmaPlot 12.5 software (Systat Software, Inc). A two-tailed Student *t*-test was performed to analyze the statistical significance of differences between RNA-expression of aged and control oocytes and comparisons of fold change ($2^{-\Delta\Delta Ct}$) of oligo$(dT)_{16}$-primed cDNA with random hexamer-primed cDNA. The normal distribution of data was validated using the Shapiro-Wilk Normality test. When this test failed, as was the case for the number of oocytes retrieved per mouse, H3K9me3, Ybx2, BrUTP-incorporation and DNA-methylation analysis, a Mann-Whitney U Rank Sum test was applied instead. The α-level was set at 0.05 to determine statistically significant differences.

3 Results

3.1 Oocyte retrieval after preovulatory aging

The number of oocytes isolated per mouse was counted in the control group and after 3 and 4 d of preovulatory *in vivo* aging (Figure 6A). All mice, also control mice, received the GnRH antagonist cetrorelix (control +cetro). An additional control group that did not receive cetrorelix (control –cetro) was included in the analysis to see if the cetrorelix itself had an impact on oocyte output.

An average of 25.16 oocytes per mouse was isolated from control –cetro mice. When applying cetrorelix to control mice during oocyte maturation, this number decreased significantly to 17.92 oocytes per mouse (control –cetro: $n = 68$, control +cetro: $n = 49$, Mann-Whitney U test: $p < 0.05$). Aging reduced the oocyte number further to a mean of 11.91 oocytes after 3 d of aging ($n = 48$) and 9.91 oocytes after 4 d of aging ($n = 33$). The difference between the control +cetro group and the aged groups was significant after 3 d (Mann-Whitney U test: $p < 0.05$) and 4 days (Mann-Whitney U test: $p < 0.01$). Thus, aging showed a major effect on oocyte retrieval rates. Since the GnRH treatment itself also seemed to affect oocyte growth and maturation rates the control +cetro group was used for all further experiments (in the following this group will be referred to as control).

To investigate whether this reduced oocyte number upon aging is caused by degradation of oocytes, the number of degraded oocytes after ovulation was counted. The mean percentage of degraded oocytes relative to total oocytes per mouse was calculated for each group (Figure 6B). The percentage of degraded oocytes varied between the groups from 17.6% in 3 d preovulatory-aged oocytes to 28.6% in the control –cetro group. No significant differences were found between the analyzed groups, indicating that the lower oocyte number after aging is not due to increased degradation.

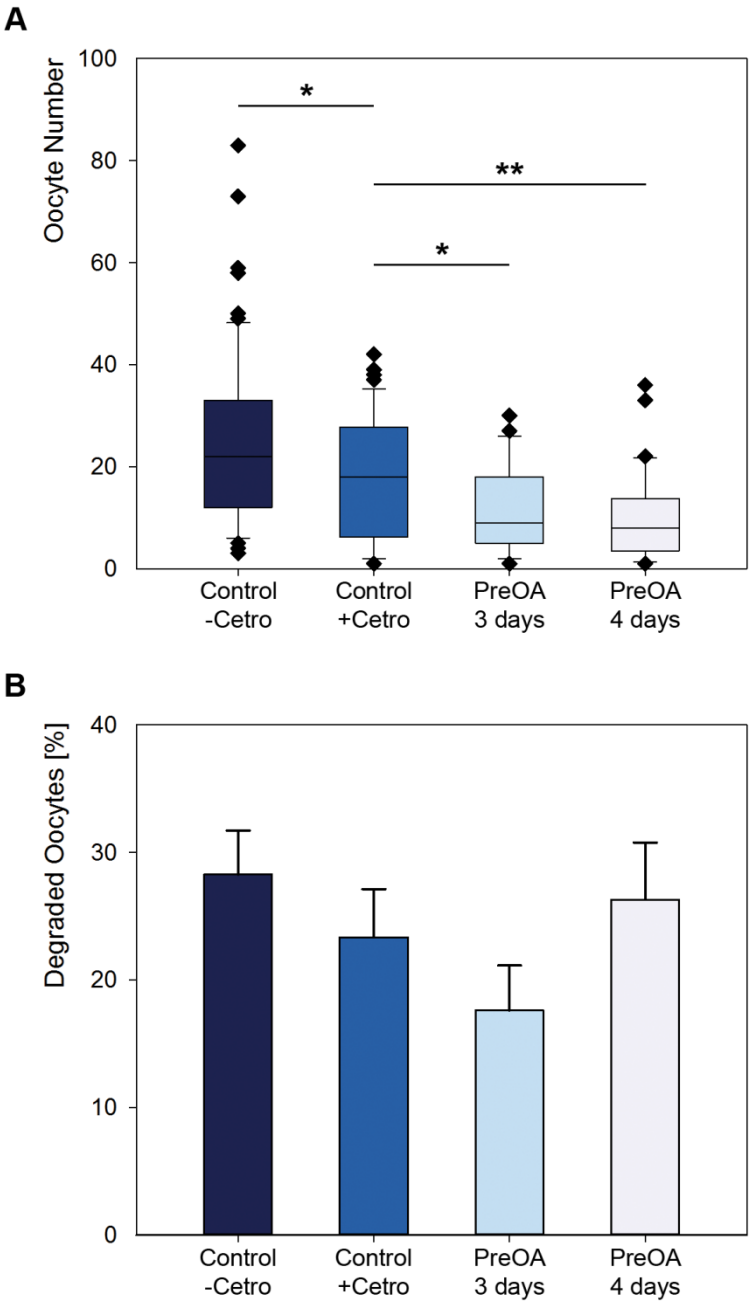

Figure 6: Oocyte retrieval from control and preovulatory-aged mice. A) Boxplots demonstrate oocyte numbers isolated from mice after superovulation. Control mice are split into two groups, one that did not receive cetrorelix (control –cetro) and another that received cetrorelix (control +cetro). Preovulatory aging (PreOA) was conducted for either 3 or 4 days in the presence of cetrorelix. Cetrorelix treatment reduced oocyte numbers in control mice. Preovulatory aging further lowered the oocyte number. **B)** Graph shows the percentage of degraded oocytes per mouse (Mean±SEM), which did not differ significantly between the groups. Control –Cetro: $n = 68$, Control +Cetro: $n = 49$, PreOA 3d: $n = 48$, PreOA 4d: $n = 33$, Mann-Whitney U test: * $p < 0.05$; ** $p < 0.01$.

3.2 H3K9me3 histone methylation

It is not clear what causes the observed decline in oocyte maturation rates upon preovulatory aging. One crucial step in oocyte maturation is the transcriptional silencing of the maternal genome during prophase I of meiosis. This is mediated by repressive epigenetic histone modifications such as the trimethylation of histone H3 lysine K9 (H3K9me3; Kageyama et al. 2007). H3K9me3 is further important for chromosome integrity and genome stability (Peters et al. 2001). Therefore, the effect of preovulatory aging on the level of H3K9me3 in oocytes was investigated using immunofluorescence (IF) analysis. H3K9me3 was visualized in control (n = 106) and 4 d preovulatory-aged (n = 65) oocytes and relative signal intensity was compared by quantification with ImageJ (Figure 7). In both control and aged oocytes the H3K9me3 signal co-localized with the chromosomes in the cell nucleus (Figure 7A). Relative quantification of fluorescent staining intensities showed no significant difference between aged and control oocytes (Mann-Whitney U test: p = 0.973; Figure 7B). The mean signal intensity of control oocytes was set to 1 ± 0.06 a.u. (mean ± SEM) and compared to controls the mean signal intensity of the aged oocytes was 0.97 ± 0.05 a.u. The results indicate that preovulatory aging does not affect the level of H3K9 trimethylation.

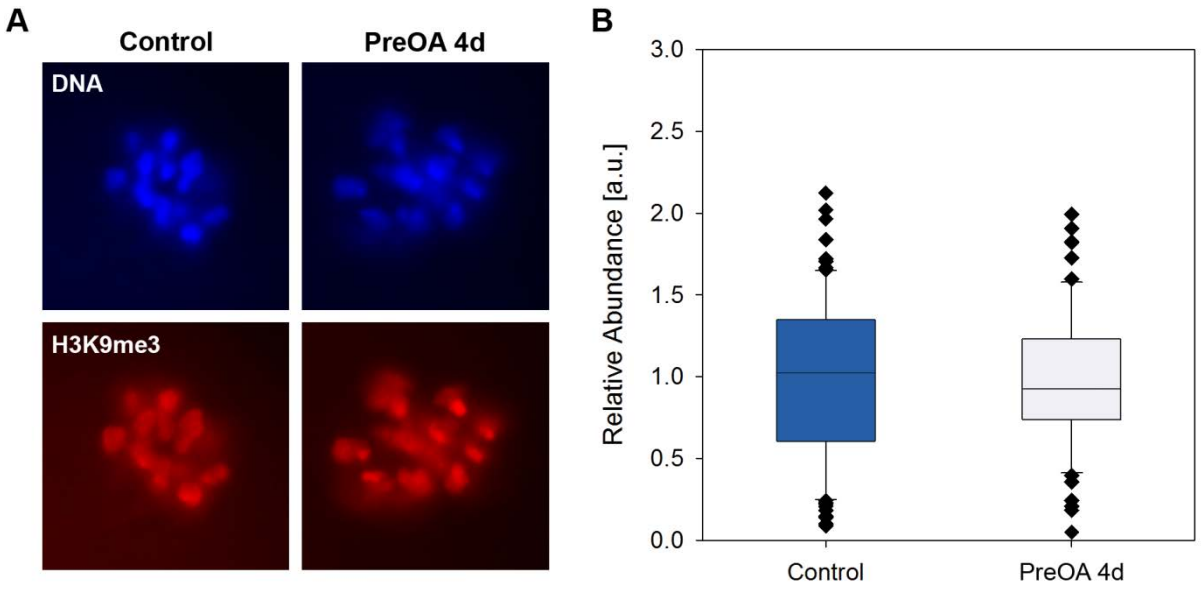

Figure 7: Immunohistochemical analysis of histone methylation H3K9me3 in control and 4 d preovulatory-aged (PreOA 4d) oocytes. A) Representative DAPI and anti-H3K9me3 stainings of cell nuclei of control and preovulatory-aged oocytes. **B)** Relative quantification of fluorescent signal intensities showed no significant difference between control and aged oocytes. Control: n = 106, PreOA 4d: n = 65; a.u.: arbitrary units.

3.3 *Ybx2* transcript and Ybx2 protein expression

For the storage of maternal transcripts and stabilization of the poly(A) tail length the Ybx2 protein is essential (Medvedev et al. 2011). Transcript levels of *Ybx2* were analyzed in 4 control oocyte pools and in 3 pools of 4 d preovulatory-aged oocytes by qRT-PCR after cDNA-synthesis with random hexamer primers. Each pool contained 10 oocytes. Transcript levels decreased with a normalized fold change of 0.35 in aged oocytes compared to controls, although this decline was not significant due to high variation between the control pools (*t*-test: $p = 0.137$; Figure 8).

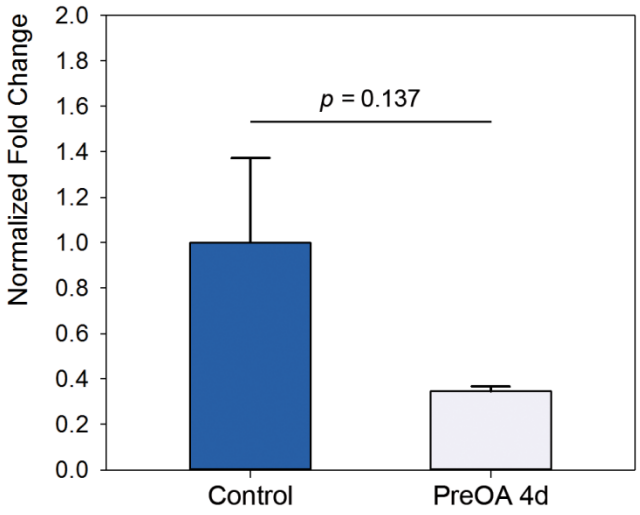

Figure 8: Transcript levels of *Ybx2* in control and 4 d preovulatory-aged (PreOA 4d) oocytes. Indicated is the fold change of aged oocytes compared to controls, which was normalized against a *Luciferase* standard curve. The cDNA was primed with random hexamers and the two groups were compared using a *t*-test. No significant difference of transcript expression was observed. Indicated is the Mean±SEM. Control: $n = 4$, PreOA 4d: $n = 3$.

Next the protein expression of Ybx2 was investigated using IF analysis (Figure 9). Staining of Ybx2 was documented by CLSM by Dr. Tom Trapphoff. In control oocytes, Ybx2 expression was observed throughout the whole cytoplasm, but was enriched in the subcortical RNP (ribonucleoprotein particles) domain (SCRD) (Figure 9A). Furthermore, expression was also seen in the chromosome spindle complex (arrowheads in Figure 9A'). Here, Ybx2 localized in the proximal kinetochore area of the chromosomes left and right to the equatorial plate in the spindle halves. It was absent in the area of the interpolar microtubules, in the center of the spindle with the chromosomes and in the polar part of the spindle and the anastral spindle poles.

After 4 d of preovulatory aging Ybx2 expression decreased in the subcortical area as well as in the rest of the cytoplasm (Figure 9B). Also, the spindle complex surrounding the chromosomes showed less Ybx2 signal after aging (Figure 9B'). The signal intensity of Ybx2 was quantified by X-axis profiling of the relative Ybx2 mean abundance through a cross-section of the entire cell (Figure 9C). This demonstrated enrichment of Ybx2 in the cortex of control and aged oocytes and also a decline in transcript abundance after aging. This uniform decline was also confirmed by determination of the relative staining intensity of the overall ooplasm, or the subcortical and the inner cytoplasmic regions separately (Figure 9D). Staining intensity of 83 control oocytes was compared to that of 120 aged oocytes after normalization against background staining. In the SCRD and in the inner cytoplasm Ybx2 expression was significantly lower in aged oocytes relative to controls (Mann-Whitney U test: $p < 0.001$ for both regions; Figure 9E). It is therefore not surprising that also a highly significant decrease in protein level in the total cytoplasm was observed after preovulatory aging (Mann-Whitney U test: $p < 0.001$). The decrease in transcript and protein levels of Ybx2 might have implications for RNA stability in the oocyte.

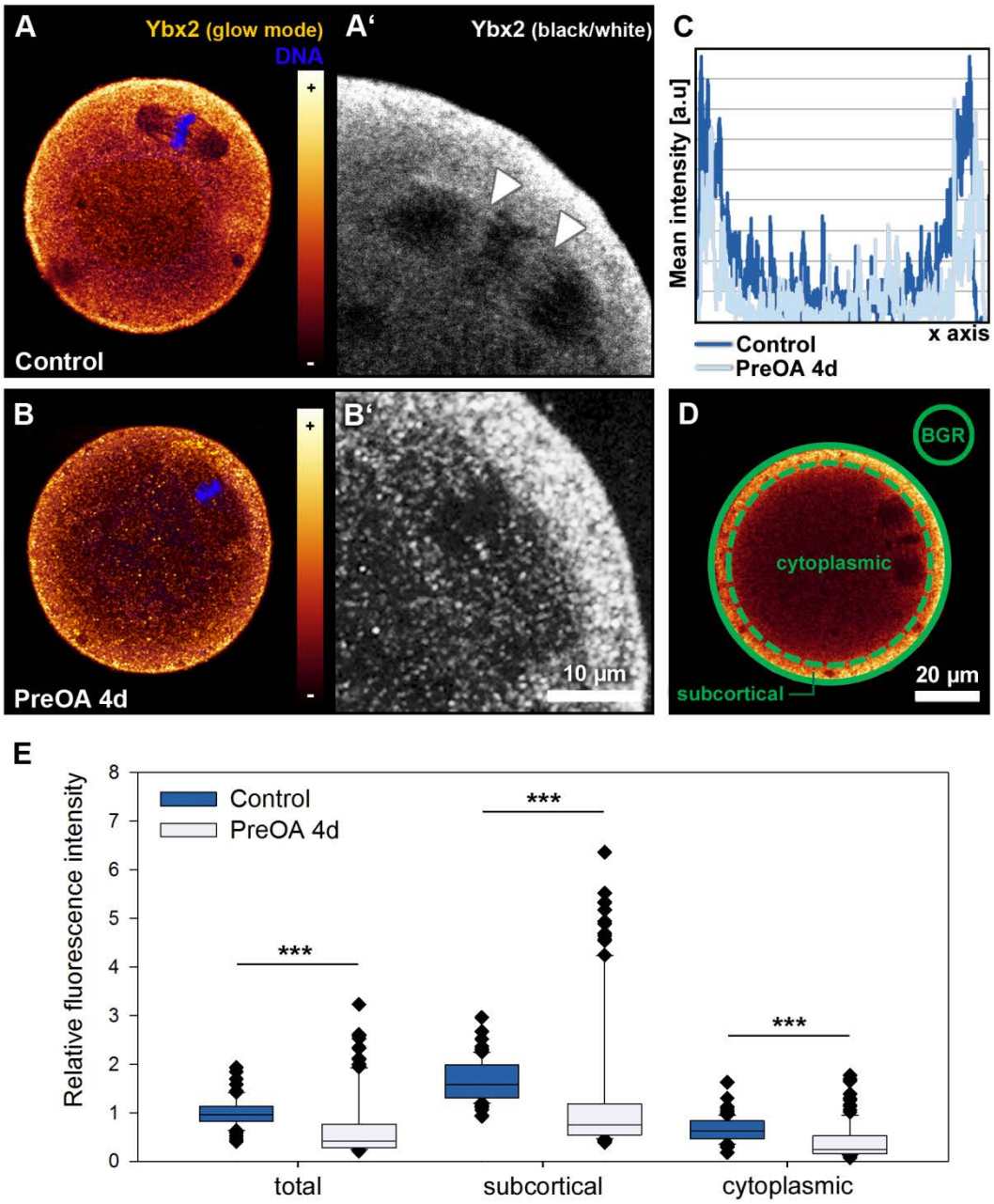

Figure 9: Ybx2 protein localization and relative protein abundance in control and 4 d preovulatory-aged (PreOA 4d) oocytes investigated by confocal laser scanning microscopy. Representative figures of Ybx2 expression in control **(A)** and aged oocytes **(B)**. **A, A')** Ybx2 protein is enriched in the subcortical RNA domain, but also detectable in the cytoplasm, as well as in the spindle chromosome complex (arrowheads in close-up **A'**). **B, B')** Reduced staining for Ybx2 was observed in preovulatory-aged oocytes and no enrichment in the spindle of the aged oocyte. **C)** X-axis-scanning through an entire cell revealed an even decline in protein abundance in aged oocytes in comparison to controls. **D, E)** This decrease in overall protein abundance was confirmed by semi-quantification of relative fluorescence intensity of the subcortical and inner cytoplasmatic region as well as total ooplasm, normalized against background fluorescence (BGR). Scale bar in **D** also applies to **A** and **B** and scale bar in **B'** also to **A'**. Control: $n = 83$, PreOA 4d: $n = 120$, Mann-Whitney U test: *** $p < 0.001$.

3.4 Transcript levels and poly(A) content of maternal effect genes

Since Ybx2 levels are reduced in oocytes after preovulatory aging, the effect on mRNA level and poly(A) tail stability of transcripts of maternal effect (ME) genes was assessed. ME genes are of crucial importance for early embryonic development (Li et al. 2010). It was analyzed by qRT-PCR if 3 d of preovulatory aging affects the expression of 10 selected candidate ME genes (Figure 10). Three pools of 20 oocytes each were analyzed for every experimental group. Preovulatory aging in vivo as well as in follicle culture was assessed. For cDNA synthesis total RNA was either primed with random hexamers or with oligo(dT) primers. This allows investigation of the poly(A) content of the ME transcripts, which is interesting because poly(A) tail length is an important regulator of translation efficiency in the oocyte (Clarke 2012). Changes in total transcript levels can be visualized by the fold change of the random primed cDNA. The oligo(dT) primers bind to the poly(A) tail of a transcript. Therefore, comparison of oligo(dT)-primed cDNA to random-primed cDNA provided information about the poly(A) content of the transcripts: If the poly(A) content stays stable during aging, the fold change of oligo(dT)-primed cDNA should change in a similar amount as the fold change of random-primed cDNA (e.g. *Zfp57* in Figure 10B). If however, the length of the poly(A) tail of a transcript changes, this can be observed as a difference in fold change between random- and oligo(dT)-primed cDNA (e.g. *Smarca4* in Figure 10A).

After oocyte maturation and 3 d of preovulatory aging in vivo, the mean transcript levels of *Smarca4* and *Tet3* decreased significantly by approximately two-fold compared to controls (Figure 10A; *Smarca4*: Fold change = 0.53, *t*-test: $p < 0.01$; *Tet3*: Fold change = 0.48, *t*-test: $p < 0.05$), as indicated by the normalized fold change of random hexamer-primed cDNA. *Zfp57* transcript levels also tended to decrease after aging (Fold change = 0.54, *t*-test: $p = 0.0602$). The other analyzed genes, *Trim28*, *Dnmt1*, *Nlrp2*, *Nlrp5*, *Nlrp14*, *Pou5f1* and *Zar1* did not show significant changes in total transcript levels in aged oocytes compared to controls. When comparing the fold change of random- and oligo(dT)-primed cDNA, *Smarca4* showed a trend towards an increased poly(A) content (Oligo(dT) fold change = 1.42, *t*-test: $p = 0.0567$). The other ME-genes did not show significant differences between random- and oligo(dT)-primed cDNA. The tendency towards an increased poly(A)content was visible for all genes though.

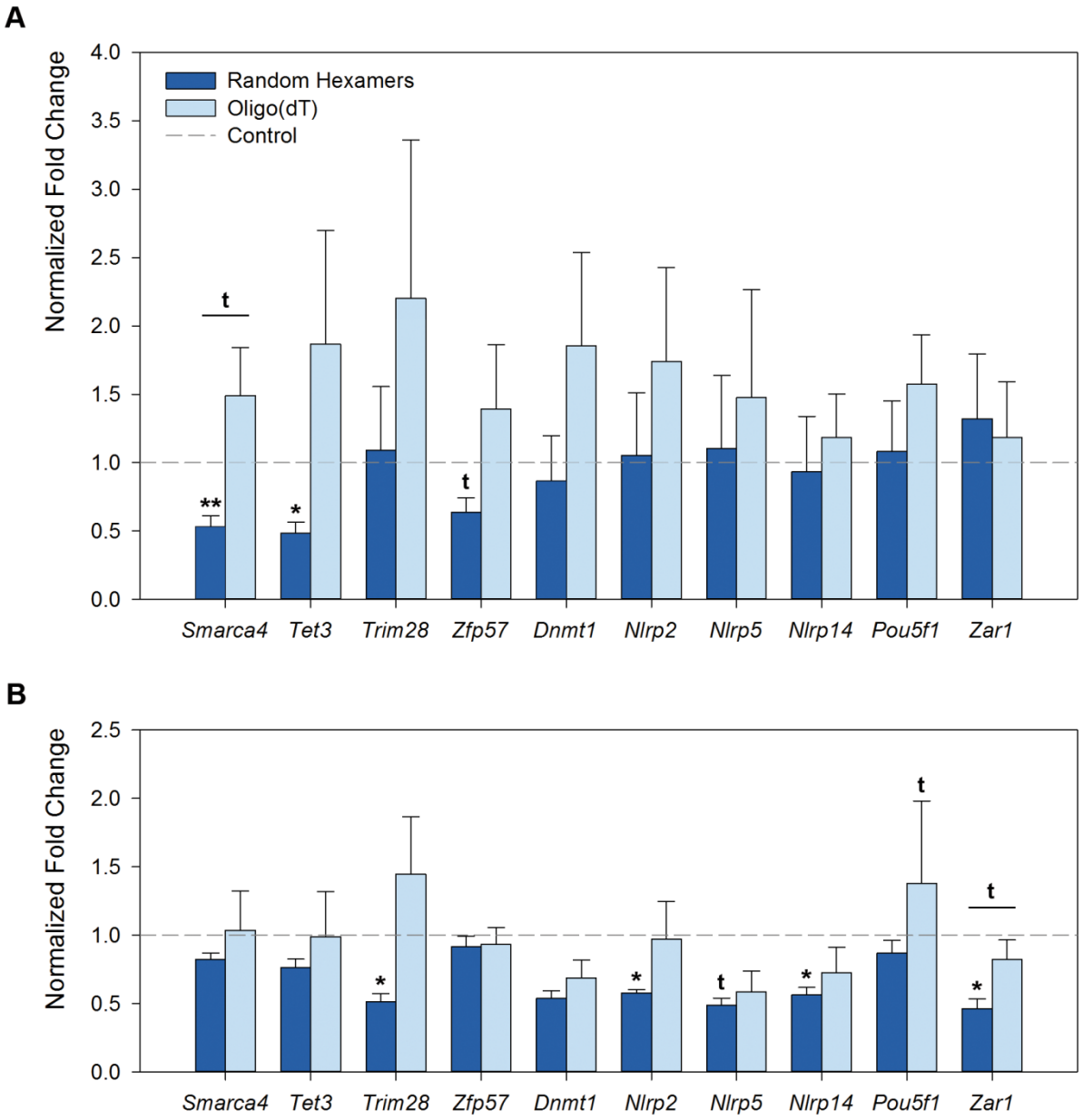

Figure 10: Transcript levels and poly(A) content of ME genes of 3 d in vivo (A) or in vitro (B) preovulatory-aged oocytes compared to controls. Indicated is the normalized fold change of 10 ME genes of aged oocytes compared to control oocytes. cDNA of oocytes was either primed with random hexamers to show total transcript levels or with oligo(dT) primers. Comparing the fold change of random- and oligo(dT)-primed cDNA indicates the poly(A) content of transcripts. **A)** In vivo aging of oocytes led to significantly reduced transcript levels of *Smarca4* and *Tet3* and a general tendency of poly(A) content increase. **B)** In vitro aging caused transcript decline of *Trim28*, *Nlrp2*, *Nlrp14* and *Zar1*. Indicated is the Mean±SEM. Three pools of 20 oocytes were analyzed for each group; *t*-test: t: $p < 0.10$, * $p < 0.05$, ** $p < 0.01$. This figure was modified from Dankert et al. 2014.

Mean transcript levels of in vitro preovulatory-aged oocytes were significantly lower compared to controls for *Trim28* (Fold change = 0.51, *t*-test: $p < 0.05$), *Nlrp2* (Fold change = 0.58, *t*-test: $p < 0.05$), *Nlrp14* (Fold change = 0.56, *t*-test: $p < 0.05$) and *Zar1* (Fold

change = 0.46, *t*-test: $p < 0.05$; Figure 10B). A trend towards decreased transcript levels in aged oocytes compared to controls was also observed for *Nlrp5* (Fold change = 0.49, *t*-test: $p = 0.0541$). Comparing random- and oligo(dT)-primed cDNA of *in vitro*-aged oocytes showed a trend of increased poly(A) content of *Zar1* (Oligo(dT) fold change = 0.82, *t*-test: $p = 0.752$). Again this tendency was also observed for other analyzed genes, although not as pronounced as for in vivo-aged oocytes.

Overall, the results show a decrease of transcript level for certain genes after preovulatory aging, although different genes were affected in vivo than in vitro. The poly(A) content of transcripts tends to increase upon aging, although only few significant changes were observed, due to high variation between samples.

3.5 Transcriptome-wide analysis of poly(A) tail length

After having seen effects of preovulatory aging on poly(A) tail length in some of the investigated candidate genes, the poly(A) tail length during aging was analyzed on a transcriptome-wide level. Total RNA was fractionated into 3 fractions with different poly(A) tail length. Establishment of the method was carried out using postovulatory-aged oocytes instead of preovulatory-aged oocytes because these oocytes are easier and cheaper to obtain. Poly(A) tail length of postovulatory-aged oocytes was compared to control oocytes. Successful poly(A) fractionation was verified for *Dnmt1* and *Zar1* with an extension poly(A) test (ePAT) by Dr. Debora Dankert (Dankert 2015).

3.5.1 Poly(A)-sequencing analysis

All fractions where sequenced on the Illumina HiSeq 2500 and reads were mapped against the mouse transcriptome. The number of mapped reads lay between 918,565 and 22,791,961 reads depending on group and fraction, which corresponded to 27-79% of total read number (Supplementary Table S4). More reads were found in the control group in comparison to the postovulatory-aged oocytes. The duplicate rate was relatively high, varying between 58 and 84%. The number of reads which coded for known genes was determined (counts). Fraction 1 contained the majority of counts (Control: F1 = 11,625,270 counts; PostOA: F1 = 13,480,406 counts) and in Fraction 2 and 3 less than half of the counts were found (Control: F2 = 7,319,693 counts, F3 = 3,814,821 counts; PostOA: F2 = 807,163 counts, F3 = 664,657 counts). Most of these counts encoded protein-coding genes (between 75 and 99%).

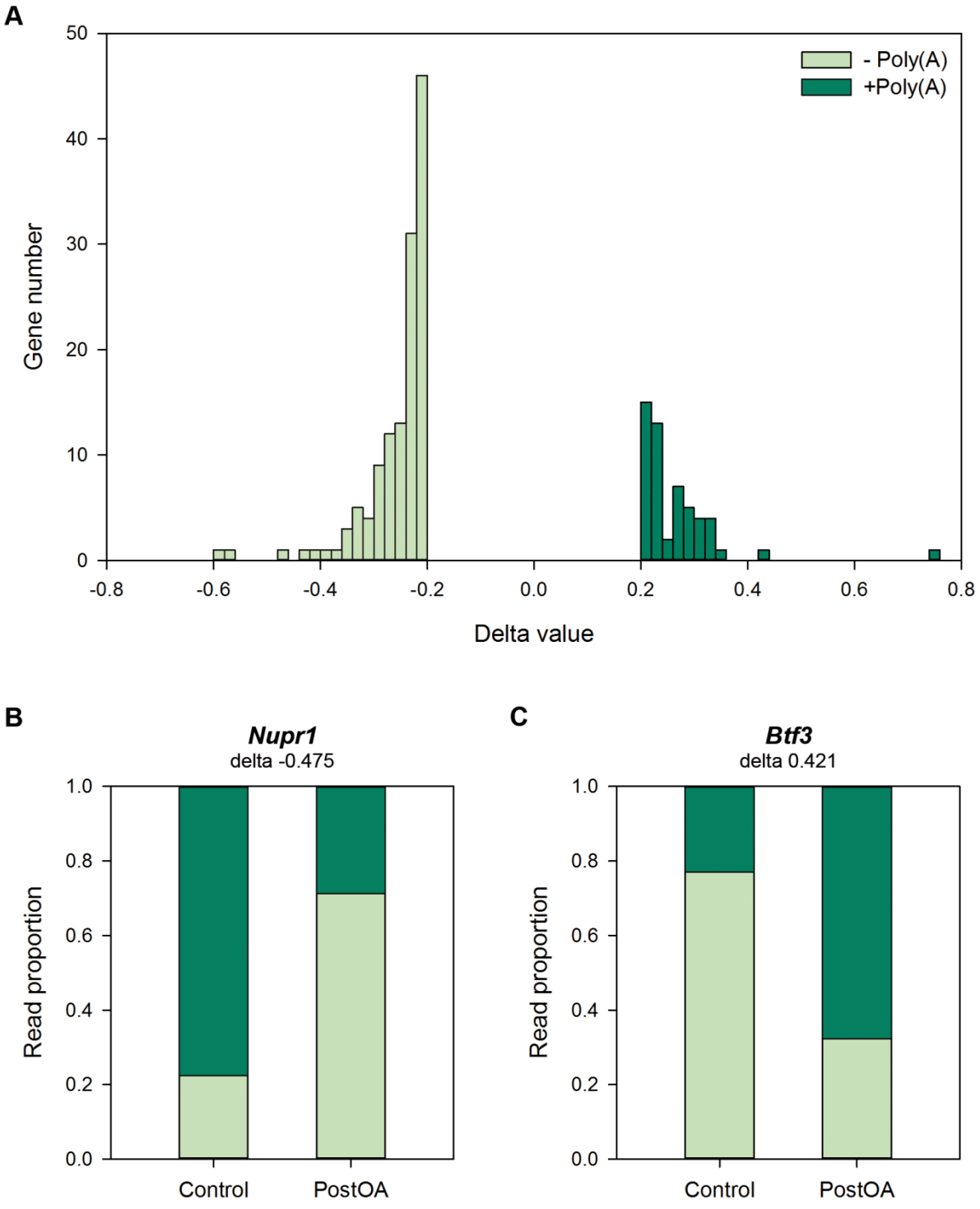

Figure 11: Poly(A)-sequencing analysis of control and postovulatory-aged (PostOA) oocytes. A delta-score showing the change in poly(A) tail length between control and PostOA oocytes is visualized. **A)** The number of genes which had a differential poly(A) tail length is shown in relation to their delta-score, demonstrating that the majority of genes with a change in poly(A) tail length show deadenylation in aged oocytes. **B, C)** The ratio between counts without and with a poly(A) tail are shown for *Nupr1*, a gene with a delta-score indicating loss of poly(A) tail length **(B)** and for *Btf3*, which shows polyadenylation in PostOA oocytes **(C)**. Differential poly(A) tail length: delta value < -0.2 or delta value >0.2.

The delta-score was used to compare control and postovulatory-aged oocytes and to determine poly(A) tail changes between the two groups. Fraction 2 and 3 were combined and it was just distinguished between mRNA without and with poly(A) tail (-poly(A) fraction and +Poly(A) fraction), to improve the robustness of the analysis. In total, 183 genes with a differential poly(A) tail length where found, of which 130 showed a loss of poly(A) tail and 53 genes showed a gain in polyadenylation (Figure 11A and Supplementary Table S5). In Figure 11B and C examples of genes where the delta-score indicated a clear loss or gain of the poly(A) tail length are shown. For *Nupr1* (delta -0.435) 71% of counts in control oocytes were found in the +poly(A) fraction and after postovulatory aging, only 29% of counts had a poly(A) tail. The opposite was found for *Btf3* (delta 0.421), where the +poly(A) fraction increased after postovulatory aging from 23% to 68% of total counts. A gene ontology analysis did not find any biological processes, molecular functions or cellular compartments enriched within these gene groups, which could indicate that it is not a specific process, function or location that is affected by poly(A) tail changes due to postovulatory aging. All interpretations should be taken with caution since it was not possible to repeat this experiment and analysis. Three subsequent trials failed due to low sequencing library quality or because it was not possible to normalize the data to the Luciferase RNA or to the controls (total RNA and pool of F1-F3).

3.5.2 ePAT analysis

To verify the results obtained from the single poly(A) sequencing analysis, an ePAT was performed allowing the investigation of the poly(A) tail length for individual genes. Since the ePAT showed unspecific fragments during agarose gel electrophoresis, the fragment of the expected size was eluted and verified by Sanger sequencing. After this validation, the ePAT of 4 genes (*Btf3*, *Prdx2*, *Ddx3x* and *Nupr1*) was assessed on an Agilent DNA 1000 or DNA High Sensitivity chip. A region of interest containing the peak with the expected fragment size was defined and the concentration and average fragment size within this region was determined. The ePAT of *Btf3*, which in the sequencing analysis showed a decline in poly(A) content after postovulatory aging, showed a decrease in transcript levels after postovulatory aging from 8.85 ng/µl to 6.88 ng/µl (Supplementary Table S6). It was not possible to see a clear shift in the peak size between control and postovulatory-aged oocytes, indicating no change in poly(A) tail length (Figure 12A). This is not in accordance with the RNA sequencing results. Another example for polyadenylation, *Prdx2* was investigated, which had a delta value of 0.244 during the poly(A) sequencing analysis. This gene showed no clear

decline in transcript levels (control: 1.08 ng/µl; PostOA: 1.01 ng/µl). The peak size changed from an average size of 429 bp in control oocytes to 471 bp in aged oocytes, indicating an increase in poly(A) tail length in agreement with the sequencing results (Figure 12B). *Ddx3x* showed no change in poly(A) tail length during the sequencing analysis (delta value: 0.090). The ePAT confirmed this result, since there was no visible shift in peak size between control and postovulatory-aged oocytes (Figure 12C). It also showed a decrease in transcript level of aged oocytes (control: 2.55 ng/µl; PostOA: 2.40 ng/µl). *Nupr1* showed deadenylation after aging during the sequencing experiment. We were not able to detect a signal for this transcript after postovulatory aging in two trials with 200 pooled oocytes each, probably due to a severe transcript decline upon aging (Figure 12D). Of the other 3 genes only 2 confirmed the sequencing data. Taken together with the 3 unsuccessful trials to reproduce the poly(A) sequencing experiment, it seems that this method is not reliable with the experimental set up used here. This is possibly due to the low input amount when using mammalian oocytes. Therefore, the transcriptome-wide approach was not used to investigate poly(A) tail length in preovulatory-aged oocytes.

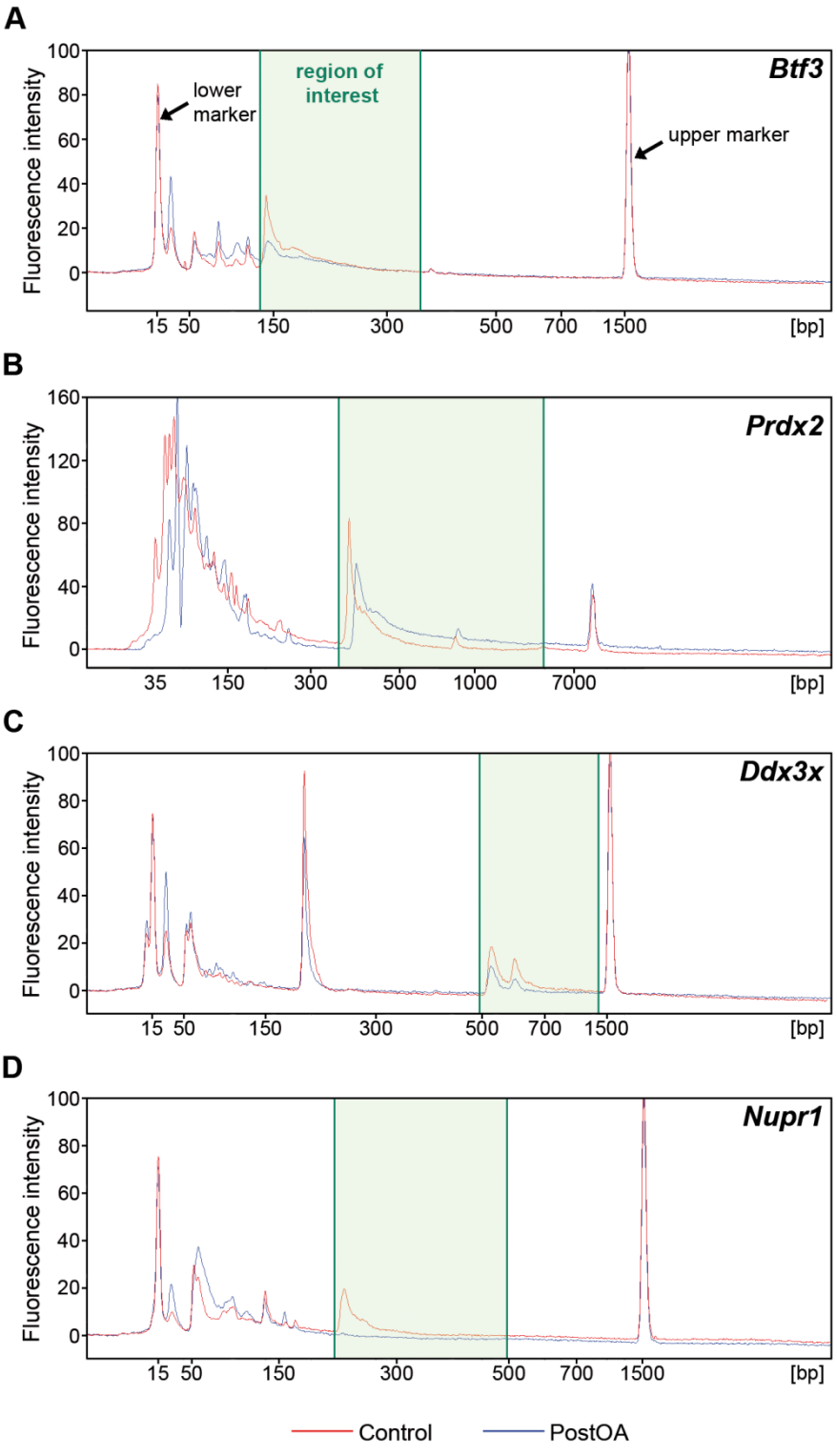

Figure 12: Poly(A) tail length of 200 pooled control and 200 pooled postovulatory-aged (PostOA) oocytes as determined by ePAT of the transcripts *Btf3* (A), *Prdx2* (B), *Ddx3x* (C) and *Nupr1* (D). Shown is the fluorescence intensity of DNA fragments as measured with an Agilent DNA 1000 chip (*Btf3*, *Ddx3x*, *Nupr1*) or DNA High Sensitivity chip (*Prdx2*). The peaks for the upper and lower marker are indicated by the arrows and the region of interest (green), containing the amplicon peak with the possible poly(A) tail. A shift in poly(A) tail length was observed only for *Prdx2*.

3.6 Fertilization rates after preovulatory aging

To analyze the developmental capacity of preovulatory-aged oocytes in comparison to control oocytes, female C57Bl/6J mice were mated either with C57Bl/6JxCBA hybrid males or CAST/EiJ males (see also 2.2.9). The hybrid males were used for mating instead of C57Bl/6J males to avoid inbred depression, which was shown to affect the fertilization rates of IVF (Dankert 2015). A mating was counted successful when the female had a vaginal plug the next morning after mating and 2-cell embryos were found in the oviduct 36 h after mating. The number of 2-cell embryos and unfertilized oocytes of every mating was recorded. The ratio of 2-cell embryos to total oocyte number found in the oviduct was defined as fertilization rate.

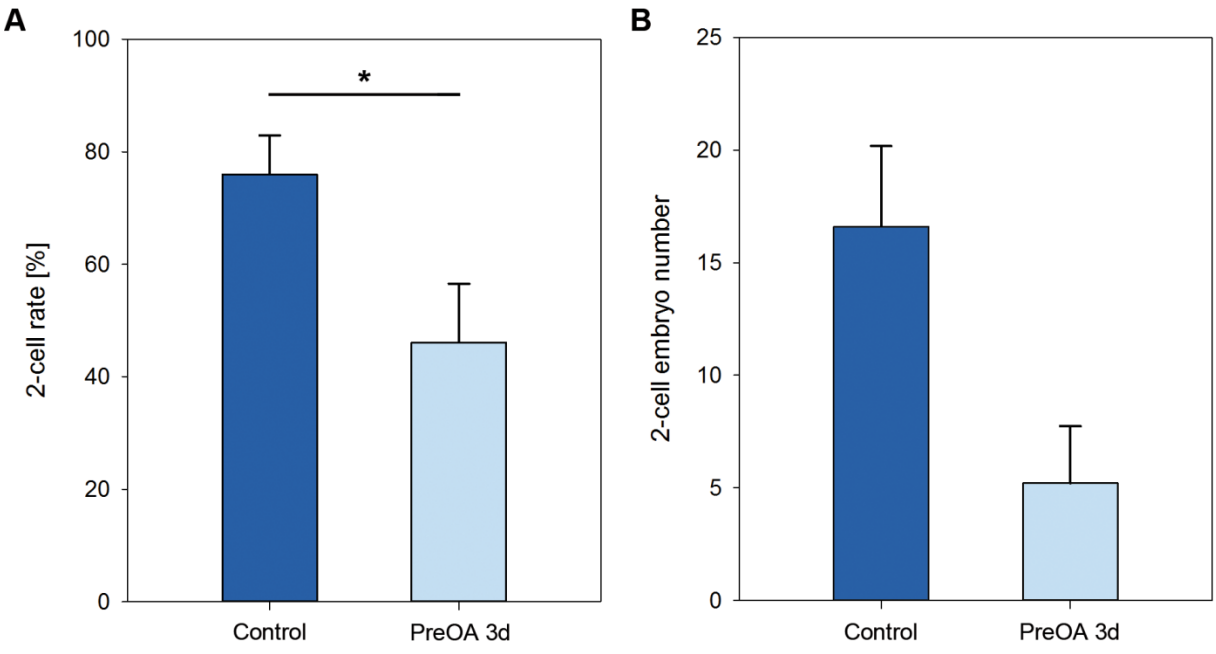

Figure 13: Two-cell rate as indicator of fertilization rate (A) and absolute number of 2-cell embryos (B) after mating of C57Bl/6J females with C57Bl/6JxCBA hybrid males. Fertilization of oocytes after 3 d of preovulatory aging (PreOA 3d) was significantly reduced after aging compared to controls as demonstrated by the decreased 2-cell rate. Also, the total number of 2-cell embryos decreased after aging. Indicated is the Mean±SEM. Control: $n = 10$, PreOA: $n = 5$, *t*-test: * $p < 0.05$.

In total, 10 of 18 control females were effectively mated with C57Bl/6JxCBA hybrid males. In contrast, only 5 of 16 matings with females with 3 d preovulatory-aged oocytes were successful. The fertilization rate of control mice lay at 76% ($n = 10$, SEM = 6.93; Figure 13A). After preovulatory aging the fertilization rate dropped significantly to 46% ($n = 5$, SEM = 10.45, *t*-test: $p = 0.0299$). This is a drop of almost one third. When looking at

total number of embryos that derived from each mating the difference between control and preovulatory oocytes was even greater: the mean embryo number derived from control embryos was 16.6 (SEM = 3.58; Figure 13B) and after preovulatory aging the number declined to an average of 5.2 (SEM = 2.54; *t*-test: $p = 0.0563$). This is a decrease of more than two third. The low number of embryos can be explained by a combination of low fertilization rates and a reduced oocyte number after preovulatory aging in vivo (see 3.1). So there are fewer oocytes available for fertilization after preovulatory aging and these oocytes seem more difficult to fertilize. Taken together, the data point to a reduced developmental competence of oocytes after 3 d of preovulatory aging.

To distinguish between paternal and maternal genetic background during the DNA methylation analysis of 8-cell embryos, males of the CAST/EiJ mouse strain were used for mating with C57Bl/6J females. Two-cell embryos were collected from the oviduct 36 h after mating. In general, the mating rate was very low: 3 out of 8 control matings and only 3 out of 21 matings after aging were successful. The fertilization rate was similar to C57Bl/6JxCBA hybrid males (control: 83% ± 11.5 SEM and PreOA 54% ± 4.1 SEM). Due to the low number of trials the difference was not significant. The number of embryos retrieved per mating was similar between the control and aged group. From control mice an average of 13 ± 3.8 SEM embryos was retrieved and after preovulatory aging the number dropped to 10 ±1.0 SEM embryos. Embryos were further cultured in vitro to the 8-cell stage. The developmental rates did not differ greatly between the 2 groups (control: 84.0%; PreOA: 88.9%). In summary, it seems that preovulatory-aged oocytes are more difficult to fertilize, but that those that are successfully fertilized develop in a similar rate as controls.

3.7 Transcription onset in 2-cell embryos

To investigate the embryonic genome activation, transcriptional activity of embryos at the 2-cell stage was assessed. At this time point the first major wave of embryonic genome activation should occur (Schultz 1993; Hamatani et al. 2004; Wang et al. 2004). Two-cell embryos derived from control and 3 d in vivo preovulatory-aged oocytes were incubated in BrUTP. During transcription BrUTP is incorporated into nascent RNA and is converted to BrU. The BrUTP incorporation into 2-cell embryos was visualized with a FITC-labeled antibody against BrU (Figure 14A). BrU was mainly present in the cell nuclei of control and aged embryos, where it was enriched in nucleoli-like structures. In embryos derived from preovulatory-aged oocytes, the BrU signal was more intense than in control embryos. The fluorescent signal of the cell nucleus was semi-quantified by Image J, normalized against

background staining and a fold change of embryos from aged oocytes in comparison to control embryos was calculated (Figure 14B). A total of 61 control embryo cells and 43 cells from embryos derived after oocyte aging were analyzed. Embryos from preovulatory aged oocytes showed a highly significant increased fold change of 2.85-fold in comparison to control embryos (Mann-Whitney U test: $p < 0.001$). This indicates a higher transcription rate in 2-cell embryos derived from aged oocytes.

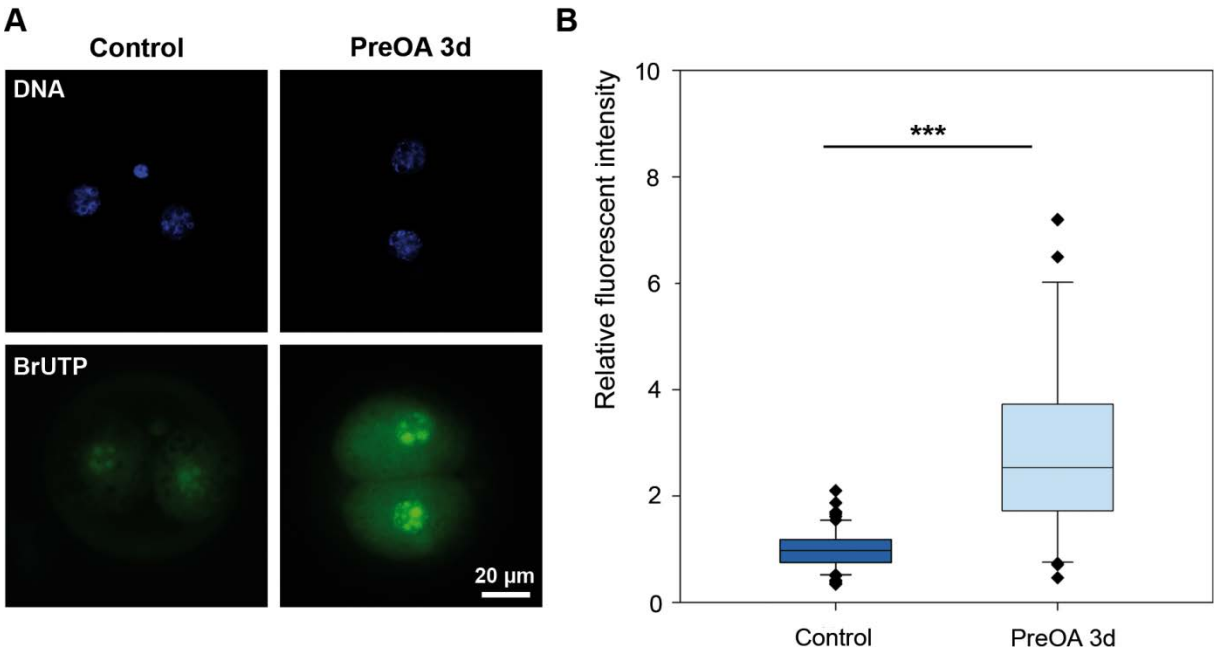

Figure 14: BrUTP incorporation in 2-cell embryos derived from control or 3 days preovulatory-aged (PreOA 3d) oocytes. A) Shown are representative 2-cell embryos derived from either control embryos or after preovulatory oocyte aging, which had been incubated in BrUTP. BrUTP is incorporated into nascent RNA during transcription and converted into BrU. DNA was stained with DAPI and BrUTP incorporation with a FITC-labeled antibody against BrU. **B)** The normalized fluorescence intensity shows a significant increase in the PreOA group in comparison to controls. Control: $n = 61$, PreOA: $n = 43$;Mann-Whitney U test: *** $p < 0.001$.

3.8 DNA methylation of imprinted genes in 8-cell embryos

Differential DNA methylation of imprinted genes is maintained throughout embryonic reprogramming. Imprint maintenance was assessed of 15 control and 14 embryos derived from preovulatory-aged oocytes by analyzing DNA methylation levels of 3 imprinted loci at the 8-cell stage (*H19*, *Snrpn*, *Igf2r*). At this time point in embryonic development all cells are still pluripotent, but the embryonic genome is already fully active. *Pou5f1* was analyzed as a control gene that should undergo reprogramming and should be fully demethylated at the 8-cell stage (El Hajj et al. 2011). Deep-amplicon bisulfite sequencing of single embryos showed indeed methylation levels of nearly 0% for *Pou5f1* for most control and preovulatory-aged embryos on both the maternal and paternal allele (Figure 15A, Supplementary Figures S1 and S2, Supplementary Table S7). Of the 3 imprinted loci analyzed *H19* is the only one with imprint methylation on the paternal allele, which was indeed observed (Figure 15B, Supplementary Figures S3 and S4, Supplementary Table S8). The amplicon included 4 CpGs, but the methylation on the paternal allele of the first CpG was unstable in both control and preovulatory-aged embryos, so it was excluded from the analysis. As expected, *Snrpn* and *Igf2r* both showed methylation of the maternal and not the paternal allele (Figure 15C and D, Supplementary Figures S5-S8, Supplementary Table S9 and S10). PCR template switching was observed on the *Snrpn* locus and, although to a lesser extent, the *H19* locus. It was not possible to observe fully methylated and fully unmethylated alleles for these loci. Therefore, for the further analysis the mean methylation levels of the maternal and paternal alleles were analyzed to compensate the template switches. In Figure 15E an example of an embryo with aberrant methylation is shown for the *Igf2r* locus. In this example the maternal allele is hypomethylated, while the paternal allele shows low methylation as expected. This hypomethylation of the maternal allele could indicate failure in imprint setting or an impairment of imprint maintenance during embryonic development.

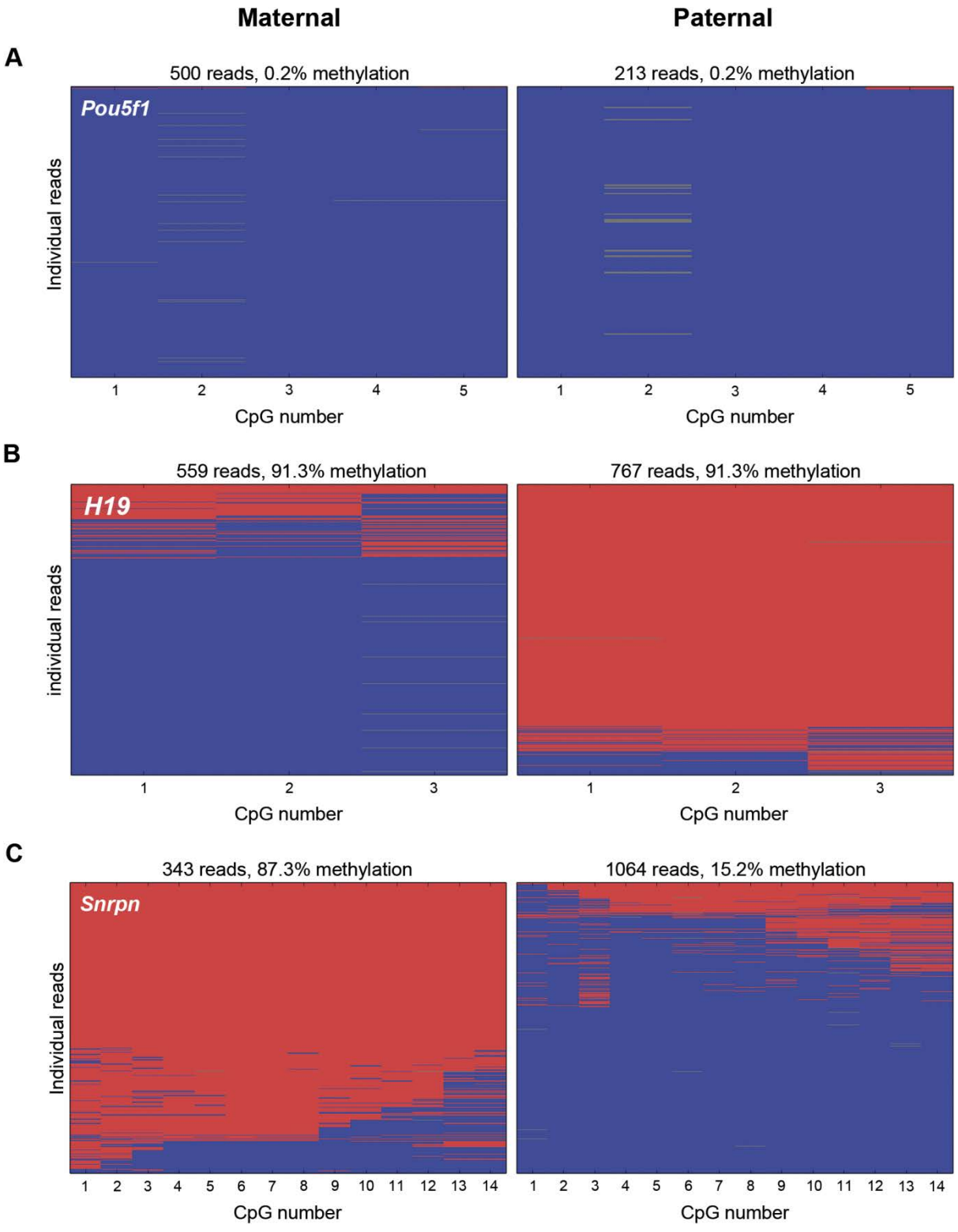
Maternal
Paternal
A
500 reads, 0.2% methylation
213 reads, 0.2% methylation
Pou5f1
Individual reads
1 2 3 4 5
CpG number
B
559 reads, 91.3% methylation
767 reads, 91.3% methylation
H19
individual reads
1 2 3
CpG number
C
343 reads, 87.3% methylation
1064 reads, 15.2% methylation
Snrpn
Individual reads
1 2 3 4 5 6 7 8 9 10 11 12 13 14
CpG number

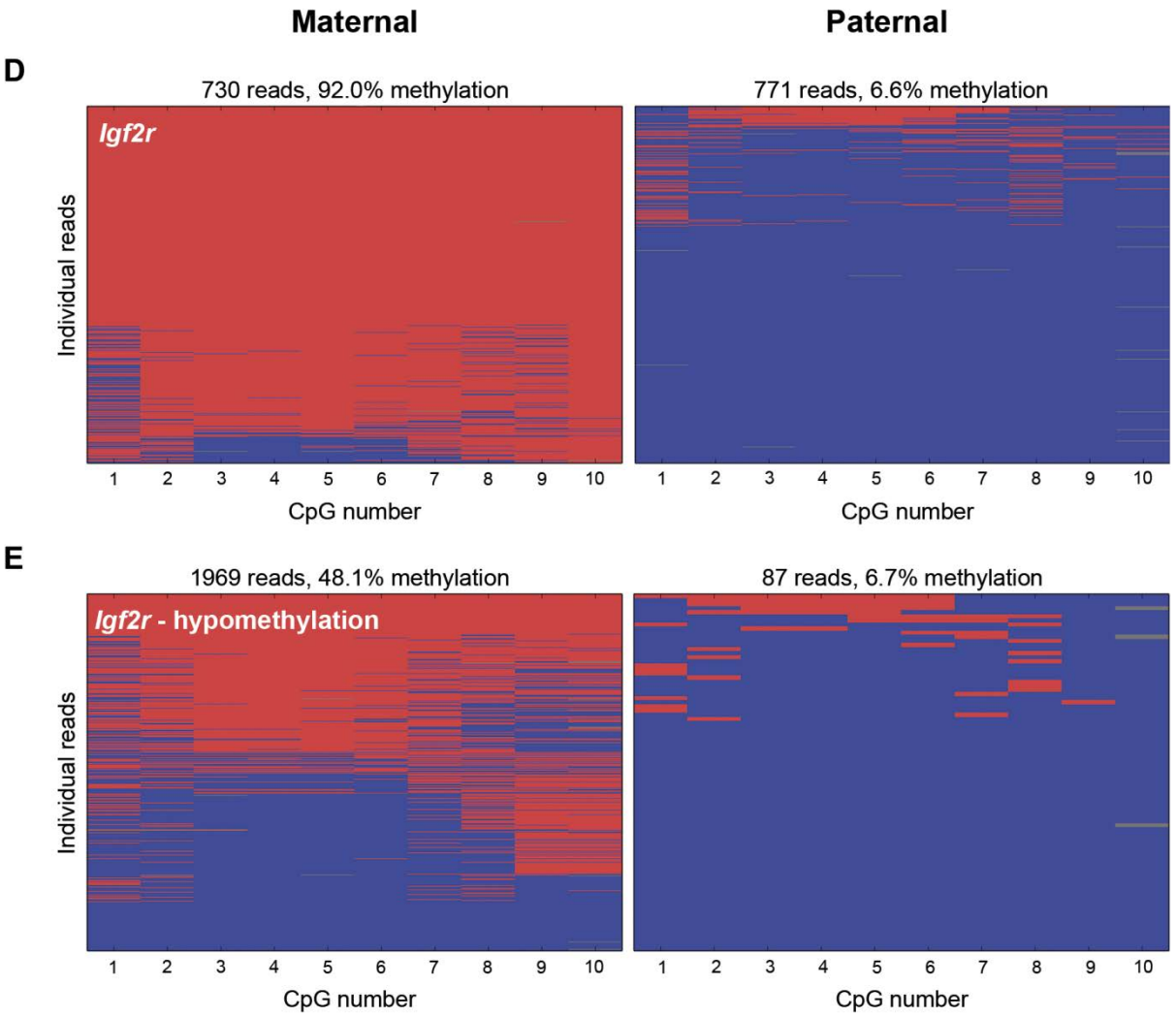

Figure 15: DNA methylation on the maternal and paternal allel for representative single 8-cell control embryos assessed by deep amplicon bisulfite-sequencing. Individual reads are shown in rows, single CpG sites are shown in columns. Methylation status for each CpG is indicated in red (methylated) or blue (unmethylated). The total number of reads and average methylation rate are shown per allele at the top of each figure. **A)** *Pou5f1* is a control gene, which was expected to be fully demethylated at the 8-cell stage. **B-D)** Three imprinted genes were analyzed: *H19*, which was expected to be paternally methylated **(B)** and *Snrpn* and *Igf2r*, which were expected to be maternally methylated **(C, D)**. **E)** An example for aberrant DNA methylation of an embryo is shown for the *Igf2r* locus where the maternal allele is hypomethylated.

The mean methylation of the maternal and paternal allele of *Pou5f1* was close to 0% for both control and preovulatory-aged embryos (Control = 6.1%; PreOA 3d = 1.4%; Figure 16A). Embryos derived from preovulatory-aged oocytes actually showed 0% methylation for all but one, whereas 8 of 15 control embryos showed methylation levels over 0%. The difference between control and aged embryos was not significant. All imprinted genes showed average methylation levels around 50% when combining the methylation levels of the maternal and paternal alleles. For *H19* the mean methylation level of control embryos was 49.6% and 46.4% for aged embryos (Figure 16B). Again there was no significant change between control

and aged embryos. Similar results were obtained for *Snrpn* (control = 42.9%; PreOA 3d = 49.8%; Figure 16C) and *Igf2r* (control = 47.6%; PreOA 3d = 47.5%; Figure 16D).

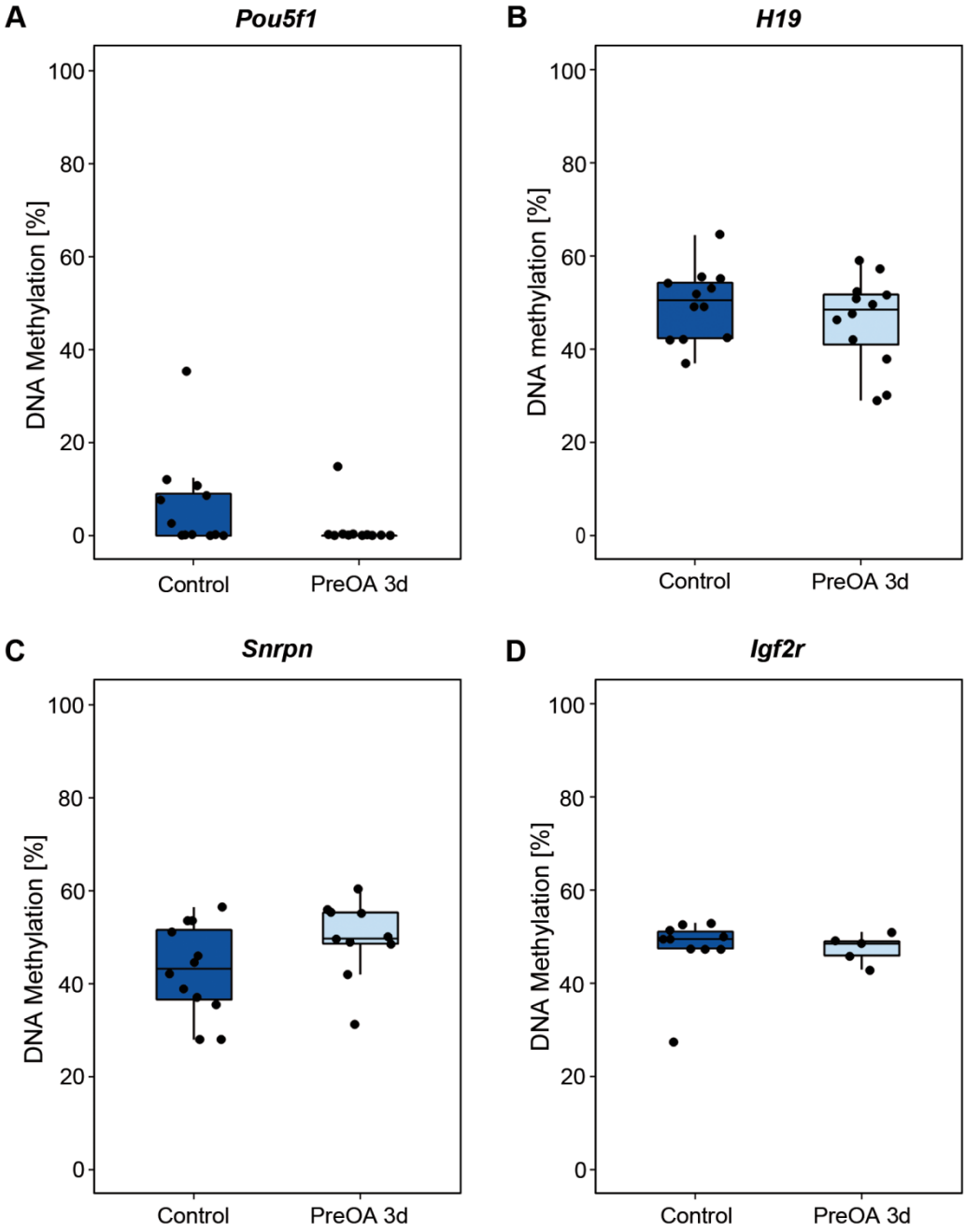

Figure 16: DNA methylation levels in embryos of control and 3 d preovulatory-aged (PreOA 3d) oocytes. Boxplots indicate the mean methylation levels of the maternal and paternal allele, which for *Pou5f1* **(A)** lies close to 0% and for the imprinted genes *H19* **(B)**, *Snrpn* **(C)** and *Igf2r* **(D)** around 50%. Dots visualize the mean methylation level for single embryos. No significant differences were observed between control and aged embryos for any of the investigated loci. Control: n = 15, PreOA: n = 14.

To determine the number of embryos with aberrant methylation, mean methylation levels of single embryos were assessed and an embryo with over 10% divergence from the expected methylation was defined as having methylation impairment. For *Pou5f1* 3 of 15 analyzed control embryos and 1 of 12 analyzed preovulatory-aged embryos showed aberrant methylation of over 10% (Figure 17A). This is not a big difference but more control than preovulatory-aged embryos showed a methylation failure, which is in line with the higher mean methylation level observed for the control group. For *H19* more embryos of aged oocytes with a methylation failure were detected (control: 2/13; PreOA 3d: 3/14; Figure 17B). *Snrpn* was the locus where most embryos with aberrant methylation were found: 5 of 15 control embryos and 2 of 14 embryos from preovulatory-aged oocytes had mean methylation levels below 40% or above 60% (Figure 17C). No embryos of preovulatory-aged oocytes showed methylation abnormalities for *Igf2r* and only 2 of 15 control embryos displayed abnormal methylation on this locus (Figure 17D).

Overall, there were no clear differences between the number of embryos with methylation aberrations of the control and preovulatory-aged group. This is consistent with a lack of significant differences in average methylation levels between the two groups. These results demonstrate that preovulatory aging does not affect DNA methylation of the 4 analyzed genes.

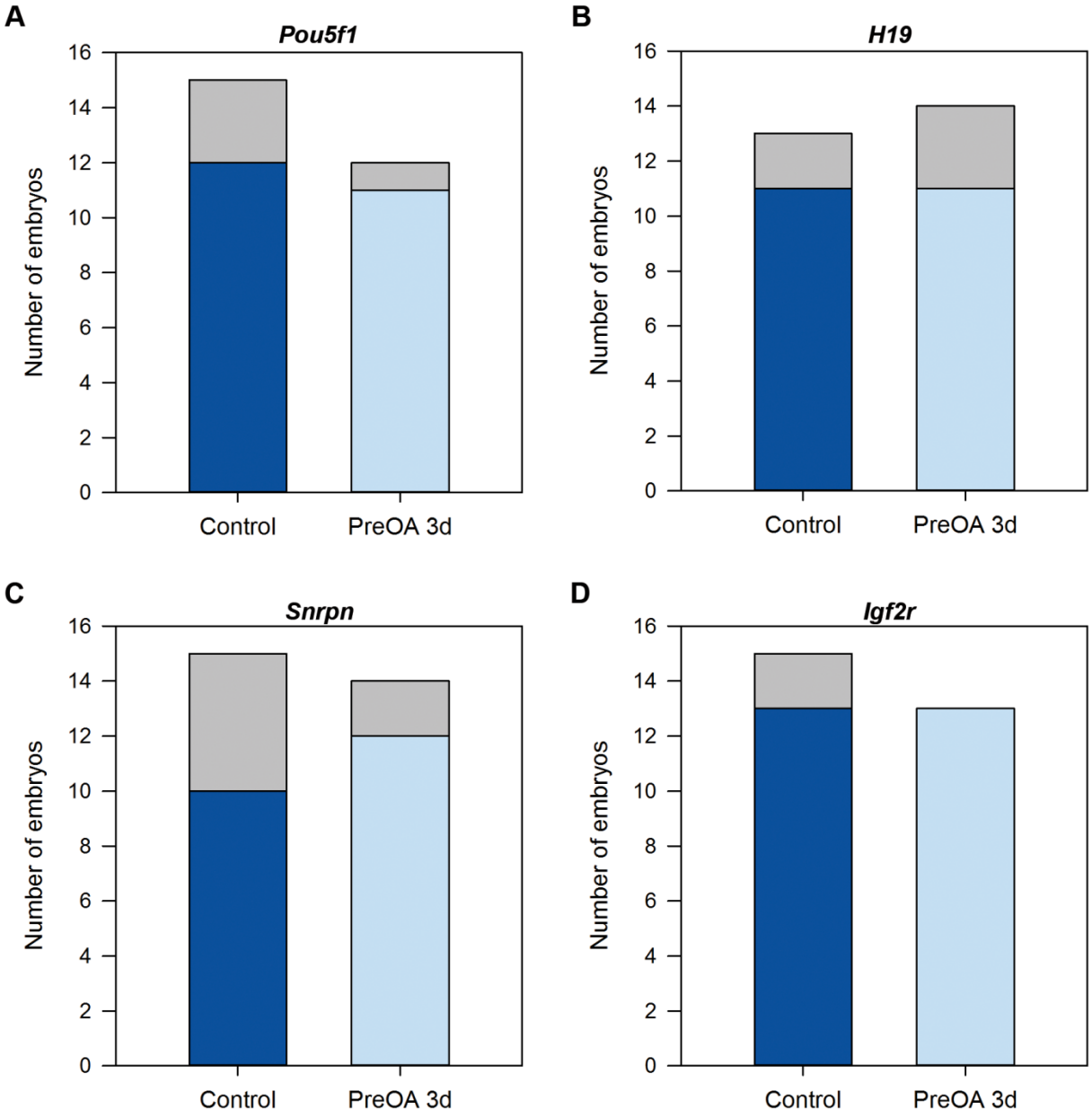

Figure 17: Number of embryos with aberrant methylation levels derived from control or 3 d preovulatory-aged (PreOA 3d) oocytes. The number of analyzed embryos is shown, with embryos with impaired methylation levels indicated in grey for *Pou5f1* **(A)**, *H19* **(B)**, *Snrpn* **(C)** and *Igf2r* **(D)**. No clear effect of aging on methylation failure can be observed.

4 Discussion

Growth and maturation of the mammalian oocyte are tightly regulated and perturbations of these processes can have severe effects on the developmental potential of the oocyte. The present study focused on the molecular effects of prolonged oocyte maturation known as preovulatory aging. Hardly anything is known about this form of oocyte overripeness making this study to the most detailed analysis about the molecular mechanisms of preovulatory aging so far. An in vivo mouse model was used in which ovulation was delayed with the GnRH antagonist cetrorelix. The effects of delayed ovulation on RNA storage potential, transcript levels and poly(A) tail length, as well as on epigenetic histone modifications were investigated in oocytes. To assess the developmental capacity of the preovulatory-aged oocytes several aspects of early embryonic development were analyzed. It was found that certain but not all processes were impaired by preovulatory aging demonstrating that there is a distinct regulation of these processes.

4.1 Preovulatory aging reduces oocyte number and fertilization rates

Ovulation is a critical step in each menstrual cycle. Since preovulatory aging is caused by deregulation of the menstrual cycle it was interesting to see if it would interfere with oocyte maturation. Furthermore, fertilization rates were determined to investigate the quality and developmental potential of oocytes after preovulatory aging.

4.1.1 Effects of cetrorelix on oocyte numbers during regular menstrual cycles

The cetrorelix mouse model of the present study is the first in vivo model for preovulatory aging induced by hormonal manipulation of the menstrual cycle. The GnRH antagonist cetrorelix suppresses gonadotropins during ovarian stimulation and thus prevents a premature LH surge. It has found broad application in human assisted reproductive techniques (ART). Before the introduction of GnRH antagonists GnRH agonists were used in ART to diminish gonadotropins during ovarian stimulation. Over 200 studies have compared the benefits and disadvantages of both protocols with conflicting results. Meta-analyses found lower oocyte numbers as well as slightly reduced pregnancy rates using a GnRH antagonist protocol (Al-Inany 2007; Al-Inany et al. 2011). The reduced oocyte numbers are in line with the results of the present study. Since the difference in pregnancy rate between the two protocols did not differ much, and antagonists have many benefits such as a shorter treatment period and less side-effects in comparison to agonists they are still widely used (Depalo et al. 2012).

It is not known why GnRH antagonists lead to a lower number of oocytes. Since in human ART oocytes are not ovulated but retrieved directly from the ripe follicles, the antagonist is likely to affect oocyte maturation before ovulation. Antagonists bind competitively to GnRH receptors and directly prevent GnRH to stimulate the pituitary cells to produce gonadotropins. This leads to a deep suppression of LH secretion, which has been proposed to affect follicle maturation and oocyte ripening. Indeed, it is known for another antagonist, ganirelix, that with increasing antagonist dosage the LH and estrogen levels drop and implantation and ongoing pregnancy rates decline (The ganirelix dose-finding study group 1998). However, studies trying to overcome this problem by LH substitution showed no effect on oocyte retrieval or embryo numbers and pregnancy or delivery rate, which contradicts this hypothesis (Aboulghar et al. 2004; Cedrin-Durnerin et al. 2004; Baruffi et al. 2007). Another postulated explanation for the observed effects in humans is that not the absolute LH levels are associated with low pregnancy rates after GnRH antagonist treatment but the large changes in LH levels during treatment. Oocyte maturation could also be affected by FSH suppression during cetrorelix treatment. In the present study, control mice that did not receive cetrorelix secreted intrinsic FSH next to injected PMSG that supports follicle and oocyte development. In case that these intrinsic hormone levels are suppressed due to cetrorelix this might lead to recruitment of fewer follicles and therefore to lower oocyte numbers at the time point of ovulation.

In order to study the influence of intrafollicular aging rather than suppression of LH, the control mice in the present study received cetrorelix but were stimulated to ovulate without delay. Nevertheless, it cannot be excluded that the effects seen in the in vivo model for preovulatory aging are at least partly an effect of prolonged cetrorelix treatment instead of prolonged ripening.

4.1.2 Effects of preovulatory aging on oocyte numbers

In line with previous studies in other vertebrate species including studies in rodents and humans (Smits et al. 1995), a decrease in number of ovulated oocytes after preovulatory aging was observed. These oocytes were of good quality as no increase in the number of degenerated oocytes was observed. However, degeneration of oocytes could occur before ovulation and lead to oocyte death in atretic follicles. Another possibility is that less oocytes ovulate due to maturation or growth arrest during preovulatory aging in the ovary. Both theories are supported by data on preovulatory aging in the in vitro follicle culture system revealing an increase of maturation arrest and oocyte degeneration, which correlated with a

decreased percentage of maturated MII oocytes (Demond et al. submitted). In comparison to control oocytes, more preovulatory-aged oocytes arrested in the germinal vesicle stage or were not able to complete germinal vesicle breakdown during meiosis I. It is likely that such a developmental arrest also occurs during in vivo preovulatory aging and that these arrested oocytes retain in the ovary upon induction of ovulation due to e.g. deregulated folliculogenesis, granulosa cell maturation or cumulus expansion.

4.1.3 Effects of preovulatory aging on fertilization

Not only ovulation but also fertilization was affected by preovulatory aging as indicated by a decrease of the 2-cell embryo rate after preovulatory aging from 76% to 46%. Similar results have been published for rats where preovulatory aging lowered the fertilization success as well (Fugo and Butcher 1966). The difference of total number of 2-cell embryos retrieved after in vivo preovulatory aging in comparison to controls was even more striking; decreasing from an average of 16.6 to 5.2 embryos per mouse. This major decline is likely due to a combination of the lower oocyte numbers that ovulate and lower fertilization rates after preovulatory aging.

In addition to preovulatory aging, also postovulatory aging that starts after ovulation is known to affect fertilization rates. The optimal time window for fertilization in the mouse lies between 8 and 12 h after ovulation (Austin 1974). If fertilization is delayed the oocyte starts to degenerate and fertilization rates reduce. For example, in vivo fertilization of postovulatory aged-oocytes 21-25 h after hCG application decreased the 2-cell rate significantly (Marston and Chang 1964). Using in vitro fertilization, no effect on fertilization rates was observed after postovulatory aging for up to 8 h (Dankert 2015). However, after 13 h the fertilization rates had previously been shown to drop and after 24 h no fertilization seems to be possible (Lacham-Kaplan and Trounson 2008). The present study shows that degeneration of the oocyte does not only happen after ovulation but can also happen before, when ovulation is delayed, having similar consequences for fertilization. However, the time frame in which aging occurs is different before ovulation than after considering that fertilization was still possible after 3 d of preovulatory aging. So in the ovary the oocytes seem to be more protected.

4.2 Stable H3K9 trimethylation in preovulatory-aged oocytes

The reduced fertilization rates after preovulatory aging point to an impaired oocyte quality and developmental potential. Therefore, several aspects were addressed in the following to search for possible causes for the reduced quality of preovulatory-aged oocytes.

Trimethylation of H3K9 is an epigenetic histone modification which occurs during oocyte growth (Kageyama et al. 2007). It is a chromatin repressive mark required for genome stability and thought to be associated with transcriptional silencing in the maturating oocyte and (Peters et al. 2001, Kageyama et al. 2007). H3K9me3 was first discovered to be mainly present in constitutive heterochromatin but recent work has found that it plays a key role in cell differentiation (Becker et al. 2016). After preovulatory in vivo aging no effect on H3K9me3 levels was observed. This is in contrast to in vitro preovulatory aging in follicle culture where a decrease after aging was found (Demond et al. submitted). Also other forms of oocyte overripeness show effects on H3K9me3. Postovulatory aging shows a similar decline in H3K9me3 levels as in vitro preovulatory aging (Trapphoff et al. 2010). Maternal aging of mice has an even more severe impact on H3K9me3 and can lead to complete depletion of methylation marks (Manosalva and Gonzalez 2010; Van den Berg et al. 2011). Absence of H3K9me3 leads to genome instability, chromosome disruption during meiosis and methylation deficiency (Peters et al. 2001). It was indeed found that H3K9me3-deficient vitro preovulatory-aged and postovulatory-aged oocytes had an increased rate of chromosome misalignments (Trapphoff et al. 2015; Demond et al. submitted). For comparison, it would be interesting to investigate chromosome alignment and spindle formation of in vivo preovulatory-aged oocytes in subsequent studies. Overall the studies show differences between pre- and postovulatory aging and between the in vivo situation and the follicle culture system. Methylation of H3K9 might be better protected in the ovary than in vitro.

4.3 Loss of Ybx2 protein levels may impair RNA storage potential

Ybx2 is a germ cell specific RNA binding protein, required for mRNA storage and poly(A) tail stability in the oocyte (Gu et al. 1998; Medvedev et al. 2011). After preovulatory aging transcript levels of *Ybx2* tended to decrease even though not significantly due to a high sample variation between the oocyte pools. A similar variation was observed during qPCR analysis of maternal effect genes. It appeared that there is a high variation between single oocytes in transcript levels and that it might be better to increase the oocyte number of the pools or to analyze more pools.

The tendency of decreased transcript levels was supported by a significant decline in protein levels of Ybx2 after preovulatory aging. Also, after postovulatory aging a decrease in Ybx2 mRNA and protein levels has been described and a relocation of Ybx2 protein in the cell was observed (Trapphoff et al. 2015). Normally, Ybx2 is localized in the cytoplasm where it is enriched in the subcortical RNP domain (SCRD; Flemr et al. 2010). There it co-localizes with poly(A)-mRNA, the RNA helicase Ddx6 and Edc4, a component of cytoplasmic RNA granules (also known as P-bodies; Flemr et al. 2010). Ybx2 is not located in the chromosome-spindle-complex except for the proximal kinetochore area of the chromosomes (Trapphoff et al. 2015). After postovulatory aging Ybx2 protein localization was disturbed and was enriched in the center of the ooplasm. In the current study Ybx2 did not show a reallocation but a general loss in protein abundance in preovulatory-aged oocytes.

The loss in Ybx2 protein levels after preovulatory aging might have a serious impact on RNA storage potential. Ybx2 is one of the most abundant proteins in the oocyte and loss of Ybx2 leads to alterations of the entire transcriptome and failure in transcriptional silencing and ultimately results in infertility (Yang et al. 2005; Medvedev et al. 2011). Following germinal vesicle breakdown during oocyte maturation Ybx2 protein is phosphorylated by the Cdc2a kinase, which in turn leads to mRNA instability and the maturation-associated degradation of mRNAs in the oocyte (Medvedev et al. 2008). This transcript instability is associated with translation of factors needed for the oocyte-to-embryo transition. Following fertilization the amounts of *Ybx2* mRNA and Ybx2 protein decrease such that little Ybx2 protein is detected in 2-cell embryos (Yu et al. 2001). It could be possible that the observed decline in Ybx2 protein levels in preovulatory-aged oocytes is a consequence of precocious dephosphorylation and degradation.

4.4 Preovulatory aging affects poly(A) tail length and expression of maternal effect genes

Disturbances of maternal effect (ME) genes affect oocyte quality. Since the reduced Ybx2 levels might affect mRNA and poly(A) tail stability after preovulatory aging, transcript levels and poly(A) tail length of selected ME genes were analyzed. ME genes are of special importance for the developmental potential since they encode transcripts that are expressed in the oocyte but function in the early embryo (Li et al. 2010). Expression levels and poly(A) tail length of ME genes in preovulatory-aged oocytes derived in vivo and in follicle culture were assessed by qRT-PCR. The results of the poly(A) tail length analysis by comparison of random hexamer and oligo(dT)-primed cDNA was confirmed using an ePAT analysis for

Zar1 and *Dnmt1* in postovulatory-aged oocytes (Dankert et al. 2014). In postovulatory-aged oocytes the poly(A) tail length of *Zar1* showed no significant effect, whereas *Dnmt1* showed a decrease in length. The results of the ePAT were in line with the qRT-PCR data, indicating that the method is reliable.

4.4.1 Polyadenylation of transcripts after preovulatory in vivo aging

After preovulatory aging of in vivo matured oocytes mRNA levels of *Smarca4* and *Tet3* were significantly reduced. This is likely to disturb protein levels that could affect chromatin remodeling and DNA demethylation in the course of embryonic genome reprogramming and activation (Bultman et al. 2006; Gu et al. 2011). Loss of transcript could therefore affect the embryonic genome activation. *Zfp57* mRNA levels tended to decrease as well although not significantly. Loss of *Zfp57* expression is known to interfere with DNA methylation maintenance of imprinted genes during epigenetic reprogramming in the preimplantation embryo (Li et al. 2008b).

It was surprising to see a tendency towards increased poly(A) tail length of most investigated ME genes in oocytes after in vivo preovulatory aging. An increased poly(A) tail length has also been previously described for *BUB1B* and *MAD2L1* transcripts in in vitro-matured human oocytes with a low developmental competence (Jones and Cram 2013). These two genes encode spindle and cell cycle regulating factors. In contrast, postovulatory aging from in vivo-matured oocytes is associated with a decrease in poly(A) tail length for many genes in both *Xenopus* and mice (Kosubek et al. 2010; Dankert et al. 2014). The poly(A) tail length is an important regulator of posttranscriptional control during oocyte maturation when transcription is repressed (Weill et al. 2012). During oocyte growth, mRNAs accumulate in the ooplasm. To store them in a dormant state, the poly(A) tail is shortened, which leads to translational repression of the transcripts. When the transcripts need to be recruited for protein translation during oocyte maturation, the poly(A) tail can be elongated again through a process known as cytoplasmic polyadenylation. The best investigated mechanism of cytoplasmic polyadenylation is mediated by CPEB, which binds to the CPE (Figure 2; McGrew et al. 1989, Gebauer et al. 1994). Of the 10 selected ME genes only *Brg1*, *Tet3* and *Dnmt1* contain a CPE in their 3'UTR (Dankert et al. 2014). Since these 3 genes all show a trend towards an increased poly(A) tail length after preovulatory in vivo aging, it is likely that CPE-dependent polyadenylation occurred in these cases. However, this cannot be the only mechanism working in preovulatory-aged oocytes since also other transcripts without a CPE showed polyadenylation.

The qRT-PCR analysis showed a high standard variation between the oocyte pools resulting in significant changes in poly(A) tail length for only few genes. But a concordant effect of poly(A) tail status was seen for almost all investigated genes supporting that the effects observed are reliable. The results indicate that prolonged meiotic arrest may cause increased re-adenlyation of mRNAs during preovulatory aging. This might be a signal for precocious recruitment of transcripts for translation in the preovulatory-aged oocytes, which would fit with the loss of Ybx2 protein levels. It is important to analyze in subsequent studies whether the increased polyadenylation after preovulatory in vivo aging also results in increased protein levels, which could explain the reduced oocyte quality in this mouse model.

4.4.2 Preovulatory in vitro aging affects transcript levels

The current results show that ME genes are distinctly regulated and transcript levels of the selected genes react differently to preovulatory aging in vitro. Transcript levels of *Dnmt3a*, *Dnmt3l* and *Zfp57* have previously been shown not to be affected in in vitro-matured mouse oocytes (Anckaert et al. 2013b). This is in is in agreement with the present study that also did not show any significant changes in *Zfp57* mRNA levels after preovulatory aging in the in vitro follicle culture system. However, in the present study the in vitro follicle culture model in vitro preovulatory-aged oocytes showed a significant decrease in transcript levels for *Trim28*, *Nlrp2*, *Nlrp 14* and *Zar1*, and a similar trend for *Nlrp5*. Trim28 protein interacts with Zfp57 and is also required in imprint maintenance during early embryonic development (Messerschmidt et al. 2012). It is not exactly known how *Nlrp2* and *Nlrp14* function in the oocyte, but both are needed for embryonic development past the 2-cell stage (Horikawa et al. 2005; Peng et al. 2012). In humans, mutations in *NLRP2* and *NLRP7* are responsible for imprinting defects (Murdoch et al. 2006; Meyer et al. 2009). It remains to be determined whether murine Nlrp proteins might have similar functions.

Nlrp5 showed a decrease in total transcript levels in preovulatory-aged in vitro-grown MII oocytes compared to controls. A similar reduction was also observed for Nlrp5 protein abundance of in vitro preovulatory-aged GV oocytes (Demond et al. submitted). Although the abundance of this protein was not analyzed in MII oocytes, the decrease found at GV stage suggests a perturbation of the normal expression pattern of Nlrp5 before ovulation that may also affect preimplantation embryogenesis after fertilization. The same study found Smarca4 protein levels to be altered as well. Here, an increase in protein abundance was observed at GV stage. In contrast, the MII transcript-data did not show an effect of preovulatory aging on *Smarca4* mRNA levels. This could mean that transcript expression levels or polyadenylation

status are not directly predictive for abundance of a protein, which is supported by data on transcript and protein expression after postovulatory aging (Dankert et al. 2014; Trapphoff et al. 2015). However, the comparison of GV protein levels and MII transcript levels has to be regarded with caution. It cannot be ruled out that transcript and protein levels change during the transition from GV to MII stage. It would therefore be interesting to investigate protein levels in MII in vitro-grown oocytes to have a direct comparison of transcript and protein expression after preovulatory aging in vitro.

The present data demonstrates clear differences between in vivo and in vitro preovulatory aging of oocytes. This is in line with a study by Sanchéz and colleagues (2009) who found reduced total transcript levels for *Bmp15*, *Gdf9*, *Nlrp5*, *Zar1* and *Fgf8* in immature in vitro-grown oocytes in comparison to in vivo-grown oocytes. The current study also analyzed *Zar1* transcript levels, which is an oocyte specific gene involved in syngamy (Wu et al. 2003). A decrease in total transcript levels of *Zar1* was observed after preovulatory aging in vitro. Furthermore, *Zar1* showed a trend towards an increased poly(A) tail length. This tendency was observed for other genes as well, which is in accordance with the data on preovulatory in vivo aging. However, polyadenylation was observed less consistently in vitro than in vivo and not for the same genes. Along with the differences in total transcript levels between the in vivo and the in vitro mouse model, environmental factors seem to influence mRNA stability and poly(A) tail length in the oocyte and are different in the ovary compared to follicle culture. Indeed, oocytes from follicle culture are still of lower quality than in vivo-matured oocytes even though culture methods improved (Smitz et al. 2010).

4.5 Transcriptome-wide analysis of poly(A) tail dynamics

It was aimed to establish a poly(A) RNA sequencing analysis to investigate the poly(A) tail dynamics during oocyte aging on a transcriptome-wide level. For this, a method described by Meijer and coworkers was adapted (Meijer et al. 2007). Meijer separated RNA from 10 *Xenopus* oocytes into 6 fractions of increasing poly(A) tail length, which was verified by urea polyacrylamide gel electrophoresis. In the present study, this method was adapted for 200 mouse oocytes using oligo(dT) Dynabeads for separation of the RNA. Elution of 200 control oocytes into 4 fractions was successfully analyzed by ePAT for *Zar1* and *Dnmt1*, demonstrating an increase in poly(A) tail length in the fractions when eluting in buffers of decreasing salt concentration (Dankert 2015). Subsequently, transcriptome-wide sequencing analysis was used investigate an effect of postovulatory aging on mammalian oocytes. A transcriptome-wide decrease of polyadenylated transcripts had been previously described for

Xenopus but not mammalian oocytes (Kosubek et al. 2010). Since postovulatory aging coincides with a decrease in total RNA levels, the transcriptome was separated in only 3 fractions with different poly(A) length (unbound -poly(A) mRNA, oligoadenylated mRNA and polyadenylated mRNA) to maximize the RNA amount in each fraction. As normalization of the data was still difficult it was only distinguished between -poly(A) RNA and +poly(A) RNA for the final analysis. A decrease in poly(A) tail length was observed for the majority of genes after postovulatory aging, which is in line with the study on *Xenopus* oocytes (Kosubek et al. 2010). It was recently described for immature bovine oocytes that transcripts required for early embryonic development are predominantly deadenylated (20-50 adenosines), whereas the majority of RNAs associated with short-term processes for meiotic resumption or cell survival have a long poly(A) tail of over 200 adenosines (Gohin et al. 2014). A gene ontology analysis of transcripts with a poly(A) tail length that changes during postovulatory aging did not reveal an enrichment for certain processes or biological functions in the current study.

Unfortunately, it was not possible to repeat the analysis. Three consecutive trials failed due to low RNA quality of the libraries or because there were problems with the normalization. It is possible that the RNA amount of 200 oocytes is not enough when using postovulatory-aged oocytes, due to the loss of maternal RNAs that has been described for this form of aging (Kosubek et al. 2010). Indeed, the RNA sequencing analysis showed less reads in fractions from postovulatory-aged oocytes than controls.

Another possibility is that the external *Luciferase* RNA was not an optimal reference. An external reference RNA was needed because internal reference genes, often referred to as house-keeping genes, were not suitable as a standard for two reasons: 1) the expression level of housekeeping RNAs might be affected by the aging process and 2) their poly(A) length might differ after aging, which would affect the fractionation. This is why synthetic *Luciferase* RNA with a standardized poly(A) tail length of 30 adenosines was chosen as a reference in the present study. To ensure that each fraction contained the same amount of *Luciferase* RNA it was added after fractionation and before the library generation. However, working with such limited material increases the risk for biases when adding a reference manually. A recent study overcame this problem by using several synthetic mRNA-like standards each with a different poly(A) tail length (Subtelny et al. 2014). Even though a different approach was used to analyze the poly(A) tail length on a transcriptome-wide level such a cocktail of references might have been useful for the present study as well, since it would be possible to add the mixture before fractionation. This might help to increase the

repeatability of the present experiment and with that the reliability of the results in combination with a higher number of oocytes as input especially after postovulatory aging.

4.6 Preovulatory aging leads to precocious embryonic genome activation

Since the results discussed so far showed that preovulatory aging affects RNA storage potential, expression and poly(A) tail length, the developmental competence of aged oocytes was analyzed. The results from the current as well as previous studies on fertilization rates already indicated that the developmental competence might be affected (see 4.1.3 and Smits et al. 1995). Early embryonic development depends greatly on transcripts and proteins of ME genes that are stored in the oocyte (Li et al. 2010). With the start of embryonic genome activation, these maternal factors are replaced by embryonic factors to ensure development beyond the 2-cell stage (Minami et al. 2007). But the first waves of embryonic genome activation still depend majorly on maternal factors (Hamatani et al. 2007). *Tet3* and *Smarca4*, two ME genes involved in processing of the parental genomes, showed decreased transcript levels after preovulatory aging (Gu et al. 2011, Bultman et al. 2006). Therefore, it was interesting to see if the embryonic genome activation at the 2-cell stage would be also affected.

Transcription at the first major wave of embryonic genome activation was assessed by BrUTP incorporation into 2-cell embryos. BrUTP is a nucleotide analog that is incorporated into nascent RNA of transcriptionally active cells. BrUTP was detected in nucleoli-like structures of both control and preovulatory-aged embryos. In the nucleoli rRNA is synthesized starting from the 2-cell stage (Knowland and Graham 1972). The majority of total RNA consists of rRNA, which may explain that most transcriptional activity was found in this nuclear compartment. The results are in conflict with a previous study that detected BrUTP mainly in the nucleus and observed only minor signals in the nucleoli (Inoue et al. 2012). Inoue and colleagues therefore suggested that BrUTP is mainly incorporated by RNA polymerase II. Another study though has detected incorporation of BrUTP by RNA polymerase I, which transcribes rRNA in the nucleoli (Wansink et al. 1993). This is in line with the present results.

Surprisingly, an increase in transcription, as measured by BrUTP incorporation, was observed in 2-cell embryos that derived from preovulatory-aged oocytes compared to controls. One explanation could be that the cell cycle is disturbed after preovulatory aging. The initiation of transcription correlates with DNA replication and it was thought that embryonic genome activation might be triggered by DNA replication at the zygote stage (Aoki et al. 1997).

However, cleavage of the zygote seems to be independent of transcription since transcription continues to increase when cleavage is inhibited (Aoki et al. 1997). Therefore, it is more likely that the increase of transcription after preovulatory aging indicates a premature activation of the zygotic genome prior to the 2-cell stage. Similar evidence is found for postovulatory-aged oocytes. After 4 h of postovulatory aging an increase in transcriptional activity has been described (Dankert 2015). In the case of postovulatory aging more facts are known supporting the hypothesis of precocious transcription. It has been shown that postovulatory aging of 22 h leads to a transcriptional activation, resumption of the cell cycle and release of cortical granules in absence of fertilization (Xu et al. 1997). Furthermore, the protein synthesis of factors required for embryonic genome activation is increased in the postovulatory-aged oocyte (Wang and Latham 1997).

Thus, after postovulatory aging the oocyte initiates events of egg activation, which might explain the premature transcriptional activation observed. Similar effects might occur after preovulatory aging, which is also supported by the altered Ybx2 protein expression and the polyadenylation of ME effect genes observed in the present study. Both the data on pre- and postovulatory aging together suggest that many processes, such as translation of transcripts in the oocyte or embryonic genome activation, are regulated in a continuous, time-dependent manner. If events such as ovulation or fertilization are delayed these processes do not adapt to this delay, which leads to a desynchronization and impairment of oocyte quality with potentially long-term effects on reproductive success and longevity of the offspring (Tarin et al. 2002).

4.7 Stable imprint maintenance after preovulatory aging

Embryonic genome activation is a highly regulated process during early embryonic development, which depends on reprogramming of the parental genomes (Messerschmidt 2012). The decrease in mRNA expression of the ME genes *Tet3* and *Smarca4* together with the increased transcriptional activity provide evidence that preovulatory aging disturbs the epigenetic reprogramming processes. Another interesting aspect is that transcript levels of *Zfp57* tended to decrease after preovulatory aging.

Zfp57 is an ME gene involved in the DNA methylation maintenance of imprinted genes but also in the acquirement of methylation imprints (Li et al. 2008b). In humans loss-of-function mutations in the *ZFP57* gene are associated with hypomethylation at multiple imprinted regions in individuals affected by transient neonatal diabetes (Mackay et al. 2008). In mice

maternal Zfp57 protein is present all the way throughout embryonic preimplantation development (Li et al. 2008b). The embryo itself also expresses Zfp57 and both the maternal and the embryonic protein are required for full maintenance of differential DNA methylation at ICRs (Li et al. 2008b). Zfp57 protein binds to a hexanucleotide sequence that is found in all mouse ICRs, which would explain its specific maintenance function of differentially methylated loci (Quenneville et al. 2011). Zfp57 seems to have a second function in imprint establishment, at least at the *Snrpn* ICR: Loss of oocyte *Zfp57* in mice leads to failure in maternal imprint establishment during oocyte growth. This loss can be compensated by expression of zygotic *Zfp57* leading to a gain of methylation during embryonic development at the ICR of *Snrpn.* Zfp57 protein binds directly to the *Snrpn* ICR (Li et al. 2008b). Thus, a decrease in *Zfp57* expression after preovulatory aging might affect DNA methylation levels during preimplantation development.

Therefore, the current study investigated the methylation levels of 3 imprinted genes (*H19*, *Snrpn*, *Igf2r*) and 1 unmethylated gene (*Pou5f1*) at the 8-cell stage. DNA methylation of single embryos was analyzed using deep-amplicon bisulfite sequencing. The data indicate a stable maintenance of DNA methylation at the investigated imprinted loci as well as successful demethylation of *Pou5f1* during epigenetic reprogramming in embryos from preovulatory-aged oocytes. The lower transcript levels of *Zfp57* after preovulatory aging seem not to interfere with imprint establishment or maintenance. The transcript expression of *Zfp57* was lowered by half, which might still be sufficient for stable imprint maintenance. It is also unknown if the decrease in transcript level of *Zfp57* is reflected in protein levels. Furthermore, it was shown that loss of maternal *Zfp57* can be partly rescued by embryonic *Zfp57* (Li et al. 2008b). Since transcription starts premature after preovulatory aging, this might further ameliorate the effects of decreased maternal Zfp57 expression by making embryonic Zfp57 earlier available.

Expression of other factors involved in imprint methylation maintenance was stable after preovulatory aging (*Dnmt1*, *Trim28*) and might have compensated for the loss of *Zfp57*. Trim28 protein is a co-factor of Zfp57, which binds to it and recruits heterochromatin-inducing factors such as Hp1 and Set1b leading to the establishment of H3K9me3 during embryonic development (Schultz et al. 2002). Loss of *Trim28* disturbs the maintenance of DNA methylation of imprinted genes in a random way, leading to mosaicism in the blastomers of 8-cell embryos (Lorthongpanich et al. 2013). A similar effect could also happen upon loss of *Zfp57* and looking at DNA-methylation of single embryos where all 8 blastomers are pooled might not have a high enough resolution to detect such effects. The study of

Lorthongpanich and colleagues (2013) assessed DNA-methylation of single blastomers using a methylation sensitive restriction enzyme to digest DNA followed by a PCR. This method however only allows the investigation of a single CpG site. The CpGs within a CpG island can vary though in their susceptibility to methylation disturbances (Heinzmann et al. 2015). The bisulfite treatment in the current study leads to destruction of DNA making the method difficult to use for single cells, but the amplicon sequencing analysis enabled the investigation of several CpGs within a CpG island. It showed for example for *H19* unstable methylation of one of the CpGs in the ICR in both control embryos and embryos from aged oocytes underlining the need to investigate more than one CpG. Recently, bisulfite sequencing of single oocytes has been described, which might be a good approach to investigate subtle changes in DNA methylation status such as mosaicism of single blastomeres within a single preimplantation embryo (Smallwood et al. 2014).

This was the first study to investigate methylation levels in embryos after preovulatory aging. In line with the present results on preovulatory aging, previous studies on postovulatory aging showed no major, general effects on methylation status of imprinted genes. However, some studies found that certain genes are more susceptible to methylation disturbances then others after postovulatory aging. Mouse embryos at mid-gestation that were derived from postovulatory-aged oocytes showed no significant changes of methylation levels of *Igf2r* and *H19*. However, the placenta of these embryos was hypomethylated for *H19* and increased transcript levels for *H19* in comparison to controls were observed (Liang et al. 2008). Postovulatory aging showed abnormal methylation levels in mouse oocytes for the *Snrpn* DMR but not *Peg1*/*Mest* (Liang et al. 2008). In contrast, in vitro postovulatory aging of superovulated oocytes has shown to affect DNA methylation of the *Peg1/Mest* DMR in oocytes (Imamura et al. 2005). Whether these abnormal methylation levels are maintained after fertilization has not been investigated so far. Postovulatory aging of bovine oocytes derived from in vitro-maturated oocytes showed no significant differences in methylation status of *bH19*, *bSNRPN*, *bZAR1*, *bPOU5F1* and *bDNMT3A* (Heinzmann et al. 2015). Only *bDNMT3Lo* showed an increase in methylation errors in oocytes and embryos after postovulatory aging, but only for 2 of 8 analyzed CpGs and the average methylation level did not change more than 20%. Even though this effect might be significant the vast majority of postovulatory-aged oocytes and embryos showed no methylation defects and the imprinted genes investigated were not affected (Heinzmann et al. 2015).

4.8 Conclusion

This study used a previously established in vivo mouse model to investigate molecular effects of preovulatory aging on oocytes and their developmental capacity. In this mouse model it has been shown that preovulatory aging increases the number of embryo resorption sites and lowers embryonic weight during pregnancy (Bittner et al. 2011). This was a first indication that preovulatory-aged oocytes may be of lower quality. The present study supported this observation by noticing lower ovulation and fertilization rates. However, not all investigated processes were affected by preovulatory aging. Normal levels of the epigenetic histone modification H3K9me3 were observed in preovulatory-aged oocytes. Only 3 out of 10 selected ME genes showed a decrease in RNA expression levels after aging. Embryos derived after preovulatory aging showed successful DNA methylation maintenance at the investigated imprinted genes. This demonstrates that molecular mechanisms in the oocyte and preimplantation embryo are distinctly regulated.

For postovulatory aging it has been proposed that molecular processes are regulated in a time-dependent manner and that a delay in fertilization leads to a deregulation of these processes (Xu et al. 1997, Kosubek et al. 2010, Trapphoff et al. 2015). The current results suggest that the same might occur during preovulatory aging. A premature loss of the RNA storage protein Ybx2 was observed, which coincided with an increase in poly(A) tail length of transcripts from selected ME genes. Both are indicators of a precocious recruitment of mRNAs for protein translation. The synthesis of proteins from stored transcripts is required for the initiation of transcription after fertilization in the course of embryonic genome activation (Wang and Latham 1997). Indeed, embryonic genome activation was premature showing an early increase in transcription in embryos after preovulatory aging. Taken together, it seems that RNA storage, poly(A) tail dynamics and embryonic genome activation are not (exclusively) timed by ovulation, but at least partly regulated by events in the growing or maturing oocyte. A delay in ovulation desynchronizes physiological processes in the oocyte, which may consequently affect the embryonic programs resulting in potentially long-lasting effects for the offspring.

5 Summary

Preovulatory aging of oocytes is caused by a delay in ovulation and it is known to impair postimplantation embryonic development. However, hardly anything is known about the molecular mechanisms associated with preovulatory aging. To investigate several aspects of RNA dynamics in the preovulatory-aged oocytes and possible consequences on early preimplantation development, the present study used a mouse model in which ovulation was postponed with the GnRH antagonist cetrorelix.

Preovulatory aging led to a lower number of ovulated oocytes. Furthermore, preovulatory-aged oocytes were more difficult to fertilize, as was demonstrated by a decrease in 2-cell embryo rate after mating compared to controls. These results are in accordance with previous studies on preovulatory aging in several vertebrate models including rats and humans.

As an indicator for transcriptional silencing and genome stability during oocyte growth, the epigenetic histone modification H3K9 trimethylation was analyzed using immunofluorescence. No effect of preovulatory aging on H3K9 trimethylation levels was observed. Before transcriptional silencing, mRNAs are stored in the oocyte until recruitment for protein translation later during oocyte maturation. One major key player in the storage and recruitment of maternal transcripts is the RNA-binding protein Ybx2. Immunofluorescent staining showed a significant decrease in Ybx2 protein abundance after preovulatory aging, which might have severe implications for RNA dynamics in the oocyte.

Since the RNA-storage potential seemed impaired, transcript levels of selected maternal effect genes were analyzed by qRT-PCR. Maternal effect genes are of crucial importance for oocyte developmental potential because they function in the early embryo before transcription initiates again. Transcript levels of 2 out of 10 investigated ME genes (*Smarca4* and *Tet3*) decreased significantly after preovulatory aging. Additionally, oligo(dT) priming allowed investigation of poly(A) tail length of mRNAs of the candidate maternal effect genes by qRT-PCR. The poly(A) tail determines the translation efficiency of transcripts in the oocyte and early embryo. The majority of genes showed elongation of poly(A) tail length after preovulatory aging. Similar results were also found after in vitro preovulatory aging of oocytes grown in follicle culture, although not the same genes were affected than in vivo.

Loss of Ybx2 protein and polyadenylation of maternal effect gene transcripts should occur later during oocyte maturation. Therefore, the results imply premature recruitment of mRNAs for protein translation. This assumption is supported by experiments determining the start of

transcription at the 2-cell stage of embryonic preimplantation development in the course of embryonic genome activation. Embryos were incubated in BrUTP, which intercalates into nascent RNA and can by visualized by immunofluorescence. Compared to controls, in embryos derived from preovulatory-aged oocytes an increase in transcription was observed, indicating a precocious start of embryonic genome activation.

Last, DNA methylation maintenance of three imprinted genes (*H19*, *Snrpn*, *Igf2r*) during epigenetic reprogramming in the preimplantation embryo was analyzed. Deep amplicon bisulfite sequencing of single 8-cell embryos showed stable maintenance of DNA methylation at the investigated loci.

Overall, the results show that the investigated processes are distinctly regulated in the oocyte and early embryo and not all of them are susceptible to preovulatory aging. Nevertheless, preovulatory aging impairs oocyte quality with possible long-term effects on embryonic development and reproductive success.

6 Zusammenfassung

Eine Verzögerung des Eisprungs führt zu präovulatorischer Überreife der Oozyte und dies kann die Entwicklung des Embryos nach der Einnistung in die Gebärmutter beeinträchtigen. Über die molekularen Mechanismen, die das Entwicklungspotenzial der überreifen Oozyte beeinflussen und die Auswirkungen auf die frühe Embryonalentwicklung ist nur wenig bekannt. Mit Hilfe eines Mausmodells, in dem der Eisprung mit Hilfe des GnRH Antagonisten Cetrorelix hinausgezögert wurde, wurden in dieser Studie verschiedene Aspekte der RNA Dynamik in der überreifen Oozyte und mögliche Konsequenzen für die frühe Embryonalentwicklung vor der Einnistung untersucht.

Die Verzögerung des Eisprungs führte zu einer verringerten Anzahl von ovulierten, reifen Oozyten. Außerdem ließen sich überreife Oozyten schlechter befruchten, was zu einer Abnahme der Zahl von 2-Zell-Embryonen nach Verpaarung führte. Diese Ergebnisse stimmen mit vorhergegangenen Studien zur präovulatorischen Überreife in verschiedenen Vertebraten, u.a. Ratten und Menschen, überein.

Während des Oozyten-Wachstums wird die Transkription eingestellt. Dieser Prozess wurde mittels Immunofluoreszenz gegen die epigenetische Histonmodifikation H3K9-Trimethylierung untersucht. Dabei wurde kein Effekt der präovulatorischen Überreife auf das Ausmaß der H3K9-Trimethylierung beobachtet. Vor dem transkriptionellen Arrest werden mRNAs in der Oozyte gespeichert, bis sie im späteren Verlauf der Oozyten-Reifung für die Translation von Proteinen rekrutiert werden. Ein wichtiger Faktor für die Speicherung und Rekrutierung von mRNA in der Oozyte ist das RNA-Bindeprotein Ybx2. Mittels Immunofluoreszenz konnte eine signifikante Abnahme der Ybx2 Proteinmenge nach präovulatorischer Überreife gezeigt werden. Dies könnte zu Störungen der RNA-Speicherung in der Oozyte führen. Um dies zu ermitteln wurde die Transkriptmenge von ausgewählten maternalen Effektgenen (ME-Genen) mittels qRT-PCR untersucht. Transkripte der ME-Gene sind entscheidend für das Entwicklungspotential der Oozyte, da sie im frühen Embryo, dessen Transkription noch nicht begonnen hat, wirken. Von zwei der 10 untersuchten ME-Gene (*Smarca4* und *Tet3*) waren die Transkriptmengen, im Vergleich zu den Kontrollen, in überreifen Oozyten signifikant reduziert. Außerdem wurde die Poly(A)-Schwanzlänge von ME-Genen untersucht, da diese die Effizienz der Translation eines Transkriptes in der Oozyte bestimmt. In überreifen Oozyten zeigte der Großteil der analysierten Kandidatengene eine Verlängerung des Poly(A)-Schwanzes. Ähnliche Ergebnisse wurden auch bei in vitro

präovulatorisch überreifen Oozyten aus einer Follikelkultur beobachtet, obwohl hier nicht die gleichen ME-Gene beeinträchtigt waren.

Die beobachtete Abnahme von Ybx2-Protein und die Verlängerung des Poly(A)-Schwanzes der ME-Transkripte sind Prozesse, die während der Eizell-Reifung eigentlich später stattfinden. Die Beobachtung, dass diese Prozesse bei präovulatorischer Alterung früher stattfinden, impliziert, dass auch die Rekrutierung von mRNA für die Proteintranslation verfrüht stattfinden könnte, was die Transkription im Embryo beeinflussen kann. Diese Annahme wird durch Analysen zur Aktivierung der Transkription im 2-Zell-Embryo unterstützt. Embryonen wurden in BrUTP inkubiert, welches sich während der Transkription in die RNA einlagert und mit Immunofluoreszenz nachgewiesen werden kann. Dieses Experiment zeigte, im Vergleich zu Kontrollen, eine Zunahme der Transkription in Embryonen von überreifen Oozyten, was auf einen vorzeitigen Start der embryonalen Genomaktivierung hindeutet.

Zuletzt wurde die DNA-Methylierung von drei Genen, die dem Imprinting unterliegen (*H19, Snrpn, Igf2r*), in einzelnen 8-Zell-Embryonen analysiert. Deep amplicon bisulifte sequencing zeigte einen stabilen Erhalt der DNA-Methylierung nach präovulatorischer Überreife in den untersuchten Loci.

Insgesamt zeigen diese Ergebnisse, dass die untersuchten Prozesse in der Oozyte und im frühen Embryo individuell reguliert sind und nicht alle durch präovulatorische Überreife gestört werden. Dennoch lässt sich sagen, dass präovulatorische Überreife die Qualität der Oozyte beeinträchtigt, mit möglichen Langzeiteffekten auf die Embryo-Entwicklung und den Reproduktionserfolg.

7 References

Aboulghar MA, Mansour RT, Serour GI, Al-Inany HG, Amin YM, Aboulghar MM. 2004. Increasing the dose of human menopausal gonadotrophins on day of GnRH antagonist administration: randomized controlled trial. *Reprod Biomed Online* **8**: 524-527.

Acevedo N, Smith GD. 2005. Oocyte-specific gene signaling and its regulation of mammalian reproductive potential. *Front Biosci* **10**: 2335-2345.

Al-Inany HG. 2007. Gonadotrophin-releasing hormone antagonists for assisted conception: a Cochrane Review. *Reprod BioMed Online* **14**: 640-649.

Al-Inany HG, Youssef MA, Aboulghar M, Broekmans F, Sterrenburg M, Smit J, Abou-Setta AM. 2011. GnRH antagonists are safer than agonists: an update of a Cochrane review. *Hum Reprod Update* **17**: 435.

Anckaert E, Sanchez F, Billooye K, Smitz J. 2013b. Dynamics of imprinted DNA methylation and gene transcription for imprinting establishment in mouse oocytes in relation to culture duration variability. *Biol Reprod* **89**: 130-138.

Aoki F, Worrad DM, Schultz RM. 1997. Regulation of transcriptional activity during the first and second cell cycles in the preimplantation mouse embryo. *Dev Biol* **181**: 296-307.

Austin CR. 1974. Principles of fertilization. *Proc R Soc Med* **67**: 925-927.

Bachvarova R, De Leon V, Johnson A, Kaplan G, Paynton BV. 1985. Changes in total RNA, polyadenylated RNA, and actin mRNA during meiotic maturation of mouse oocytes. *Dev Biol* **108**: 325-331.

Bannister AJ, Zegerman P, Partridge JF, Miska EA, Thomas JO, Allshire RC, Kouzarides T. 2001. Selective recognition of methylated lysine 9 on histone H3 by the HP1 chromo domain. *Nature* **410**: 120-124.

Barlow DP. 2011. Genomic imprinting: a mammalian epigenetic discovery model. *Annu Rev Genet* **45**: 379-403.

Barnard DC, Ryan K, Manley JL, Richter JD. 2004. Symplekin and xGLD-2 are required for CPEB-mediated cytoplasmic polyadenylation. *Cell* **119**: 641-651.

Bartolomei MS, Webber AL, Brunkow ME, Tilghman SM. 1993. Epigenetic mechanisms underlying the imprinting of the mouse H19 gene. *Genes Dev* **7**: 1663-1673.

Barton SC, Surani MA, Norris ML. 1984. Role of paternal and maternal genomes in mouse development. *Nature* **311**: 374-376.

Baruffi RL, Mauri AL, Petersen CG, Felipe V, Martins AM, Cornicelli J, Cavagna M, Oliveira JB, Franco JG, Jr. 2007. Recombinant LH supplementation to recombinant FSH during induced ovarian stimulation in the GnRH-antagonist protocol: a meta-analysis. *Reprod Biomed Online* **14**: 14-25.

Bazett-Jones DP, Cote J, Landel CC, Peterson CL, Workman JL. 1999. The SWI/SNF complex creates loop domains in DNA and polynucleosome arrays and can disrupt DNA-histone contacts within these domains. *Mol Cell Biol* **19**: 1470-1478.

Becker JS, Nicetto D, Zaret KS. 2016. H3K9me3-Dependent Heterochromatin: Barrier to Cell Fate Changes. *Trends Genet* **32**: 29-41.

Beilharz TH, Preiss T. 2007. Widespread use of poly(A) tail length control to accentuate expression of the yeast transcriptome. *RNA* **13**: 982-997.

Bell AC, Felsenfeld G. 2000. Methylation of a CTCF-dependent boundary controls imprinted expression of the Igf2 gene. *Nature* **405**: 482-485.

Bestor T, Laudano A, Mattaliano R, Ingram V. 1988. Cloning and sequencing of a cDNA encoding DNA methyltransferase of mouse cells. The carboxyl-terminal domain of the mammalian enzymes is related to bacterial restriction methyltransferases. *J Mol Biol* **203**: 971-983.

Bestor TH. 2000. The DNA methyltransferases of mammals. *Hum Mol Genet* **9**: 2395-2402.

Bittner AK, Horsthemke B, Winterhager E, Grümmer R. 2011. Hormone-induced delayed ovulation affects early embryonic development. *Fertil Steril* **95**: 2390-2394.

Borowczyk E, Mohan KN, D'Aiuto L, Cirio MC, Chaillet JR. 2009. Identification of a region of the DNMT1 methyltransferase that regulates the maintenance of genomic imprints. *Proc Natl Acad Sci U S A* **106**: 20806-20811.

Bourc'his D, Xu GL, Lin CS, Bollman B, Bestor TH. 2001. Dnmt3L and the establishment of maternal genomic imprints. *Science* **294**: 2536-2539.

Brockdorff N. 2011. Chromosome silencing mechanisms in X-chromosome inactivation: unknown unknowns. *Development* **138**: 5057-5065.

Bultman SJ, Gebuhr TC, Pan H, Svoboda P, Schultz RM, Magnuson T. 2006. Maternal BRG1 regulates zygotic genome activation in the mouse. *Genes Dev* **20**: 1744-1754.

Butcher RL. 1976. Pre-ovulatory and post-ovulatory overripeness. *Int J Gynaecol Obstet* **14**: 105-110.

Carlson LL, Page AW, Bestor TH. 1992. Properties and localization of DNA methyltransferase in preimplantation mouse embryos: implications for genomic imprinting. *Genes Dev* **6**: 2536-2541.

Cedar H, Bergman Y. 2009. Linking DNA methylation and histone modification: patterns and paradigms. *Nat Rev Genet* **10**: 295-304.

Cedrin-Durnerin I, Grange-Dujardin D, Laffy A, Parneix I, Massin N, Galey J, Theron L, Wolf JP, Conord C, Clement P et al. 2004. Recombinant human LH supplementation during GnRH antagonist administration in IVF/ICSI cycles: a prospective randomized study. *Hum Reprod* **19**: 1979-1984.

Chamberlain SJ, Brannan CI. 2001. The Prader-Willi syndrome imprinting center activates the paternally expressed murine Ube3a antisense transcript but represses paternal Ube3a. *Genomics* **73**: 316-322.

Chen J, Melton C, Suh N, Oh JS, Horner K, Xie F, Sette C, Blelloch R, Conti M. 2011. Genome-wide analysis of translation reveals a critical role for deleted in azoospermia-like (Dazl) at the oocyte-to-zygote transition. *Genes Dev* **25**: 755-766.

Chi MM, Manchester JK, Yang VC, Curato AD, Strickler RC, Lowry OH. 1988. Contrast in levels of metabolic enzymes in human and mouse ova. *Biol Reprod* **39**: 295-307.

Chian RC, Uzelac PS, Nargund G. 2013. In vitro maturation of human immature oocytes for fertility preservation. *Fertil Steril* **99**: 1173-1181.

Cirio MC, Ratnam S, Ding F, Reinhart B, Navara C, Chaillet JR. 2008. Preimplantation expression of the somatic form of Dnmt1 suggests a role in the inheritance of genomic imprints. *BMC Dev Biol* **8**: 9.

Clarke HJ. 2012. *Post-transcriptional control of gene expression during mouse oogenesis*. Springer-Verlag, Berlin Heidelberg.

Cortvrindt RG, Smitz JE. 2002. Follicle culture in reproductive toxicology: a tool for in-vitro testing of ovarian function? *Hum Reprod Update* **8**: 243-254.

Dankert D. 2015. Auswirkung einer postovulatorischen Alterung auf molekulare Parameter und die Entwicklungskompetenz muriner Oozyten. in *Institut für Anatomie*. Universität Duisburg-Essen, Essen.

Dankert D, Demond H, Trapphoff T, Heiligentag M, Rademacher K, Eichenlaub-Ritter U, Horsthemke B, Grummer R. 2014. Pre- and postovulatory aging of murine oocytes affect the transcript level and poly(A) tail length of maternal effect genes. *PLoS One* **9**: e108907.

Davis TL, Yang GJ, McCarrey JR, Bartolomei MS. 2000. The H19 methylation imprint is erased and re-established differentially on the parental alleles during male germ cell development. *Hum Mol Genet* **9**: 2885-2894.

Dean W, Lucifero D, Santos F. 2005. DNA methylation in mammalian development and disease. *Birth Defects Res C Embryo Today* **75**: 98-111.

Dean W, Santos F, Reik W. 2003. Epigenetic reprogramming in early mammalian development and following somatic nuclear transfer. *Semin Cell Dev Biol* **14**: 93-100.

Deaton AM, Bird A. 2011. CpG islands and the regulation of transcription. *Genes Dev* **25**: 1010-1022.

Demant M, Trapphoff T, Frohlich T, Arnold GJ, Eichenlaub-Ritter U. 2012. Vitrification at the pre-antral stage transiently alters inner mitochondrial membrane potential but proteome of in vitro grown and matured mouse oocytes appears unaffected. *Hum Reprod* **27**: 1096-1111.

Demond H, Trapphoff T, Dankert D, Heiligentag M, Grummer R, Horsthemke B, Eichenlaub-Ritter U. submitted. Preovulatory aging in vivo and in vitro affects maturation rates, abundance of selected proteins, histone methylation and spindle integrity in murine oocytes. *Mol Hum Reprod*.

Depalo R, Jayakrishan K, Garruti G, Totaro I, Panzarino M, Giorgino F, Selvaggi LE. 2012. GnRH agonist versus GnRH antagonist in in vitro fertilization and embryo transfer (IVF/ET). *Reprod Biol Endocrin* **10**: 26.

Dickson KS, Bilger A, Ballantyne S, Wickens MP. 1999. The cleavage and polyadenylation specificity factor in Xenopus laevis oocytes is a cytoplasmic factor involved in regulated polyadenylation. *Mol Cell Biol* **19**: 5707-5717.

Eggermann T. 2009. Silver-Russell and Beckwith-Wiedemann syndromes: opposite (epi)mutations in 11p15 result in opposite clinical pictures. *Horm Res* **71 Suppl 2**: 30-35.

El Hajj N, Trapphoff T, Linke M, May A, Hansmann T, Kuhtz J, Reifenberg K, Heinzmann J, Niemann H, Daser A et al. 2011. Limiting dilution bisulfite (pyro)sequencing reveals parent-specific methylation patterns in single early mouse embryos and bovine oocytes. *Epigenetics* **6**: 1176-1188.

Flemr M, Ma J, Schultz RM, Svoboda P. 2010. P-body loss is concomitant with formation of a messenger RNA storage domain in mouse oocytes. *Biol Reprod* **82**: 1008-1017.

Foygel K, Choi B, Jun S, Leong DE, Lee A, Wong CC, Zuo E, Eckart M, Reijo Pera RA, Wong WH et al. 2008. A novel and critical role for Oct4 as a regulator of the maternal-embryonic transition. *PLoS One* **3**: e4109.

Fugo NW, Butcher RL. 1966. Overripeness and the mammalian ova. I. Overripeness and early embryonic development. *Fertil Steril* **17**: 804-814.

Gaudet F, Rideout WM, 3rd, Meissner A, Dausman J, Leonhardt H, Jaenisch R. 2004. Dnmt1 expression in pre- and postimplantation embryogenesis and the maintenance of IAP silencing. *Mol Cell Biol* **24**: 1640-1648.

Gebauer F, Xu W, Cooper GM, Richter JD. 1994. Translational control by cytoplasmic polyadenylation of c-mos mRNA is necessary for oocyte maturation in the mouse. *EMBO J* **13**: 5712-5720.

Gohin M, Fournier E, Dufort I, Sirard MA. 2014. Discovery, identification and sequence analysis of RNAs selected for very short or long poly A tail in immature bovine oocytes. *Mol Hum Reprod* **20**: 127-138.

Goll MG, Bestor TH. 2005. Eukaryotic cytosine methyltransferases. *Annu Rev Biochem* **74**: 481-514.

Goll MG, Kirpekar F, Maggert KA, Yoder JA, Hsieh CL, Zhang X, Golic KG, Jacobsen SE, Bestor TH. 2006. Methylation of tRNAAsp by the DNA methyltransferase homolog Dnmt2. *Science* **311**: 395-398.

Grewal SI, Jia S. 2007. Heterochromatin revisited. *Nat Rev Genet* **8**: 35-46.

Gu TP, Guo F, Yang H, Wu HP, Xu GF, Liu W, Xie ZG, Shi L, He X, Jin SG et al. 2011. The role of Tet3 DNA dioxygenase in epigenetic reprogramming by oocytes. *Nature* **477**: 606-610.

Gu W, Tekur S, Reinbold R, Eppig JJ, Choi YC, Zheng JZ, Murray MT, Hecht NB. 1998. Mammalian male and female germ cells express a germ cell-specific Y-Box protein, MSY2. *Biol Reprod* **59**: 1266-1274.

Hajkova P, Erhardt S, Lane N, Haaf T, El-Maarri O, Reik W, Walter J, Surani MA. 2002. Epigenetic reprogramming in mouse primordial germ cells. *Mech Dev* **117**: 15-23.

Hake LE, Richter JD. 1994. CPEB is a specificity factor that mediates cytoplasmic polyadenylation during Xenopus oocyte maturation. *Cell* **79**: 617-627.

Hamatani T, Carter MG, Sharov AA, Ko MS. 2004. Dynamics of global gene expression changes during mouse preimplantation development. *Dev Cell* **6**: 117-131.

Hark AT, Schoenherr CJ, Katz DJ, Ingram RS, Levorse JM, Tilghman SM. 2000. CTCF mediates methylation-sensitive enhancer-blocking activity at the H19/Igf2 locus. *Nature* **405**: 486-489.

Hata K, Okano M, Lei H, Li E. 2002. Dnmt3L cooperates with the Dnmt3 family of de novo DNA methyltransferases to establish maternal imprints in mice. *Development* **129**: 1983-1993.

Hawkins RD, Hon GC, Lee LK, Ngo Q, Lister R, Pelizzola M, Edsall LE, Kuan S, Luu Y, Klugman S et al. 2010. Distinct epigenomic landscapes of pluripotent and lineage-committed human cells. *Cell Stem Cell* **6**: 479-491.

Heinzmann J, Mattern F, Aldag P, Bernal-Ulloa SM, Schneider T, Haaf T, Niemann H. 2015. Extended in vitro maturation affects gene expression and DNA methylation in bovine oocytes. *Mol Hum Reprod* **21**: 770-782.

Hirasawa R, Chiba H, Kaneda M, Tajima S, Li E, Jaenisch R, Sasaki H. 2008. Maternal and zygotic Dnmt1 are necessary and sufficient for the maintenance of DNA methylation imprints during preimplantation development. *Genes Dev* **22**: 1607-1616.

Horikawa M, Kirkman NJ, Mayo KE, Mulders SM, Zhou J, Bondy CA, Hsu SY, King GJ, Adashi EY. 2005. The mouse germ-cell-specific leucine-rich repeat protein NALP14: a member of the NACHT nucleoside triphosphatase family. *Biol Reprod* **72**: 879-889.

Horsthemke B, Wagstaff J. 2008. Mechanisms of imprinting of the Prader-Willi/Angelman region. *Am J Med Genet A***146A**: 2041-2052.

Howell CY, Bestor TH, Ding F, Latham KE, Mertineit C, Trasler JM, Chaillet JR. 2001. Genomic imprinting disrupted by a maternal effect mutation in the Dnmt1 gene. *Cell* **104**: 829-838.

Imamura T, Kerjean A, Heams T, Kupiec JJ, Thenevin C, Paldi A. 2005. Dynamic CpG and non-CpG methylation of the Peg1/Mest gene in the mouse oocyte and preimplantation embryo. *J Biol Chem* **280**: 20171-20175.

Inoue A, Matoba S, Zhang Y. 2012. Transcriptional activation of transposable elements in mouse zygotes is independent of Tet3-mediated 5-methylcytosine oxidation. *Cell Res* **22**: 1640-1649.

Jackson DA, Hassan AB, Errington RJ, Cook PR. 1993. Visualization of focal sites of transcription within human nuclei. *EMBO J* **12**: 1059-1065.

Jänicke A, Vancuylenberg J, Boag PR, Traven A, Beilharz TH. 2012. ePAT: a simple method to tag adenylated RNA to measure poly(A)-tail length and other 3' RACE applications. *RNA* **18**: 1289-1295.

Jenuwein T, Allis CD. 2001. Translating the histone code. *Science* **293**: 1074-1080.

Jia D, Jurkowska RZ, Zhang X, Jeltsch A, Cheng X. 2007. Structure of Dnmt3a bound to Dnmt3L suggests a model for de novo DNA methylation. *Nature* **449**: 248-251.

Jones DO, Cowell IG, Singh PB. 2000. Mammalian chromodomain proteins: their role in genome organisation and expression. *Bioessays* **22**: 124-137.

Jones G, Cram DS. 2013. Gene expression in human oocytes. in *Biology and Pathology of the Oocyte* (eds. A Trouson, G Gosden, U Eichenlaub-Ritter). Cambridge Univ Press.

Kageyama S, Liu H, Kaneko N, Ooga M, Nagata M, Aoki F. 2007. Alterations in epigenetic modifications during oocyte growth in mice. *Reproduction* **133**: 85-94.

Kalscheuer VM, Mariman EC, Schepens MT, Rehder H, Ropers HH. 1993. The insulin-like growth factor type-2 receptor gene is imprinted in the mouse but not in humans. *Nat Genet* **5**: 74-78.

Kaneda M, Okano M, Hata K, Sado T, Tsujimoto N, Li E, Sasaki H. 2004. Essential role for de novo DNA methyltransferase Dnmt3a in paternal and maternal imprinting. *Nature* **429**: 900-903.

Kang MK, Han SJ. 2011. Post-transcriptional and post-translational regulation during mouse oocyte maturation. *BMB Rep* **44**: 147-157.

Kim JH, Richter JD. 2006. Opposing polymerase-deadenylase activities regulate cytoplasmic polyadenylation. *Mol Cell* **24**: 173-183.

Kingston RE, Narlikar GJ. 1999. ATP-dependent remodeling and acetylation as regulators of chromatin fluidity. *Genes Dev* **13**: 2339-2352.

Knowland J, Graham C. 1972. RNA synthesis at the two-cell stage of mouse development. *J Embryol Exp Morphol* **27**: 167-176.

Kobayashi H, Sakurai T, Imai M, Takahashi N, Fukuda A, Yayoi O, Sato S, Nakabayashi K, Hata K, Sotomaru Y et al. 2012. Contribution of intragenic DNA methylation in mouse gametic DNA methylomes to establish oocyte-specific heritable marks. *PLoS Genet* **8**: e1002440.

Kosubek A, Klein-Hitpass L, Rademacher K, Horsthemke B, Ryffel GU. 2010. Aging of Xenopus tropicalis eggs leads to deadenylation of a specific set of maternal mRNAs and loss of developmental potential. *PLoS One* **5**: e13532.

Kupka MS, Ferraretti AP, de Mouzon J, Erb K, D'Hooghe T, Castilla JA, Calhaz-Jorge C, De Geyter C, Goossens V. 2014. Assisted reproductive technology in Europe, 2010: results generated from European registers by ESHREdagger. *Hum Reprod* **29**: 2099-2113.

Kurihara Y, Kawamura Y, Uchijima Y, Amamo T, Kobayashi H, Asano T, Kurihara H. 2008. Maintenance of genomic methylation patterns during preimplantation development requires the somatic form of DNA methyltransferase 1. *Dev Biol* **313**: 335-346.

Lacham-Kaplan O, Trounson A. 2008. Reduced developmental competence of immature, in-vitro matured and postovulatory aged mouse oocytes following IVF and ICSI. *Reprod Biol Endocrin* **6**: 58.

Lachner M, O'Carroll D, Rea S, Mechtler K, Jenuwein T. 2001. Methylation of histone H3 lysine 9 creates a binding site for HP1 proteins. *Nature* **410**: 116-120.

Lamphear BJ, Kirchweger R, Skern T, Rhoads RE. 1995. Mapping of functional domains in eukaryotic protein synthesis initiation factor 4G (eIF4G) with picornaviral proteases. Implications for cap-dependent and cap-independent translational initiation. *J Biol Chem* **270**: 21975-21983.

Latos PA, Pauler FM, Koerner MV, Senergin HB, Hudson QJ, Stocsits RR, Allhoff W, Stricker SH, Klement RM, Warczok KE et al. 2012. Airn transcriptional overlap, but not its lncRNA products, induces imprinted Igf2r silencing. *Science* **338**: 1469-1472.

Lee J, Inoue K, Ono R, Ogonuki N, Kohda T, Kaneko-Ishino T, Ogura A, Ishino F. 2002. Erasing genomic imprinting memory in mouse clone embryos produced from day 11.5 primordial germ cells. *Development* **129**: 1807-1817.

Leonhardt H, Page AW, Weier HU, Bestor TH. 1992. A targeting sequence directs DNA methyltransferase to sites of DNA replication in mammalian nuclei. *Cell* **71**: 865-873.

Lerchner W, Barlow DP. 1997. Paternal repression of the imprinted mouse Igf2r locus occurs during implantation and is stable in all tissues of the post-implantation mouse embryo. *Mech Dev* **61**: 141-149.

Li E. 2002. Chromatin modification and epigenetic reprogramming in mammalian development. *Nat Rev Genet* **3**: 662-673.

Li E, Beard C, Jaenisch R. 1993. Role for DNA methylation in genomic imprinting. *Nature* **366**: 362-365.

Li E, Bestor TH, Jaenisch R. 1992. Targeted mutation of the DNA methyltransferase gene results in embryonic lethality. *Cell* **69**: 915-926.

Li L, Baibakov B, Dean J. 2008a. A subcortical maternal complex essential for preimplantation mouse embryogenesis. *Dev Cell* **15**: 416-425.

Li L, Lu X, Dean J. 2013. The maternal to zygotic transition in mammals. *Mol Aspects Med* **34**: 919-938.

Li L, Zheng P, Dean J. 2010. Maternal control of early mouse development. *Development* **137**: 859-870.

Li X, Ito M, Zhou F, Youngson N, Zuo X, Leder P, Ferguson-Smith AC. 2008b. A maternal-zygotic effect gene, Zfp57, maintains both maternal and paternal imprints. *Dev Cell* **15**: 547-557.

Liang XW, Zhu JQ, Miao YL, Liu JH, Wei L, Lu SS, Hou Y, Schatten H, Lu KH, Sun QY. 2008. Loss of methylation imprint of Snrpn in postovulatory aging mouse oocyte. *Biochem Biophys Res Commun* **371**: 16-21.

Lord T, Aitken RJ. 2013. Oxidative stress and ageing of the post-ovulatory oocyte. *Reproduction* **146**: R217-227.

Lord T, Martin JH, Aitken RJ. 2015. Accumulation of electrophilic aldehydes during postovulatory aging of mouse oocytes causes reduced fertility, oxidative stress, and apoptosis. *Biol Reprod* **92**: 33.

Lorthongpanich C, Cheow LF, Balu S, Quake SR, Knowles BB, Burkholder WF, Solter D, Messerschmidt DM. 2013. Single-cell DNA-methylation analysis reveals epigenetic chimerism in preimplantation embryos. *Science* **341**: 1110-1112.

Lucifero D, Mann MR, Bartolomei MS, Trasler JM. 2004. Gene-specific timing and epigenetic memory in oocyte imprinting. *Hum Mol Genet* **13**: 839-849.

Lüllmann-Rauch R. 2003. Weibliche Geschlechtsorgane. in *Histologie - Verstehen, Lernen, Nachschlagen*. Thieme, Stuttgart.

Lyko F, Ramsahoye BH, Kashevsky H, Tudor M, Mastrangelo MA, Orr-Weaver TL, Jaenisch R. 1999. Mammalian (cytosine-5) methyltransferases cause genomic DNA methylation and lethality in Drosophila. *Nat Genet* **23**: 363-366.

Mackay DJ, Callaway JL, Marks SM, White HE, Acerini CL, Boonen SE, Dayanikli P, Firth HV, Goodship JA, Haemers AP et al. 2008. Hypomethylation of multiple imprinted loci in individuals with transient neonatal diabetes is associated with mutations in ZFP57. *Nat Genet* **40**: 949-951.

Mader S, Lee H, Pause A, Sonenberg N. 1995. The translation initiation factor eIF-4E binds to a common motif shared by the translation factor eIF-4 gamma and the translational repressors 4E-binding proteins. *Mol Cell Biol* **15**: 4990-4997.

Manosalva I, Gonzalez A. 2010. Aging changes the chromatin configuration and histone methylation of mouse oocytes at germinal vesicle stage. *Theriogenology* **74**: 1539-1547.

Marston JH, Chang MC. 1964. The fertilizable life of ova and their morphology following delayed insemination in mature and immature mice. *J Exp Zool* **155**: 237-251.

Matsumoto K, Wolffe AP. 1998. Gene regulation by Y-box proteins: coupling control of transcription and translation. *Trends Cell Biol* **8**: 318-323.

Mayer W, Niveleau A, Walter J, Fundele R, Haaf T. 2000. Demethylation of the zygotic paternal genome. *Nature* **403**: 501-502.

McGrath J, Solter D. 1984. Completion of mouse embryogenesis requires both the maternal and paternal genomes. *Cell* **37**: 179-183.

McGrew LL, Dworkin-Rastl E, Dworkin MB, Richter JD. 1989. Poly(A) elongation during Xenopus oocyte maturation is required for translational recruitment and is mediated by a short sequence element. *Genes Dev* **3**: 803-815.

Medvedev S, Pan H, Schultz RM. 2011. Absence of MSY2 in mouse oocytes perturbs oocyte growth and maturation, RNA stability, and the transcriptome. *Biol Reprod* **85**: 575-583.

Medvedev S, Yang J, Hecht NB, Schultz RM. 2008. CDC2A (CDK1)-mediated phosphorylation of MSY2 triggers maternal mRNA degradation during mouse oocyte maturation. *Dev Biol* **321**: 205-215.

Meijer HA, Bushell M, Hill K, Gant TW, Willis AE, Jones P, de Moor CH. 2007. A novel method for poly(A) fractionation reveals a large population of mRNAs with a short poly(A) tail in mammalian cells. *Nucleic Acids Res* **35**: e132.

Mertineit C, Yoder JA, Taketo T, Laird DW, Trasler JM, Bestor TH. 1998. Sex-specific exons control DNA methyltransferase in mammalian germ cells. *Development* **125**: 889-897.

Messerschmidt DM. 2012. Should I stay or should I go: protection and maintenance of DNA methylation at imprinted genes. *Epigenetics* **7**: 969-975.

Messerschmidt DM, de Vries W, Ito M, Solter D, Ferguson-Smith A, Knowles BB. 2012. Trim28 is required for epigenetic stability during mouse oocyte to embryo transition. *Science* **335**: 1499-1502.

Meyer E, Lim D, Pasha S, Tee LJ, Rahman F, Yates JR, Woods CG, Reik W, Maher ER. 2009. Germline mutation in NLRP2 (NALP2) in a familial imprinting disorder (Beckwith-Wiedemann Syndrome). *PLoS Genet* **5**: e1000423.

Miao YL, Kikuchi K, Sun QY, Schatten H. 2009. Oocyte aging: cellular and molecular changes, developmental potential and reversal possibility. *Hum Reprod Update* **15**: 573-585.

Minami N, Suzuki T, Tsukamoto S. 2007. Zygotic gene activation and maternal factors in mammals. *J Reprod Dev* **53**: 707-715.

Molyneaux KA, Stallock J, Schaible K, Wylie C. 2001. Time-lapse analysis of living mouse germ cell migration. *Dev Biol* **240**: 488-498.

Monk M, Boubelik M, Lehnert S. 1987. Temporal and regional changes in DNA methylation in the embryonic, extraembryonic and germ cell lineages during mouse embryo development. *Development* **99**: 371-382.

Moore GP, Lintern-Moore S. 1978. Transcription of the mouse oocyte genome. *Biol Reprod* **18**: 865-870.

Murdoch S, Djuric U, Mazhar B, Seoud M, Khan R, Kuick R, Bagga R, Kircheisen R, Ao A, Ratti B et al. 2006. Mutations in NALP7 cause recurrent hydatidiform moles and reproductive wastage in humans. *Nat Genet* **38**: 300-302.

Nakamura T, Arai Y, Umehara H, Masuhara M, Kimura T, Taniguchi H, Sekimoto T, Ikawa M, Yoneda Y, Okabe M et al. 2007. PGC7/Stella protects against DNA demethylation in early embryogenesis. *Nat Cell Biol* **9**: 64-71.

Newport J, Kirschner M. 1982. A major developmental transition in early Xenopus embryos: I. characterization and timing of cellular changes at the midblastula stage. *Cell* **30**: 675-686.

Nordin M, Bergman D, Halje M, Engstrom W, Ward A. 2014. Epigenetic regulation of the Igf2/H19 gene cluster. *Cell Prolif* **47**: 189-199.

Nothias JY, Miranda M, DePamphilis ML. 1996. Uncoupling of transcription and translation during zygotic gene activation in the mouse. *EMBO J* **15**: 5715-5725.

O'Geen H, Squazzo SL, Iyengar S, Blahnik K, Rinn JL, Chang HY, Green R, Farnham PJ. 2007. Genome-wide analysis of KAP1 binding suggests autoregulation of KRAB-ZNFs. *PLoS Genet* **3**: e89.

Obata Y, Kono T. 2002. Maternal primary imprinting is established at a specific time for each gene throughout oocyte growth. *J Biol Chem* **277**: 5285-5289.

Ogawa O, McNoe LA, Eccles MR, Morison IM, Reeve AE. 1993. Human insulin-like growth factor type I and type II receptors are not imprinted. *Hum Mol Genet* **2**: 2163-2165.

Okano M, Bell DW, Haber DA, Li E. 1999. DNA methyltransferases Dnmt3a and Dnmt3b are essential for de novo methylation and mammalian development. *Cell* **99**: 247-257.

Okano M, Xie S, Li E. 1998. Dnmt2 is not required for de novo and maintenance methylation of viral DNA in embryonic stem cells. *Nucleic Acids Res* **26**: 2536-2540.

Ooi SK, Qiu C, Bernstein E, Li K, Jia D, Yang Z, Erdjument-Bromage H, Tempst P, Lin SP, Allis CD et al. 2007. DNMT3L connects unmethylated lysine 4 of histone H3 to de novo methylation of DNA. *Nature* **448**: 714-717.

Oswald J, Engemann S, Lane N, Mayer W, Olek A, Fundele R, Dean W, Reik W, Walter J. 2000. Active demethylation of the paternal genome in the mouse zygote. *Curr Biol* **10**: 475-478.

Paris J, Richter JD. 1990. Maturation-specific polyadenylation and translational control: diversity of cytoplasmic polyadenylation elements, influence of poly(A) tail size, and formation of stable polyadenylation complexes. *Mol Cell Biol* **10**: 5634-5645.

Paris J, Swenson K, Piwnica-Worms H, Richter JD. 1991. Maturation-specific polyadenylation: in vitro activation by p34cdc2 and phosphorylation of a 58-kD CPE-binding protein. *Genes Dev* **5**: 1697-1708.

Parker R, Song H. 2004. The enzymes and control of eukaryotic mRNA turnover. *Nat Struct Mol Biol* **11**: 121-127.

Patterton D, Wolffe AP. 1996. Developmental roles for chromatin and chromosomal structure. *Dev Biol* **173**: 2-13.

Payer B, Saitou M, Barton SC, Thresher R, Dixon JP, Zahn D, Colledge WH, Carlton MB, Nakano T, Surani MA. 2003. Stella is a maternal effect gene required for normal early development in mice. *Curr Biol* **13**: 2110-2117.

Peat JR, Dean W, Clark SJ, Krueger F, Smallwood SA, Ficz G, Kim JK, Marioni JC, Hore TA, Reik W. 2014. Genome-wide bisulfite sequencing in zygotes identifies demethylation targets and maps the contribution of TET3 oxidation. *Cell Rep* **9**: 1990-2000.

Peng H, Chang B, Lu C, Su J, Wu Y, Lv P, Wang Y, Liu J, Zhang B, Quan F et al. 2012. Nlrp2, a maternal effect gene required for early embryonic development in the mouse. *PLoS One* **7**: e30344.

Pesce M, Wang X, Wolgemuth DJ, Scholer H. 1998. Differential expression of the Oct-4 transcription factor during mouse germ cell differentiation. *Mech Dev* **71**: 89-98.

Peters AH, O'Carroll D, Scherthan H, Mechtler K, Sauer S, Schofer C, Weipoltshammer K, Pagani M, Lachner M, Kohlmaier A et al. 2001. Loss of the Suv39h histone methyltransferases impairs mammalian heterochromatin and genome stability. *Cell* **107**: 323-337.

Peters J. 2014. The role of genomic imprinting in biology and disease: an expanding view. *Nat Rev Genet* **15**: 517-530.

Piccioni F, Zappavigna V, Verrotti AC. 2005. Translational regulation during oogenesis and early development: the cap-poly(A) tail relationship. *C R Biol* **328**: 863-881.

Pique M, Lopez JM, Foissac S, Guigo R, Mendez R. 2008. A combinatorial code for CPE-mediated translational control. *Cell* **132**: 434-448.

Preiss T, Hentze WM. 2003. Starting the protein synthesis machine: eukaryotic translation initiation. *Bioessays* **25**: 1201-1211.

Probst AV, Almouzni G. 2011. Heterochromatin establishment in the context of genome-wide epigenetic reprogramming. *Trends Genet* **27**: 177-185.

Quenneville S, Verde G, Corsinotti A, Kapopoulou A, Jakobsson J, Offner S, Baglivo I, Pedone PV, Grimaldi G, Riccio A et al. 2011. In embryonic stem cells, ZFP57/KAP1 recognize a methylated hexanucleotide to affect chromatin and DNA methylation of imprinting control regions. *Mol Cell* **44**: 361-372.

Rahmann S, Beygo J, Kanber D, Martin M, Horsthemke B, Buiting K. 2013. Amplikyzer: Automated methylation analysis of amplicons from bisulfite flowgram sequencing. *PeerJ PrePrints* **1:e122v2**.

Reik W, Walter J. 2001. Evolution of imprinting mechanisms: the battle of the sexes begins in the zygote. *Nat Genet* **27**: 255-256.

Richter JD. 2007. CPEB: a life in translation. *Trends Biochem Sci* **32**: 279-285.

Robert C, McGraw S, Massicotte L, Pravetoni M, Gandolfi F, Sirard MA. 2002. Quantification of housekeeping transcript levels during the development of bovine preimplantation embryos. *Biol Reprod* **67**: 1465-1472.

Robertson S, Lin R. 2013. The oocyte-to-embryo transition. *Adv Exp Med Biol* **757**: 351-372.

Rougeulle C, Cardoso C, Fontes M, Colleaux L, Lalande M. 1998. An imprinted antisense RNA overlaps UBE3A and a second maternally expressed transcript. *Nat Genet* **19**: 15-16.

Rougeulle C, Glatt H, Lalande M. 1997. The Angelman syndrome candidate gene, UBE3A/E6-AP, is imprinted in brain. *Nat Genet* **17**: 14-15.

Rougier N, Bourc'his D, Gomes DM, Niveleau A, Plachot M, Paldi A, Viegas-Pequignot E. 1998. Chromosome methylation patterns during mammalian preimplantation development. *Genes Dev* **12**: 2108-2113.

Sachs A. 2000. Physical and Functional Interactions between the mRNA Cap Structure and the Poly(A) Tail. in *Translational Control of Gene Expression* (eds. AL Cline, RM Bock). Cold Spring Harbor Laboratory Press, Cold Spring Harbor.

Saksouk N, Simboeck E, Dejardin J. 2015. Constitutive heterochromatin formation and transcription in mammals. *Epigenetics Chromatin* **8**: 3.

Sanchez F, Adriaenssens T, Romero S, Smitz J. 2009. Quantification of oocyte-specific transcripts in follicle-enclosed oocytes during antral development and maturation in vitro. *Mol Hum Reprod* **15**: 539-550.

Sanger F, Nicklen S, Coulson AR. 1977. DNA sequencing with chain-terminating inhibitors. *Proc Natl Acad Sci U S A* **74**: 5463-5467.

Santos F, Hendrich B, Reik W, Dean W. 2002. Dynamic reprogramming of DNA methylation in the early mouse embryo. *Dev Biol* **241**: 172-182.

Santos F, Peat J, Burgess H, Rada C, Reik W, Dean W. 2013. Active demethylation in mouse zygotes involves cytosine deamination and base excision repair. *Epigenetics Chromatin* **6**: 39.

Schultz DC, Ayyanathan K, Negorev D, Maul GG, Rauscher FJ, 3rd. 2002. SETDB1: a novel KAP-1-associated histone H3, lysine 9-specific methyltransferase that contributes to HP1-mediated silencing of euchromatic genes by KRAB zinc-finger proteins. *Genes Dev* **16**: 919-932.

Schultz RM. 1993. Regulation of zygotic gene activation in the mouse. *Bioessays* **15**: 531-538.

Schultz RM. 2002. The molecular foundations of the maternal to zygotic transition in the preimplantation embryo. *Hum Reprod Update* **8**: 323-331.

Segers I, Adriaenssens T, Ozturk E, Smitz J. 2010. Acquisition and loss of oocyte meiotic and developmental competence during in vitro antral follicle growth in mouse. *Fertil Steril* **93**: 2695-2700.

Shemer R, Birger Y, Riggs AD, Razin A. 1997. Structure of the imprinted mouse Snrpn gene and establishment of its parental-specific methylation pattern. *Proc Natl Acad Sci U S A* **94**: 10267-10272.

Sleutels F, Zwart R, Barlow DP. 2002. The non-coding Air RNA is required for silencing autosomal imprinted genes. *Nature* **415**: 810-813.

Smallwood SA, Lee HJ, Angermueller C, Krueger F, Saadeh H, Peat J, Andrews SR, Stegle O, Reik W, Kelsey G. 2014. Single-cell genome-wide bisulfite sequencing for assessing epigenetic heterogeneity. *Nature methods* **11**: 817-820.

Smits LJ, Jongbloet PH, Zielhuis GA. 1995. Preovulatory overripeness of the oocyte as a cause of ovarian dysfunction in the human female. *Med Hypotheses* **45**: 441-448.

Smitz J, Dolmans MM, Donnez J, Fortune JE, Hovatta O, Jewgenow K, Picton HM, Plancha C, Shea LD, Stouffer RL et al. 2010. Current achievements and future research directions in ovarian tissue culture, in vitro follicle development and transplantation: implications for fertility preservation. *Hum Reprod Update* **16**: 395-414.

Sonenberg N, Morgan MA, Merrick WC, Shatkin AJ. 1978. A polypeptide in eukaryotic initiation factors that crosslinks specifically to the 5'-terminal cap in mRNA. *Proc Natl Acad Sci U S A* **75**: 4843-4847.

Sonenberg N, Rupprecht KM, Hecht SM, Shatkin AJ. 1979. Eukaryotic mRNA cap binding protein: purification by affinity chromatography on sepharose-coupled m7GDP. *Proc Natl Acad Sci U S A* **76**: 4345-4349.

Soufi A, Donahue G, Zaret KS. 2012. Facilitators and impediments of the pluripotency reprogramming factors' initial engagement with the genome. *Cell* **151**: 994-1004.

Spira A, Spira N, Papiernik-Berkauer E, Schwartz D. 1985. Pattern of menstrual cycles and incidence of congenital malformations. *Early Hum Dev* **11**: 317-324.

Stewart KR, Veselovska L, Kim J, Huang J, Saadeh H, Tomizawa S, Smallwood SA, Chen T, Kelsey G. 2015. Dynamic changes in histone modifications precede de novo DNA methylation in oocytes. *Genes Dev* **29**: 2449-2462.

Stoger R, Kubicka P, Liu CG, Kafri T, Razin A, Cedar H, Barlow DP. 1993. Maternal-specific methylation of the imprinted mouse Igf2r locus identifies the expressed locus as carrying the imprinting signal. *Cell* **73**: 61-71.

Subtelny AO, Eichhorn SW, Chen GR, Sive H, Bartel DP. 2014. Poly(A)-tail profiling reveals an embryonic switch in translational control. *Nature* **508**: 66-71.

Sun F, Betzendahl I, Shen Y, Cortvrindt R, Smitz J, Eichenlaub-Ritter U. 2004. Preantral follicle culture as a novel in vitro assay in reproductive toxicology testing in mammalian oocytes. *Mutagenesis* **19**: 13-25.

Surani MA, Barton SC, Norris ML. 1984. Development of reconstituted mouse eggs suggests imprinting of the genome during gametogenesis. *Nature* **308**: 548-550.

Tachibana M, Sugimoto K, Nozaki M, Ueda J, Ohta T, Ohki M, Fukuda M, Takeda N, Niida H, Kato H et al. 2002. G9a histone methyltransferase plays a dominant role in euchromatic histone H3 lysine 9 methylation and is essential for early embryogenesis. *Genes Dev* **16**: 1779-1791.

Tam PP, Snow MH. 1981. Proliferation and migration of primordial germ cells during compensatory growth in mouse embryos. *J Embryol Exp Morphol* **64**: 133-147.

Tarin JJ, Perez-Albala S, Perez-Hoyos S, Cano A. 2002. Postovulatory aging of oocytes decreases reproductive fitness and longevity of offspring. *Biol Reprod* **66**: 495-499.

Tarun SZ, Jr., Sachs AB. 1995. A common function for mRNA 5' and 3' ends in translation initiation in yeast. *Genes Dev* **9**: 2997-3007.

Tarun SZ, Jr., Sachs AB. 1996. Association of the yeast poly(A) tail binding protein with translation initiation factor eIF-4G. *EMBO J* **15**: 7168-7177.

Tekur S, Pawlak A, Guellaen G, Hecht NB. 1999. Contrin, the human homologue of a germ-cell Y-box-binding protein: cloning, expression, and chromosomal localization. *J Androl* **20**: 135-144.

Telford NA, Watson AJ, Schultz GA. 1990. Transition from maternal to embryonic control in early mammalian development: a comparison of several species. *Mol Reprod Dev* **26**: 90-100.

The ganirelix dose-finding study group. 1998. A double-blind, randomized, dose-finding study to assess the efficacy of the gonadotrophin-releasing hormone antagonist ganirelix (Org 37462) to prevent premature luteinizing hormone surges in women undergoing ovarian stimulation with recombinant follicle stimulating hormone (Puregon). The ganirelix dose-finding study group. *Hum Reprod* **13**: 3023-3031.

Tian X, Pascal G, Monget P. 2009. Evolution and functional divergence of NLRP genes in mammalian reproductive systems. *BMC Evol Biol* **9**: 202.

Tong ZB, Gold L, Pfeifer KE, Dorward H, Lee E, Bondy CA, Dean J, Nelson LM. 2000. Mater, a maternal effect gene required for early embryonic development in mice. *Nat Genet* **26**: 267-268.

Trapphoff T, El Hajj N, Zechner U, Haaf T, Eichenlaub-Ritter U. 2010. DNA integrity, growth pattern, spindle formation, chromosomal constitution and imprinting patterns of mouse oocytes from vitrified pre-antral follicles. *Hum Reprod* **25**: 3025-3042.

Trapphoff T, Heiligentag M, Dankert D, Demond H, Deutsch D, Frohlich T, Arnold GJ, Grummer R, Horsthemke B, Eichenlaub-Ritter U. 2015. Postovulatory aging affects dynamics of mRNA, expression and localization of maternal effect proteins, spindle integrity and pericentromeric proteins in mouse oocytes. *Hum Reprod*.

Trojer P, Reinberg D. 2007. Facultative heterochromatin: is there a distinctive molecular signature? *Mol Cell* **28**: 1-13.

Ueda T, Abe K, Miura A, Yuzuriha M, Zubair M, Noguchi M, Niwa K, Kawase Y, Kono T, Matsuda Y et al. 2000. The paternal methylation imprint of the mouse H19 locus is acquired in the gonocyte stage during foetal testis development. *Genes Cells* **5**: 649-659.

Van den Berg IM, Eleveld C, van der Hoeven M, Birnie E, Steegers EA, Galjaard RJ, Laven JS, van Doorninck JH. 2011. Defective deacetylation of histone 4 K12 in human oocytes is

associated with advanced maternal age and chromosome misalignment. *Hum Reprod* **26**: 1181-1190.

Vogel MJ, Guelen L, de Wit E, Peric-Hupkes D, Loden M, Talhout W, Feenstra M, Abbas B, Classen AK, van Steensel B. 2006. Human heterochromatin proteins form large domains containing KRAB-ZNF genes. *Genome Res* **16**: 1493-1504.

Vu TH, Hoffman AR. 1997. Imprinting of the Angelman syndrome gene, UBE3A, is restricted to brain. *Nat Genet* **17**: 12-13.

Wang Q, Latham KE. 1997. Requirement for protein synthesis during embryonic genome activation in mice. *Mol Reprod Dev* **47**: 265-270.

Wang QT, Piotrowska K, Ciemerych MA, Milenkovic L, Scott MP, Davis RW, Zernicka-Goetz M. 2004. A genome-wide study of gene activity reveals developmental signaling pathways in the preimplantation mouse embryo. *Dev Cell* **6**: 133-144.

Wansink DG, Schul W, van der Kraan I, van Steensel B, van Driel R, de Jong L. 1993. Fluorescent labeling of nascent RNA reveals transcription by RNA polymerase II in domains scattered throughout the nucleus. *J Cell Biol* **122**: 283-293.

Weill L, Belloc E, Bava FA, Mendez R. 2012. Translational control by changes in poly(A) tail length: recycling mRNAs. *Nat Struct Mol Biol* **19**: 577-585.

Wells SE, Hillner PE, Vale RD, Sachs AB. 1998. Circularization of mRNA by eukaryotic translation initiation factors. *Mol Cell* **2**: 135-140.

Whitehouse I, Flaus A, Cairns BR, White MF, Workman JL, Owen-Hughes T. 1999. Nucleosome mobilization catalysed by the yeast SWI/SNF complex. *Nature* **400**: 784-787.

Wiekowski M, Miranda M, DePamphilis ML. 1993. Requirements for promoter activity in mouse oocytes and embryos distinguish paternal pronuclei from maternal and zygotic nuclei. *Dev Biol* **159**: 366-378.

Wigglesworth K, Lee KB, O'Brien MJ, Peng J, Matzuk MM, Eppig JJ. 2013. Bidirectional communication between oocytes and ovarian follicular somatic cells is required for meiotic arrest of mammalian oocytes. *Proc Natl Acad Sci U S A* **110**: E3723-3729.

Worrad DM, Ram PT, Schultz RM. 1994. Regulation of gene expression in the mouse oocyte and early preimplantation embryo: developmental changes in Sp1 and TATA box-binding protein, TBP. *Development* **120**: 2347-2357.

Wossidlo M, Nakamura T, Lepikhov K, Marques CJ, Zakhartchenko V, Boiani M, Arand J, Nakano T, Reik W, Walter J. 2011. 5-Hydroxymethylcytosine in the mammalian zygote is linked with epigenetic reprogramming. *Nat Commun* **2**: 241.

Wright SJ. 1999. Sperm nuclear activation during fertilization. *Curr Top Dev Biol* **46**: 133-178.

Wu X, Viveiros MM, Eppig JJ, Bai Y, Fitzpatrick SL, Matzuk MM. 2003. Zygote arrest 1 (Zar1) is a novel maternal-effect gene critical for the oocyte-to-embryo transition. *Nat Genet* **33**: 187-191.

Wutz A, Smrzka OW, Schweifer N, Schellander K, Wagner EF, Barlow DP. 1997. Imprinted expression of the Igf2r gene depends on an intronic CpG island. *Nature* **389**: 745-749.

Xu Y, Goodyer CG, Deal C, Polychronakos C. 1993. Functional polymorphism in the parental imprinting of the human IGF2R gene. *Biochem Biophys Res Commun* **197**: 747-754.

Xu Z, Abbott A, Kopf GS, Schultz RM, Ducibella T. 1997. Spontaneous activation of ovulated mouse eggs: time-dependent effects on M-phase exit, cortical granule exocytosis, maternal messenger ribonucleic acid recruitment, and inositol 1,4,5-trisphosphate sensitivity. *Biol Reprod* **57**: 743-750.

Yamamoto TM, Cook JM, Kotter CV, Khat T, Silva KD, Ferreyros M, Holt JW, Knight JD, Charlesworth A. 2013. Zar1 represses translation in Xenopus oocytes and binds to the TCS in maternal mRNAs with different characteristics than Zar2. *Biochim Biophys Acta* **1829**: 1034-1046.

Yang J, Medvedev S, Yu J, Tang LC, Agno JE, Matzuk MM, Schultz RM, Hecht NB. 2005. Absence of the DNA-/RNA-binding protein MSY2 results in male and female infertility. *Proc Natl Acad Sci U S A* **102**: 5755-5760.

Yoder JA, Soman NS, Verdine GL, Bestor TH. 1997. DNA (cytosine-5)-methyltransferases in mouse cells and tissues. Studies with a mechanism-based probe. *J Mol Biol* **270**: 385-395.

Yu J, Hecht NB, Schultz RM. 2001. Expression of MSY2 in mouse oocytes and preimplantation embryos. *Biol Reprod* **65**: 1260-1270.

Yu XJ, Yi Z, Gao Z, Qin D, Zhai Y, Chen X, Ou-Yang Y, Wang ZB, Zheng P, Zhu MS et al. 2014. The subcortical maternal complex controls symmetric division of mouse zygotes by regulating F-actin dynamics. *Nat Commun* **5**: 4887.

Yurttas P, Morency E, Coonrod SA. 2010. Use of proteomics to identify highly abundant maternal factors that drive the egg-to-embryo transition. *Reproduction* **139**: 809-823.

Zhang N, Wakai T, Fissore RA. 2011. Caffeine alleviates the deterioration of Ca(2+) release mechanisms and fragmentation of in vitro-aged mouse eggs. *Mol Reprod Dev* **78**: 684-701.

Zhang P, Dixon M, Zucchelli M, Hambiliki F, Levkov L, Hovatta O, Kere J. 2008. Expression analysis of the NLRP gene family suggests a role in human preimplantation development. *PLoS One* **3**: e2755.

Zhu J, Adli M, Zou JY, Verstappen G, Coyne M, Zhang X, Durham T, Miri M, Deshpande V, De Jager PL et al. 2013. Genome-wide chromatin state transitions associated with developmental and environmental cues. *Cell* **152**: 642-654.

Zuccotti M, Merico V, Bellone M, Mulas F, Sacchi L, Rebuzzini P, Prigione A, Redi CA, Bellazzi R, Adjaye J et al. 2011. Gatekeeper of pluripotency: a common Oct4 transcriptional network operates in mouse eggs and embryonic stem cells. *BMC Genomics* **12**: 1-13.

8 Supplementary data

8.1 List of abbreviations

°C	Degrees Celcius
µ	Micro
5hmC	5-hydroxymethylcytosine
5mC	5-methyl-cytosine
A	Adenosine
ART	Assisted reproduction techniques
ATP	Adenosine triphosphate
BGR	Background fluorescence
bp	Base pair
BrU	5-Bromouracil
BrUTP	5-Bromouridine-5'-triphosphate
BSA	Bovine serum albumin
cDNA	Complentary DNA
cetro	Cetrorelix
CLSM	Confocal laser scanning microscopy
COC	Cumulus-oocytes-complex
CpG	Cytosine-phosphate-guanine
CTP	Cytosine triphosphate
d	Day
DAPI	4′,6-Diamidin-2-phenylindol
dATP	Deoxyadenosine triphosphate
dCTP	Deoxycytosine triphosphate
dGTP	Deoxyguanosine triphosphate
DNA	Desoxyribonucleid acid
DPBS	Dulbecco's phosphate buffered saline
dTTP/dT	Deoxythymidine triphosphate
EDTA	Ethylenediaminetetraacetic acid
EGF	Epidermal growth factor
ePAT	Extension poly(A) test
EtBr	Ethidium bromide
FAM	Fluorescein amidite
FITC	Fluorescein isothiocyanate
FSH	Follicle stimulating hormone
g	Gram
GnrH	Gonadotropin releasing hormone
GTC	Guanidine thiocyanate
GTP	Guanosine triphosphate
GV	Germinal vesicle
h	Hour
H3K9me3	Histone 3 Lysine 9 trimethylation
hCG	Human chorionic gonadotropin
i.p.	Intraperitoneal
ICR	Imprinting control region
IF	Immunofluorescence
IU	International unit
IVF	In vitro fertilization
l	Liter
LH	Luteinizing hormone
lncRNA	Long non-coding RNA
m	Milli
M	Molar
ME	Maternal effect
MID	Multiplex identifiers
MII	Meiosis II
min	Minutes
mRNA	Messenger RNA
n	Nano
p	Pico
PB	Physiological buffer
PCR	Polymerase chain reaction
PFA	Paraformaldehyde
PGC	Primordial germ cell
PMSG	Pregnant mare serum gonadotropin
PostOA	Postovulatory aging
PreOA	Preovulatory aging
qRT-PCR	Quantitative real-time PCR
r	Recombinant
RNA	Ribonucleid acid
RNP	Ribonucleioprotein particles
rRNA	Ribosomal RNA
RT	Reverse transcription
s	Second
s.c.	Subcutaneous
SCRD	Subcortical RNP domain
SEM	Standard error of the mean
SNP	Single nucleotide polymorphism
SSC	Saline sodium citrate
TAE	Tris acetate EDTA
TRITC	Tetramethylrhodamine
tRNA	Transfer RNA
UPL	Universal Probe Library
UTR	Untranslated region
v	Volume
xg	Times gravity

8.2 List of figures

8.3 List of tables

8.4 Supplementary figures

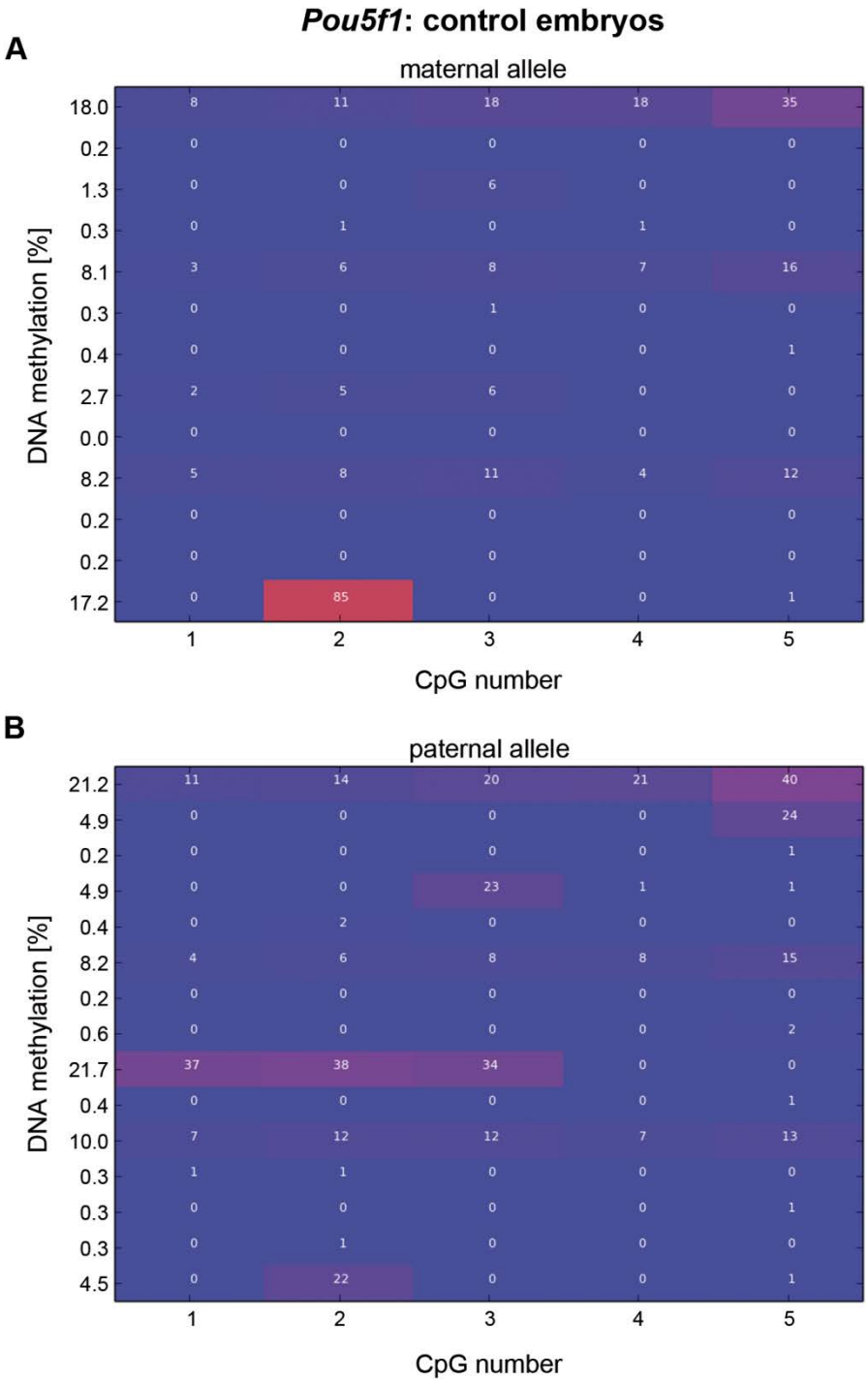

Figure S 1: Comparative analysis of DNA methylation levels at the *Pou5f1* locus of control embryos. Indicated are the mean DNA methylation levels of the entire locus per embryo of the maternal allel **(A)** and the paternal allel **(B)**. The white numbers indicate methylation levels of single CpGs. The colors represent a scale from red (100% methylation) to blue (0% methylation).

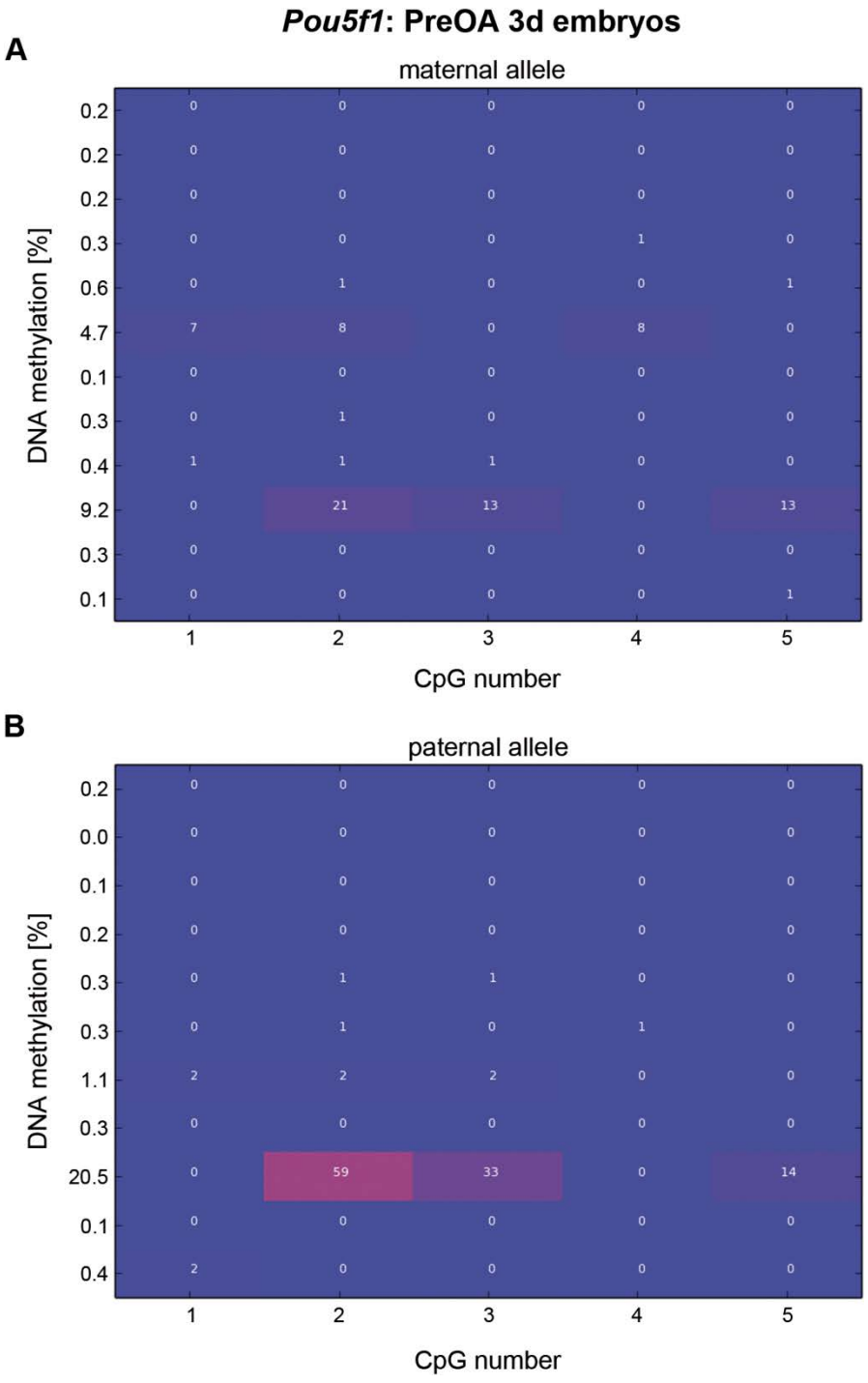

Figure S 2: Comparative analysis of DNA methylation levels at the *Pou5f1* locus of 3 days preovulatory-aged (PreOA 3d) embryos. Indicated are the mean DNA methylation levels of the entire locus per embryo of the maternal allel (A) and the paternal allel (B). The white numbers indicate methylation levels of single CpGs. The colors represent a scale from red (100% methylation) to blue (0% methylation).

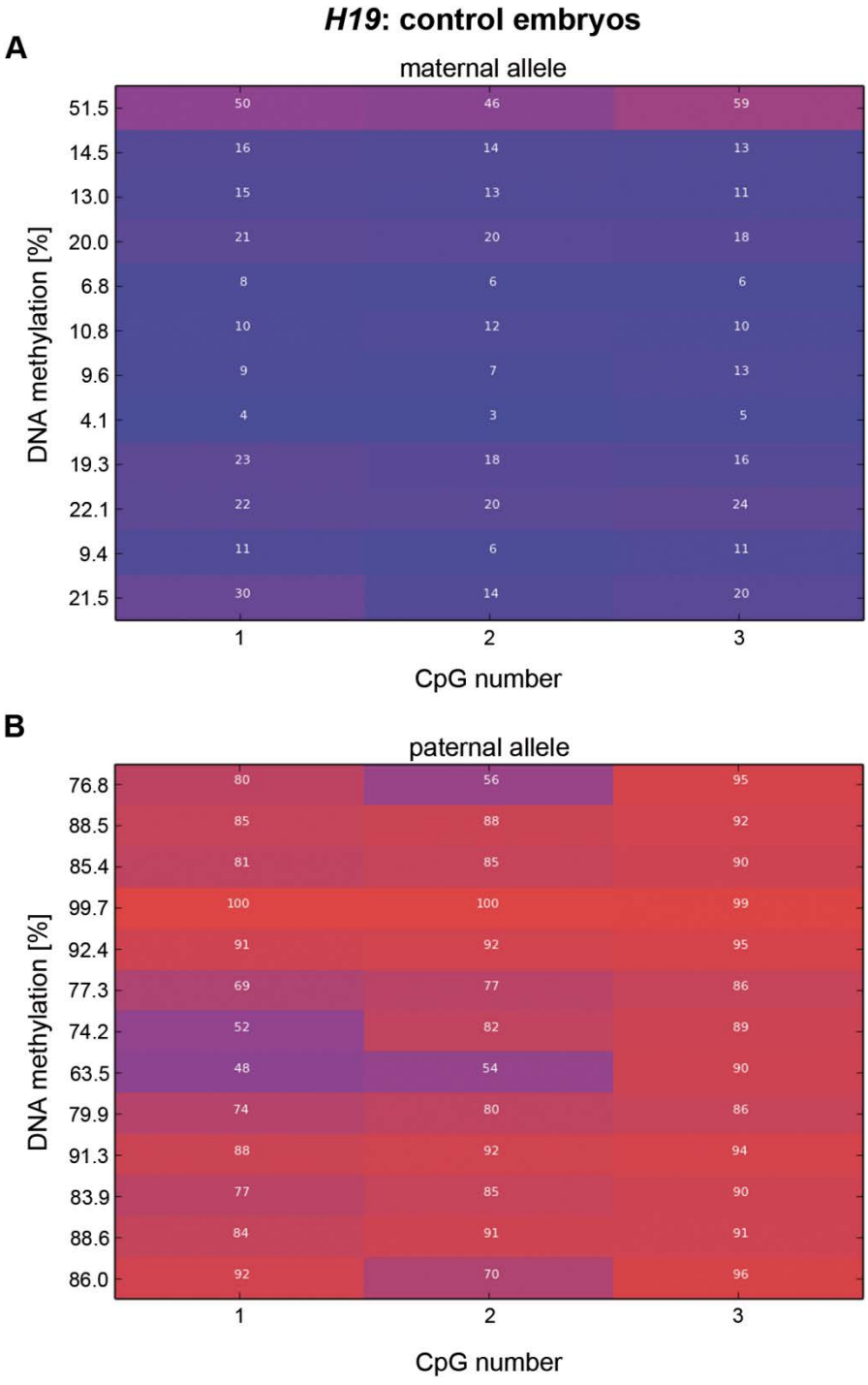

Figure S 3: Comparative analysis of DNA methylation levels at the *H19* locus of control embryos. Indicated are the mean DNA methylation levels of the entire locus per embryo of the maternal allel (A) and the paternal allel (B). The white numbers indicate methylation levels of single CpGs. The colors represent a scale from red (100% methylation) to blue (0% methylation).

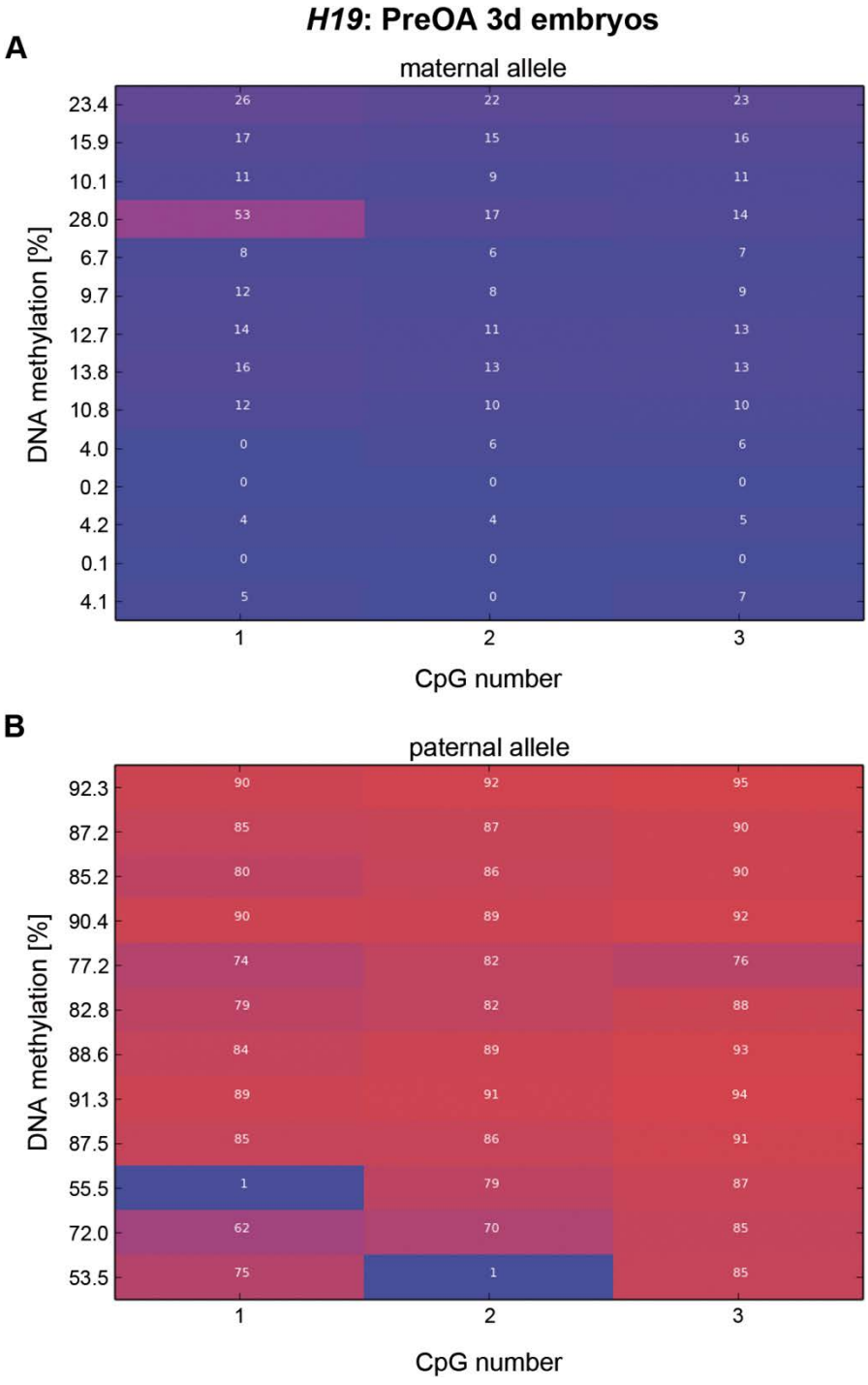

Figure S 4: Comparative analysis of DNA methylation levels at the *H19* locus of 3 days preovulatory-aged (PreOA 3d) embryos. Indicated are the mean DNA methylation levels of the entire locus per embryo of the maternal allel (A) and the paternal allel (B). The white numbers indicate methylation levels of single CpGs. The colors represent a scale from red (100% methylation) to blue (0% methylation).

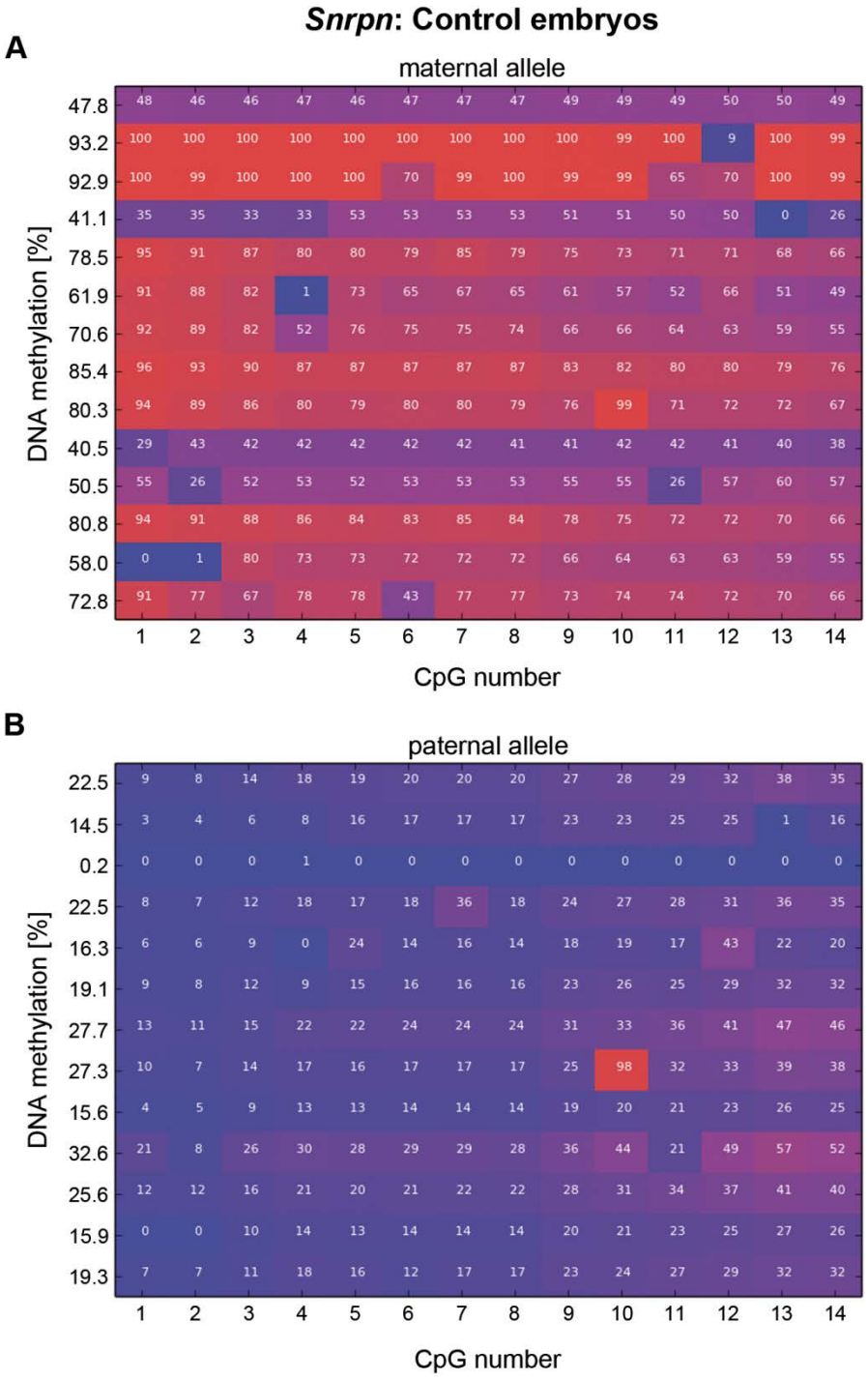

Figure S 5: Comparative analysis of DNA methylation levels at the *Snrpn* locus of control embryos. Indicated are the mean DNA methylation levels of the entire locus per embryo of the maternal allel (A) and the paternal allel (B). The white numbers indicate methylation levels of single CpGs. The colors represent a scale from red (100% methylation) to blue (0% methylation).

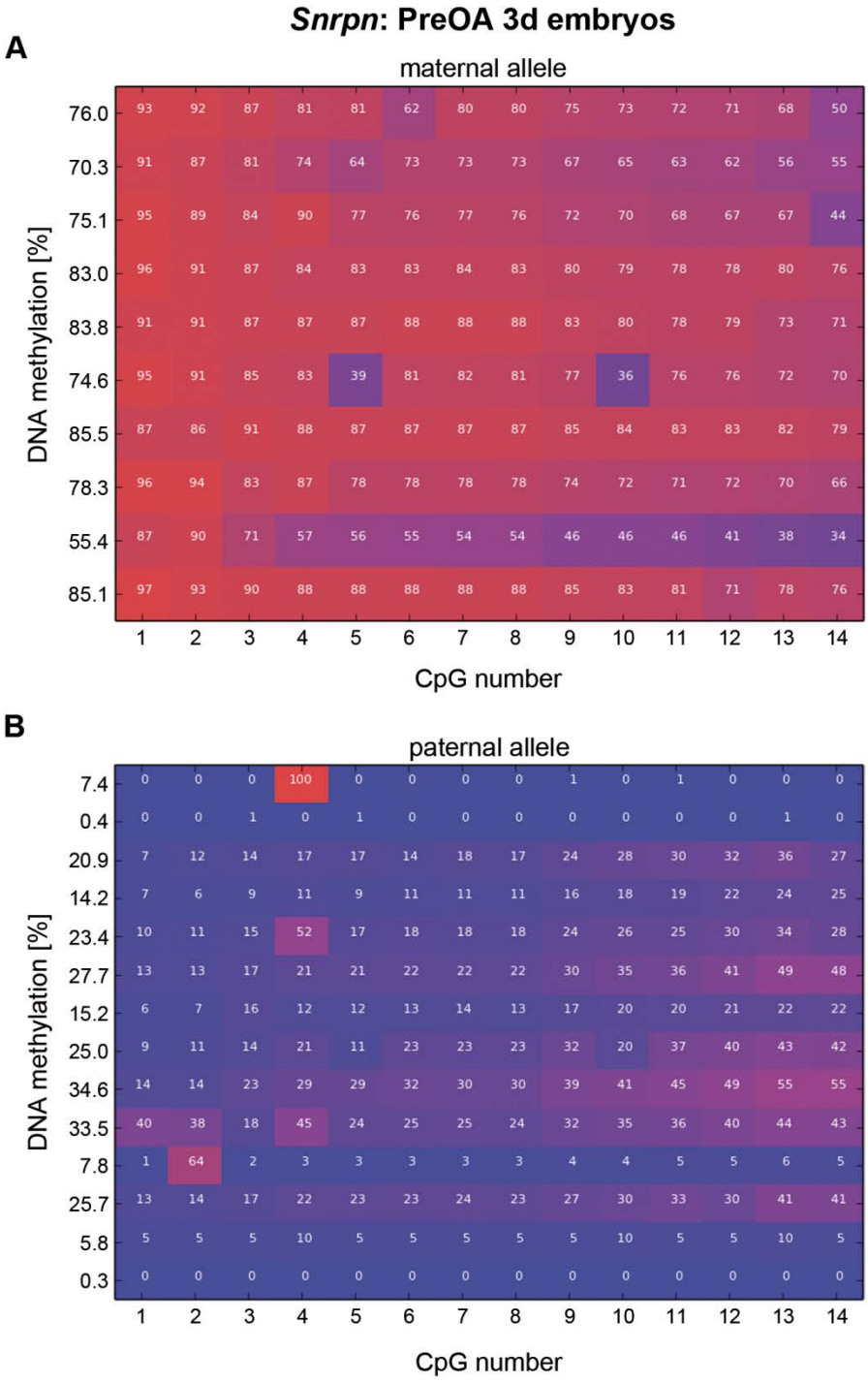

Figure S 6: Comparative analysis of DNA methylation levels at the *Snrpn* locus of 3 days preovulatory-aged (PreOA 3d) embryos. Indicated are the mean DNA methylation levels of the entire locus per embryo of the maternal allel (A) and the paternal allel (B). The white numbers indicate methylation levels of single CpGs. The colors represent a scale from red (100% methylation) to blue (0% methylation).

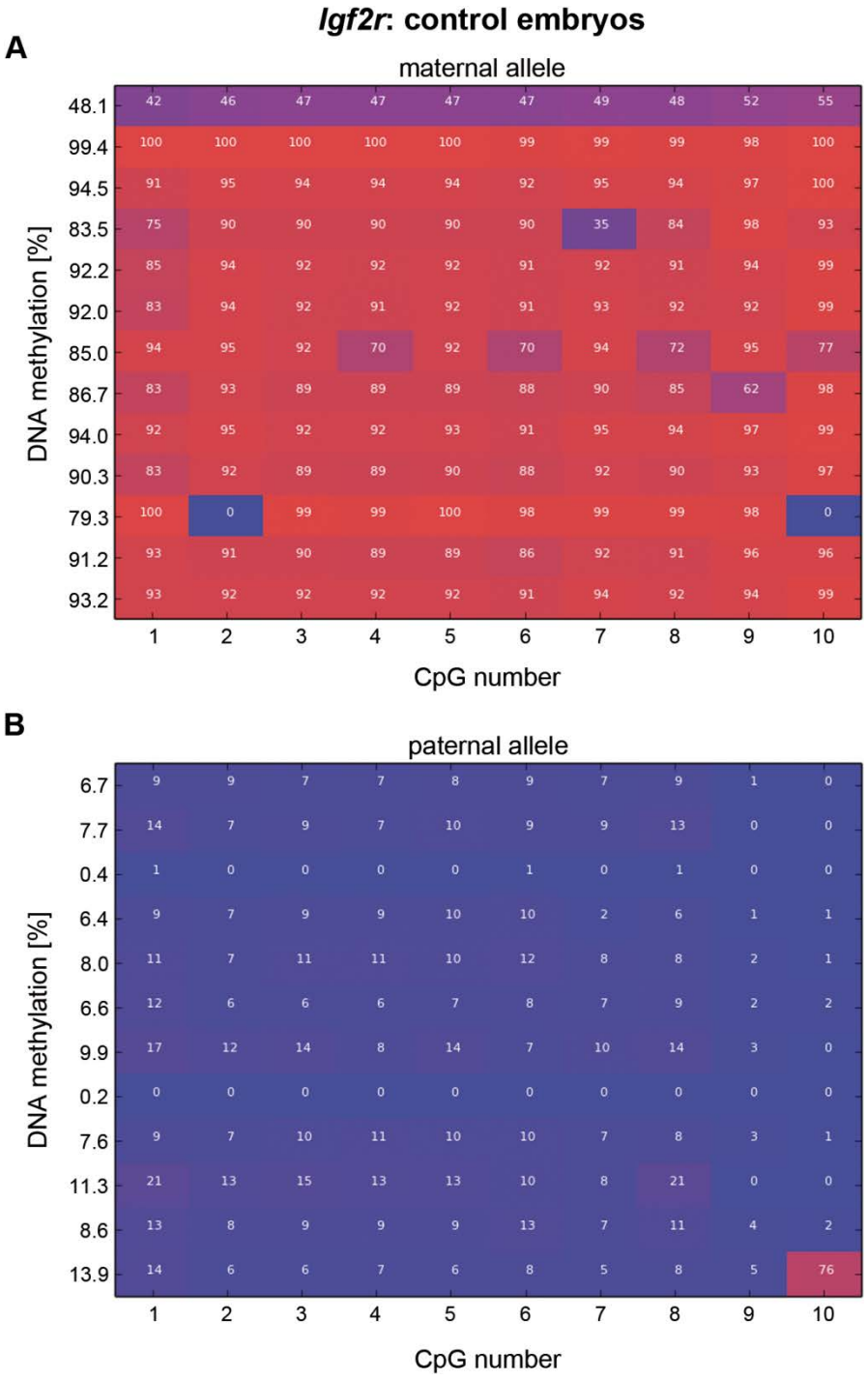

Figure S 7: Comparative analysis of DNA methylation levels at the *Igf2r* locus of control embryos. Indicated are the mean DNA methylation levels of the entire locus per embryo of the maternal allel (A) and the paternal allel (B). The white numbers indicate methylation levels of single CpGs. The colors represent a scale from red (100% methylation) to blue (0% methylation).

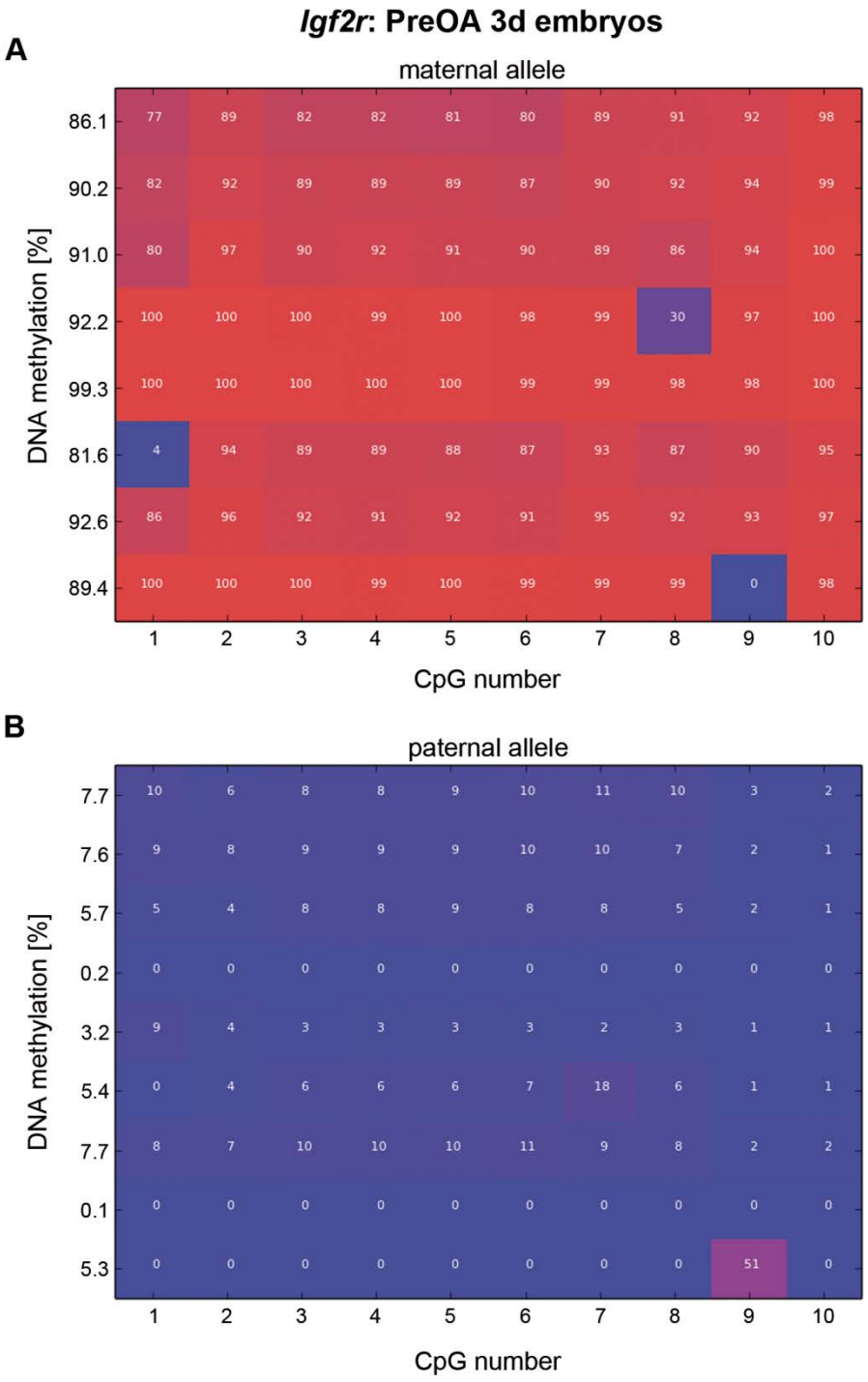

Figure S 8: Comparative analysis of DNA methylation levels at the *Igf2r* locus of 3 days preovulatory-aged (PreOA 3d) embryos. Indicated are the mean DNA methylation levels of the entire locus per embryo of the maternal allel (A) and the paternal allel (B). The white numbers indicate methylation levels of single CpGs. The colors represent a scale from red (100% methylation) to blue (0% methylation).

8.5 Supplementary tables

Table S1: Assays for qRT-PCR analysis.

Gene	Ref-Seq transcript ID	Primer sequence (5' – 3')		UPL-Probe
Brg1	NM_011417.3	F R	cggttgtgagtgacgatgac cctcactgccacttcctga	15
Tet3	NM_183138.2	F R	gcacgccagagaagatcaa ggacaatccacccttcagag	81
Trim28	NM_011588.3		Taqman assay (Mm00495594_m1)	
Zfp57	NM_001013745.2	F R	aaccttcaagaacctgacatttg ccctgtgcaactggagga	15
Dnmt1	NM_001199431.1		Taqman assay (Mm01151063)	
Nlrp2	NM_117690.3		Taqman assay (Mm00624616_m1)	
Nlrp5	NM_001039143.1		Taqman assay (Mm011143609_m1)	
Nlrp14	NM_001002894.2	F R	gcagccacactgcaatctt ccacaagccttactcgtgaga	78
Pou5f1	NM_001252452.1	F R	cacgagtggaaagcaactca gctttcatgtcctgggactc	82
Zar1	NM_174877.3	F R	ctcaggaccccggtgatt cactcggcagaactgtttga	15
Luciferase	M15077.1	F R	gtcttcccgacgatgacg gtctttccgtgctccaaaac	70

Table S2: Primers for ePAT analysis of oocytes.

Gene	Ref-Seq transcript ID	Primer Sequence (5' – 3')	Amplicon length (bp)	Annealing temp. (°C)
Anchor primer		gcgagctccgcggccgcg$(dT)_{12}$		
Btf3	NM_001170540.1	cggacactgcagctcttttc	154	58
Prdx2	NM_011563.5	cttggatttcacctgtgccc	353	58
Ddx3x	NM_010028.3	caaattaagcagacccggca	507	58
Nupr1	NM_019738.1	ggcctgcttgattctttccc	236	58

Table S3: Primers for DNA methylation analysis of embryos. Sequences were used from El Hajj et al. (2011).

Gene	Ref-Seq transcript ID	Primer sequence (5' – 3')		Amplicon length (bp)	Annealing temp. (°C)
H19	NR_130973	Outer PCR	F aaattttaattttggttgtttttgg R aatcaattaaaaaaataataaaaccc	292	52
		Inner PCR	F tggttgtttttggaatataatgtt* R aaaaacaaaacacctatacccttc*	167	57
Snrpn	NM_033174.3	Outer PCR	F ttggtagttgtttttggtaggat R ataaacccaaatctaaaatattttaatca	442	52
		Inner PCR	F ttggtagttgtttttggtaggat* R taaaatacactttcactactaaaatccac*	384	57
Igf2r	NM_010515.2	Outer PCR	F ggtattttgagggtgtaaattgta R aaccctaacacaactaaacaacat	295	52
		Inner PCR	F gaagggttttgtgattagggttaa* R aaccctaacacaactaaacaacat*	364	57
Pou5f1	NM_001252452	Outer PCR	F ttgagtgggttgtaaggatagg R aaaaaattcacctctccctcc	329	52
		Inner PCR	F gtaggggtgagaggattttgaa* R Ccaccctctaaccttaacctct*	197	57

*A tag-sequence was added in front of each inner PCR primer, which was used to adapt the MID-primers during the Re-PCR. F: cttgcttcctggcacgag; R:caggaaacagctatgac.

Table S4: Read numbers of poly(A) sequencing analysis of control and postovulatory-aged (PostOA) oocytes. Shown are the number and percentage of mapped reads in relation to total read, the duplication rate, total counts of reads mapping to genes and the number and percentage of counts for protein coding genes relative to total counts.

Group	Fraction	Mapped reads		Duplication rate	Total	Protein coding	
		Number	[%]	[%]	counts	Number	[%]
Control	Total RNA	5,381,627	67	64	4,607,724	4,345,508	94
	Fraction 1	17,384,592	79	68	11,625,270	9,910,372	85
	Fraction 2	7,825,466	65	84	7,319,693	7,221,693	99
	Fraction 3	4,353,243	51	73	3,814,821	3,771,882	99
	Pool F1-F3	14,094,147	77	64	9,854,580	8,502,255	86
PostOA	Total RNA	3,565,365	61	61	2,919,824	2,705,953	93
	Fraction 1	22,791,961	74	68	13,480,406	10,628,766	79
	Fraction 2	1,33,769	27	74	807,163	767,737	95
	Fraction 3	918,565	27	58	664,657	641,720	97
	Pool F1-F3	8,968,297	68	60	5,581,796	4,170,924	75

Table S5: List of genes with a differential poly(A) tail length after postovulatory oocyte aging according to the poly(A) sequencing analysis. Shown are the Ensembl name and gene symbol. The delta value demonstrates the change in poly(A) tail length, with a negative value indicating a loss and a positive value a gain of poly(A) tail length. The proportion of reads without (-Poly(A)) and with (+Poly(A)) are shown for control and postovulatory-aged oocytes.

Ensembl Name	Gene Name	Delta value	Control -Poly(A)	Control +Poly(A)	PostOA -Poly(A)	PostOA +Poly(A)
ENSMUSG00000082841	*Gm12994*	-0.599	0.17	0.83	0.71	0.29
ENSMUSG00000038400	*Pmepa1*	-0.571	0.33	0.67	0.94	0.06
ENSMUSG00000030717	*Nupr1*	-0.475	0.22	0.78	0.71	0.29
ENSMUSG00000022587	*Ly6e*	-0.426	0.45	0.55	0.90	0.10
ENSMUSG00000018677	*Slc25a39*	-0.414	0.45	0.55	0.91	0.09
ENSMUSG00000067594	*Krt77*	-0.382	0.53	0.47	0.94	0.06
ENSMUSG00000029166	*Mapre3*	-0.380	0.53	0.47	0.97	0.03
ENSMUSG00000021576	*Pdcd6*	-0.359	0.60	0.40	0.96	0.04
ENSMUSG00000028469	*Npr2*	-0.348	0.61	0.39	1.00	0.00
ENSMUSG00000041423	*Paqr6*	-0.343	0.56	0.44	0.98	0.02
ENSMUSG00000023336	*Wfdc1*	-0.333	0.49	0.51	0.88	0.12
ENSMUSG00000090104	*Slmapos2*	-0.326	0.54	0.46	0.91	0.09
ENSMUSG00000031156	*Slc35a2*	-0.326	0.57	0.43	0.93	0.07
ENSMUSG00000021400	*Wrnip1*	-0.325	0.52	0.48	0.95	0.05
ENSMUSG00000032551	*1110059G10Rik*	-0.324	0.63	0.37	0.98	0.02
ENSMUSG00000031532	*Saraf*	-0.309	0.58	0.42	0.93	0.07
ENSMUSG00000020321	*Mdh1*	-0.305	0.37	0.63	0.63	0.37
ENSMUSG00000043556	*Fbxl7*	-0.305	0.56	0.44	0.89	0.11
ENSMUSG00000026249	*Serpine2*	-0.305	0.49	0.51	0.82	0.18
ENSMUSG00000063229	*Ldha*	-0.292	0.65	0.35	1.00	0.00
ENSMUSG00000087601	*Uchl1os*	-0.292	0.59	0.41	0.93	0.07
ENSMUSG00000013646	*Sh3bp5l*	-0.291	0.64	0.36	1.00	0.00
ENSMUSG00000024074	*Crim1*	-0.291	0.65	0.35	0.98	0.02
ENSMUSG00000068154	*Insm1*	-0.290	0.40	0.60	0.68	0.32
ENSMUSG00000046364	*Rpl27a*	-0.287	0.54	0.46	0.99	0.01
ENSMUSG00000021721	*Htr1a*	-0.286	0.67	0.33	1.00	0.00
ENSMUSG00000002602	*Axl*	-0.285	0.68	0.32	0.99	0.01
ENSMUSG00000022634	*Yaf2*	-0.284	0.59	0.41	0.92	0.08
ENSMUSG00000096768	*Erdr1*	-0.280	0.69	0.31	1.00	0.00
ENSMUSG00000042524	*Sun2*	-0.278	0.44	0.56	0.74	0.26
ENSMUSG00000025743	*Sdc3*	-0.274	0.57	0.43	0.92	0.08
ENSMUSG00000022790	*Igsf11*	-0.274	0.49	0.51	0.84	0.16
ENSMUSG00000087531	*Gm15606*	-0.273	0.69	0.31	0.98	0.02
ENSMUSG00000039055	*Eme1*	-0.272	0.52	0.48	0.94	0.06
ENSMUSG00000018593	*Sparc*	-0.269	0.64	0.36	0.89	0.11
ENSMUSG00000020895	*Tmem107*	-0.265	0.60	0.40	0.87	0.13
ENSMUSG00000011884	*Gltp*	-0.265	0.57	0.43	0.88	0.12
ENSMUSG00000031549	*Ido2*	-0.262	0.52	0.48	0.85	0.15

Ensembl Name	Gene Name	Delta value	Control -Poly(A)	Control +Poly(A)	PostOA -Poly(A)	PostOA +Poly(A)
ENSMUSG00000026960	*Arl6ip6*	-0.260	0.61	0.39	0.89	0.11
ENSMUSG00000022180	*Slc7a8*	-0.259	0.60	0.40	0.92	0.08
ENSMUSG00000015478	*Rnf5*	-0.257	0.46	0.54	0.83	0.17
ENSMUSG00000026944	*Abca2*	-0.256	0.51	0.49	0.86	0.14
ENSMUSG00000097088	*Gm26615*	-0.249	0.55	0.45	0.97	0.03
ENSMUSG00000033161	*Atp1a1*	-0.246	0.57	0.43	0.85	0.15
ENSMUSG00000042275	*Pelo*	-0.246	0.33	0.67	0.52	0.48
ENSMUSG00000078566	*Bnip3*	-0.245	0.57	0.43	0.81	0.19
ENSMUSG00000032198	*Dock6*	-0.245	0.56	0.44	0.95	0.05
ENSMUSG00000032452	*Clstn2*	-0.243	0.65	0.35	0.92	0.08
ENSMUSG00000035395	*Pet2*	-0.243	0.54	0.46	0.91	0.09
ENSMUSG00000025082	*Vwa2*	-0.242	0.60	0.40	0.92	0.08
ENSMUSG00000028691	*Prdx1*	-0.242	0.42	0.58	0.64	0.36
ENSMUSG00000002871	*Tpra1*	-0.241	0.60	0.40	0.83	0.17
ENSMUSG00000059851	*Suv420h2*	-0.239	0.72	0.28	1.00	0.00
ENSMUSG00000038115	*Ano2*	-0.238	0.68	0.32	0.96	0.04
ENSMUSG00000090216	*Gm16549*	-0.238	0.73	0.27	1.00	0.00
ENSMUSG00000041617	*Ccdc74a*	-0.237	0.36	0.64	0.56	0.44
ENSMUSG00000026072	*Il1r1*	-0.235	0.70	0.30	0.98	0.02
ENSMUSG00000030897	*Cnga4*	-0.234	0.57	0.43	0.83	0.17
ENSMUSG00000002897	*Il17ra*	-0.233	0.61	0.39	0.89	0.11
ENSMUSG00000074934	*Grem1*	-0.233	0.68	0.32	0.96	0.04
ENSMUSG00000016179	*Camk1g*	-0.233	0.62	0.38	0.87	0.13
ENSMUSG00000031604	*Msmo1*	-0.233	0.58	0.42	0.86	0.14
ENSMUSG00000029632	*Ndufa4*	-0.232	0.62	0.38	0.87	0.13
ENSMUSG00000024940	*Ltbp3*	-0.231	0.63	0.37	0.86	0.14
ENSMUSG00000062908	*Acadm*	-0.231	0.71	0.29	0.96	0.04
ENSMUSG00000004207	*Psap*	-0.231	0.55	0.45	0.79	0.21
ENSMUSG00000020205	*Phlda1*	-0.230	0.47	0.53	0.84	0.16
ENSMUSG00000027570	*Col9a3*	-0.230	0.66	0.34	0.93	0.07
ENSMUSG00000097113	*Gm19705*	-0.230	0.62	0.38	1.00	0.00
ENSMUSG00000026112	*Coa5*	-0.230	0.55	0.45	0.79	0.21
ENSMUSG00000032572	*Col6a4*	-0.226	0.61	0.39	0.93	0.07
ENSMUSG00000036840	*Siah1a*	-0.226	0.69	0.31	0.94	0.06
ENSMUSG00000031834	*Pik3r2*	-0.226	0.61	0.39	0.89	0.11
ENSMUSG00000032577	*Mapkapk3*	-0.226	0.76	0.24	0.99	0.01
ENSMUSG00000060147	*Serpinb6a*	-0.226	0.71	0.29	0.96	0.04
ENSMUSG00000026121	*Sema4c*	-0.226	0.57	0.43	0.85	0.15
ENSMUSG00000060487	*Samd5*	-0.226	0.66	0.34	0.95	0.05
ENSMUSG00000073700	*Klhl21*	-0.225	0.62	0.38	0.89	0.11
ENSMUSG00000070056	*Mfhas1*	-0.225	0.64	0.36	0.97	0.03
ENSMUSG00000031016	*Wee1*	-0.223	0.69	0.31	1.00	0.00
ENSMUSG00000020605	*Hs1bp3*	-0.223	0.69	0.31	1.00	0.00

Ensembl Name	Gene Name	Delta value	Control -Poly(A)	Control +Poly(A)	PostOA -Poly(A)	PostOA +Poly(A)
ENSMUSG00000031823	*Zdhhc7*	-0.220	0.53	0.47	0.80	0.20
ENSMUSG00000030610	*Det1*	-0.219	0.73	0.27	0.98	0.02
ENSMUSG00000028453	*Fancg*	-0.218	0.61	0.39	0.93	0.07
ENSMUSG00000008855	*Hdac5*	-0.218	0.70	0.30	1.00	0.00
ENSMUSG00000008140	*Emc10*	-0.215	0.66	0.34	0.93	0.07
ENSMUSG00000034121	*Mks1*	-0.214	0.68	0.32	0.99	0.01
ENSMUSG00000031574	*Star*	-0.214	0.70	0.30	0.94	0.06
ENSMUSG00000040675	*Mthfd1l*	-0.212	0.63	0.37	0.94	0.06
ENSMUSG00000008730	*Hipk1*	-0.212	0.62	0.38	0.88	0.12
ENSMUSG00000029622	*Arpc1b*	-0.212	0.24	0.76	0.65	0.35
ENSMUSG00000022722	*Arl6*	-0.211	0.46	0.54	0.71	0.29
ENSMUSG00000003166	*Dgcr2*	-0.211	0.66	0.34	0.93	0.07
ENSMUSG00000032128	*Robo3*	-0.211	0.67	0.33	0.95	0.05
ENSMUSG00000063145	*Bbs5*	-0.211	0.59	0.41	0.77	0.23
ENSMUSG00000022964	*Tmem50b*	-0.209	0.67	0.33	0.95	0.05
ENSMUSG00000037656	*Slc20a2*	-0.209	0.68	0.32	0.99	0.01
ENSMUSG00000045639	*Zfp629*	-0.208	0.72	0.28	1.00	0.00
ENSMUSG00000037373	*Ctbp1*	-0.208	0.52	0.48	0.68	0.32
ENSMUSG00000030554	*Synm*	-0.207	0.63	0.37	0.88	0.12
ENSMUSG00000040860	*Crocc*	-0.207	0.56	0.44	0.84	0.16
ENSMUSG00000062270	*Morf4l1*	-0.207	0.55	0.45	0.75	0.25
ENSMUSG00000075254	*Heg1*	-0.207	0.68	0.32	0.91	0.09
ENSMUSG00000029108	*Pcdh7*	-0.207	0.75	0.25	1.00	0.00
ENSMUSG00000027748	*Trpc4*	-0.206	0.70	0.30	0.96	0.04
ENSMUSG00000029561	*Oasl2*	-0.206	0.75	0.25	0.96	0.04
ENSMUSG00000013846	*St3gal1*	-0.206	0.73	0.27	0.98	0.02
ENSMUSG00000051390	*Zbtb22*	-0.206	0.58	0.42	0.89	0.11
ENSMUSG00000048486	*Fitm2*	-0.205	0.65	0.35	0.88	0.12
ENSMUSG00000068099	*1500009C09Rik*	-0.205	0.67	0.33	0.90	0.10
ENSMUSG00000046722	*Cdc42se1*	-0.205	0.59	0.41	0.84	0.16
ENSMUSG00000078350	*Smim1*	-0.205	0.72	0.28	1.00	0.00
ENSMUSG00000021953	*Tdh*	-0.204	0.62	0.38	1.00	0.00
ENSMUSG00000021959	*Lats2*	-0.204	0.67	0.33	0.87	0.13
ENSMUSG00000038074	*Fkbp14*	-0.204	0.72	0.28	0.94	0.06
ENSMUSG00000004846	*Plod3*	-0.203	0.77	0.23	1.00	0.00
ENSMUSG00000031714	*Gab1*	-0.202	0.63	0.37	0.90	0.10
ENSMUSG00000041815	*Poldip3*	-0.202	0.68	0.32	0.93	0.07
ENSMUSG00000048706	*Lurap1l*	-0.201	0.64	0.36	0.86	0.14
ENSMUSG00000063524	*Eno1*	-0.201	0.61	0.39	0.87	0.13
ENSMUSG00000022636	*Alcam*	-0.201	0.72	0.28	0.96	0.04
ENSMUSG00000060601	*Nr1h2*	-0.201	0.58	0.42	0.76	0.24
ENSMUSG00000020413	*Hus1*	-0.201	0.70	0.30	0.92	0.08
ENSMUSG00000033396	*Spg11*	-0.201	0.68	0.32	0.95	0.05

Ensembl Name	Gene Name	Delta value	Control -Poly(A)	Control +Poly(A)	PostOA -Poly(A)	PostOA +Poly(A)
ENSMUSG00000078970	*Wdr92*	-0.200	0.73	0.27	0.96	0.04
ENSMUSG00000031654	*Cbln1*	-0.200	0.39	0.61	0.62	0.38
ENSMUSG00000030035	*Wbp1*	-0.200	0.68	0.32	0.99	0.01
ENSMUSG00000074129	*Rpl13a*	0.201	0.80	0.20	0.61	0.39
ENSMUSG00000061360	*Phf5a*	0.202	0.70	0.30	0.51	0.49
ENSMUSG00000021916	*Glt8d1*	0.204	0.75	0.25	0.58	0.42
ENSMUSG00000059060	*Rad51b*	0.206	0.98	0.02	0.71	0.29
ENSMUSG00000034278	*Dnajc17*	0.208	0.76	0.24	0.55	0.45
ENSMUSG00000025147	*Mob2*	0.208	0.82	0.18	0.59	0.41
ENSMUSG00000020440	*Arf5*	0.211	0.56	0.44	0.38	0.62
ENSMUSG00000098090	*2700099C18Rik*	0.212	0.85	0.15	0.61	0.39
ENSMUSG00000071662	*Polr2g*	0.213	0.73	0.27	0.57	0.43
ENSMUSG00000076615	*Ighg3*	0.214	0.85	0.15	0.62	0.38
ENSMUSG00000062275	*Fbxw24*	0.214	0.87	0.13	0.62	0.38
ENSMUSG00000024772	*Ehd1*	0.216	0.90	0.10	0.69	0.31
ENSMUSG00000033981	*Gria2*	0.216	0.89	0.11	0.67	0.33
ENSMUSG00000024601	*Isoc1*	0.218	0.81	0.19	0.60	0.40
ENSMUSG00000095595	*Fam177a*	0.219	0.68	0.32	0.46	0.54
ENSMUSG00000030534	*Vps33b*	0.221	0.79	0.21	0.55	0.45
ENSMUSG00000030316	*Tamm41*	0.223	0.90	0.10	0.66	0.34
ENSMUSG00000030877	*4933427G17Rik*	0.224	0.75	0.25	0.54	0.46
ENSMUSG00000076613	*Ighg2b*	0.225	0.80	0.20	0.55	0.45
ENSMUSG00000032288	*Imp3*	0.228	0.77	0.23	0.56	0.44
ENSMUSG00000053565	*Eif3k*	0.233	0.86	0.14	0.65	0.35
ENSMUSG00000020018	*Snrpf*	0.235	0.47	0.53	0.27	0.73
ENSMUSG00000023048	*Prr13*	0.235	0.88	0.12	0.58	0.42
ENSMUSG00000025580	*Eif4a3*	0.235	0.82	0.18	0.57	0.43
ENSMUSG00000066551	*Hmgb1*	0.237	0.80	0.20	0.56	0.44
ENSMUSG00000022476	*Polr3h*	0.238	0.87	0.13	0.57	0.43
ENSMUSG00000032839	*Trpc1*	0.238	0.85	0.15	0.56	0.44
ENSMUSG00000001018	*Snapin*	0.240	0.86	0.14	0.61	0.39
ENSMUSG00000031840	*Rab3a*	0.244	0.93	0.07	0.65	0.35
ENSMUSG00000005161	*Prdx2*	0.244	0.77	0.23	0.54	0.46
ENSMUSG00000029524	*Sirt4*	0.261	0.76	0.24	0.41	0.59
ENSMUSG00000003824	*Syce2*	0.264	0.83	0.17	0.56	0.44
ENSMUSG00000024863	*Mbl2*	0.268	0.87	0.13	0.58	0.42
ENSMUSG00000029465	*Arpc3*	0.268	0.80	0.20	0.48	0.52
ENSMUSG00000045690	*Wdr89*	0.269	0.81	0.19	0.60	0.40
ENSMUSG00000029649	*Pomp*	0.269	0.88	0.12	0.64	0.36
ENSMUSG00000085427	*6430710C18Rik*	0.274	0.82	0.18	0.57	0.43
ENSMUSG00000041571	*Sepw1*	0.282	0.91	0.09	0.57	0.43
ENSMUSG00000096262		0.289	0.74	0.26	0.48	0.52
ENSMUSG00000037966	*Ninj1*	0.295	0.64	0.36	0.37	0.63

Ensembl Name	Gene Name	Delta value	Control -Poly(A)	Control +Poly(A)	PostOA -Poly(A)	PostOA +Poly(A)
ENSMUSG00000036845	*Lin37*	0.296	0.81	0.19	0.51	0.49
ENSMUSG00000067702	*Tuba3a*	0.299	0.68	0.32	0.46	0.54
ENSMUSG00000076937	*Iglc2*	0.300	0.55	0.45	0.29	0.71
ENSMUSG00000024406	*Pou5f1*	0.303	0.62	0.38	0.34	0.66
ENSMUSG00000035112	*Wnk4*	0.304	0.85	0.15	0.52	0.48
ENSMUSG00000045435	*Tmem60*	0.315	0.93	0.07	0.58	0.42
ENSMUSG00000073016	*Uprt*	0.323	0.95	0.05	0.64	0.36
ENSMUSG00000043923	*Ccdc84*	0.327	0.74	0.26	0.47	0.53
ENSMUSG00000000088	*Cox5a*	0.327	0.86	0.14	0.52	0.48
ENSMUSG00000021807	*2700060E02Rik*	0.338	0.75	0.25	0.41	0.59
ENSMUSG00000010057	*Nprl2*	0.356	0.90	0.10	0.52	0.48
ENSMUSG00000021660	*Btf3*	0.421	0.77	0.23	0.32	0.68
ENSMUSG00000049214	*Skint7*	0.749	0.89	0.11	0.15	0.85

Table S6: Poly(A) tail ePAT analysis of single genes from control and postovulatory-aged oocytes on an Agilent DNA chip. Indicated is the gene symbol, the region of interest used for the assessment, the treatment of the oocytes, the average fragment size and the DNA concentration within the region.

Gene	Region (bp)		Oocytes	Average fragment size (bp)	Concentration (ng/µl)
	from	to			
Btf3	130	500	Control	218	8.85
			PostOA	228	6.88
Prdx2	360	700	Control	429	1.08
			PostOA	471	1.01
Ddx3x	500	1000	Control	617	2.55
			PostOA	612	2.40
Nupr1	220	400	Control	270	3.28
			PostOA	-	-

Table S7: DNA methylation levels of *Pou5f1* of control and 3 days preovulatory-aged embryos. Indicated is the MID of each embryo used for the deep bisulfite-sequencing and the methylation levels [%] of the maternal and paternal allel, as well as the mean methylation level over both alleles. Aberrant DNA methylation is indicated in red.

Control embryos				Preovulatory-aged embryos			
MID	**Maternal**	**Paternal**	**Mean**	**MID**	**Maternal**	**Paternal**	**Mean**
1	50	21	**25.0**	6			
2		5		7	0	0	**0.0**
3	0	0	**0.0**	8	0	0	**0.0**
4	1	5	**3.0**	9	0	0	**0.0**
5	0	0	**0.0**	10	0	0	**0.0**
11	8	8	**8.0**	16	0	0	**0.0**
12	0	0	**0.0**	17			
13	0	0	**0.0**	18	5		
14	3	22	**12.5**	19	0	0	**0.0**
15	0	0	**0.0**	20	0	0	**0.0**
21	8	10	**9.0**	26	0	0	**0.0**
22	0	0	**0.0**	27	9	21	**15.0**
23		0		28	0	0	**0.0**
24	0	0	**0.0**	29	0	0	**0.0**
25	17	5	**11.0**				
Mean	6.7	5.1	**6.1**	**Mean**	1.2	1.9	**1.4**

Table S8: DNA methylation levels of *H19* of control and 3 days preovulatory-aged embryos. Indicated is the MID of each embryo used for the deep bisulfite-sequencing and the methylation levels [%] of the maternal and paternal allel, as well as the mean methylation level over both alleles. Aberrant DNA methylation is indicated in red.

Control embryos				Preovulatory-aged embryos			
MID	**Maternal**	**Paternal**	**Mean**	**MID**	**Maternal**	**Paternal**	**Mean**
1	52	77	**64.5**	6	23	92	**57.5**
2	15	89	**52.0**	7	16	87	**51.5**
3	13	85	**49.0**	8	10	85	**47.5**
4		100		9	28	90	**59.0**
5	20	91	**55.5**	10	7	77	**42.0**
11	7	77	**42.0**	16	10	83	**46.5**
12	11	74	**42.5**	17	13	89	**51.0**
13	10	64	**37.0**	18	14	91	**52.5**
14	4	80	**42.0**	19	11	88	**49.5**
15	19	91	**55.0**	20	4	56	**30.0**
21	22	84	**53.0**	26	0		
22	9	89	**49.0**	27	4	72	**38.0**
23				28	0		
24	22	86	**54.0**	29	4	54	**29.0**
25							
Mean	17.0	83.6	**49.6**	**Mean**	10.3	80.3	**46.2**

Table S9: DNA methylation levels of *Snrpn* of control and 3 days preovulatory-aged embryos. Indicated is the MID of each embryo used for the deep bisulfite-sequencing and the methylation levels [%] of the maternal and paternal allel, as well as the mean methylation level over both alleles. Aberrant DNA methylation is indicated in red.

Control embryos				Preovulatory-aged embryos			
MID	**Maternal**	**Paternal**	**Mean**	**MID**	**Maternal**	**Paternal**	**Mean**
1	48	23	**35.5**	6		7	
2	93			7		0	
3	93			8	76	21	**48.5**
4	41	15	**28.0**	9	70	14	**42.0**
5		0		10	75	23	**49.0**
11	79	23	**51.0**	16	83	28	**55.5**
12	62	16	**39.0**	17	84	15	**49.0**
13	70	19	**44.5**	18	75	25	**50.0**
14	85	28	**56.5**	19	86	35	**60.5**
15	80	27	**53.5**	20	78	34	**56.0**
21	41	15	**28.0**	26	55	8	**31.5**
22	51	33	**42.0**	27	85	25	**55.0**
23	81	26	**53.5**	28			
24	58	16	**37.0**	29		0	
25	73	19	**46.0**				
Mean	68.2	20.0	**42.9**	**Mean**	76.7	17.2	**49.8**

Table S10: DNA methylation levels of *Igf2r* of control and 3 days preovulatory-aged embryos. Indicated is the MID of each embryo used for the deep bisulfite-sequencing and the methylation levels [%] of the maternal and paternal allel, as well as the mean methylation level over both alleles. Aberrant DNA methylation is indicated in red.

Control embryos				Preovulatory-aged embryos			
MID	**Maternal**	**Paternal**	**Mean**	**MID**	**Maternal**	**Paternal**	**Mean**
1	48	7	**27.5**	6	85	7	**46.0**
2	99			7	90	8	**49.0**
3	95	8	**51.5**	8	91	6	**48.5**
4		0		9	92		
5	88	7	**47.5**	10	99		
11	92	8	**50.0**	16		0	
12	92	7	**49.5**	17		3	
13	85	10	**47.5**	18			
14		0		19	81	5	**43.0**
15	87	8	**47.5**	20	93	9	**51.0**
21	94	12	**53.0**	26		0	
22	90	9	**49.5**	27		5	
23	79			28			
24	91	14	**52.5**	29	89		
25	93						
Mean	87.2	7.5	**47.6**	**Mean**	90.0	4.8	**47.5**

9 Acknowledgement

This project was supported by the Deutsche Forschungsgemeinschaft (DFG HO 949/21-1).

I would like to give my special thanks to Prof. Bernhard Horsthemke and Prof. Ruth Grümmer for the opportunity to work on this interesting topic but also for the exceptional guidance and supervision. It was a great experience to work in close cooperation with two institutes and to be introduced into such fascinating field of research. I am grateful for the constructive suggestions and the open and profitable discussions during our many project meetings. I am especially thankful to have had supervisors that gave me the freedom to work independently and encouraged me to pursue my own ideas, but at the same time always had an open door to support me whenever I stumbled. Their positive and calming attitudes were a great support in moments of doubt. Overall though, I did not have many of these moments and I will look happily look back at this time and the many great moments we shared.

Another very important person for me during this project was Debora Dankert, who I would like to thank for her support and friendship. It was great to be working on this project with someone I trusted so much. The opportunity to discuss all small and big problems, difficulties, successes and achievements were a major support.

For the warm welcome, fantastic work environment and great help I would like to thank all members of the Institute of Human Genetics. My special thanks goes to Laura Steenpass and her brilliant ideas in times when my experiments faltered as well as for critically reading my thesis. I would also like to thank Nicholas Wagner for proof reading my first paper and for having always time to discuss any problems that I encountered over the last years. I thank Lars Maßhöfer, who is known under many other names, for an amazing time in Lab 26/27. I had great fun, especially when Daniela Falkenstein came to visit us. I am very grateful for the support that I got from the other PhD students and postdocs, especially Jasmin Beygo, Christian Grosser, Helena Heinz, Jana Stanurova, Katrin Grothaus, Alexander Kalmbach and Tea Berulava; not just for their support in the laboratory, but more importantly for their friendship. I feel lucky to have spent my time as a PhD student in such an encouraging environment.

In addition I would also like to thank the Institute of Anatomy, who welcomed and supported me as much as if I would have been a member of their laboratory. I am thankful that Prof. Gunther Wennemuth gave me the opportunity to join the weekly seminar and the retreats to

Austria. For their support, friendship and distraction I thank Jennifer Thomczik, Janine Dreesen and Theresa Fahnenbruck.

I am grateful for the easy and successful collaboration with Prof. Ursula Eichenlaub-Ritter, Tom Trapphoff and Martyna Heiligentag. The interesting discussions and mutual help were very supportive and an experience I do not want to miss.

Finally, I thank my family and friends for their support during this time, but also for being a source of distraction and giving me other things to think about. I especially thank my parents, who were always beside me, for their love and encouragement throughout my studies. For his support, love and patience I thank Jano. I am happy to have Sarah who keeps me on the ground and Franzi, Christina, Nenja and Martina for always listening. I am also grateful for my friends in Holland that give me the feeling of coming home every time I visit. Without you all I would not be standing here today.

10 Curriculum vitae

Der Lebenslauf ist in der Online-Version aus Gründen des Datenschutzes nicht enthalten.

Der Lebenslauf ist in der Online-Version aus Gründen des Datenschutzes nicht enthalten.

11 Eidesstattliche Erklärung

Erklärung:

Hiermit erkläre ich, gem. § 6 Abs. 2, g der Promotionsordnung der Fakultät für Biologie zur Erlangung des Dr. rer. nat., dass ich das Arbeitsgebiet, dem das Thema „Effects of preovulatory aging on the developmental competence of mouse oocytes“ zuzuordnen ist, in Forschung und Lehre vertrete und den Antrag von Hannah Demond befürworte.

Essen, den _____ _____ _____

Name des wissenschaftl. Betreuers/Mitglieds der Universität Duisburg-Essen	Unterschrift d. wissenschaftl. Betreuers/ Mitglieds der Universität Duisburg-Essen

Erklärung:

Hiermit erkläre ich, gem. § 7 Abs. 2, d und f der Promotionsordnung der Fakultät für Biologie zur Erlangung des Dr. rer. nat., dass ich die vorliegende Dissertation selbständig verfasst und mich keiner anderen als der angegebenen Hilfsmittel bedient habe und alle wörtlich oder inhaltlich übernommenen Stellen als solche gekennzeichnet habe.

Essen, den _____ _____
Unterschrift des/r Doktoranden/in

Erklärung:

Hiermit erkläre ich, gem. § 7 Abs. 2, e und g der Promotionsordnung der Fakultät für Biologie zur Erlangung des Dr. rer. nat., dass ich keine anderen Promotionen bzw. Promotionsversuche in der Vergangenheit durchgeführt habe, dass diese Arbeit von keiner anderen Fakultät abgelehnt worden ist, und dass ich die Dissertation nur in diesem Verfahren einreiche.

Essen, den _____ _____
Unterschrift des/r Doktoranden/in